Master's thesis

NTNU
Norwegian University of Science and Technology
Faculty of Engineering
Department of Marine Technology

Mats Nilsen

Ice loading on Semi-Submersible

Local Analysis of Structural Response

Master's thesis in Marine Technology
Supervisor: Bernt J. Leira
July 2019

NTNU
Norwegian University of
Science and Technology

Mats Nilsen

Ice loading on Semi-Submersible

Local Analysis of Structural Response

Master's thesis in Marine Technology
Supervisor: Bernt J. Leira
July 2019

Norwegian University of Science and Technology
Faculty of Engineering
Department of Marine Technology

NTNU
Norwegian University of
Science and Technology

Master Thesis, Spring 2019

For

Stud. Techn. Mats Nilsen

Ice loading on Semi-Submersible: Local Analysis of Structural Response

Isbelastning på en Semi-Submersible: Lokal Strukturell Responsanalyse

With the entry of floating drilling and completion units for ice infested environments, development of associated structural design criteria for these units are required. It is also important that adequate algorithms for analysis of non-linear structural behaviour are available in order to quantify reserve strength properties if damage to the structural components might occur. The objective of the thesis is to address these issues in some detail.

The candidate shall address the following topics:

1. A summary of ice properties, ice mechanics and ice load formulations for floating hull structures is to be made.
2. Relevant loading conditions for floating units are to be discussed with focus on local strength requirements (e.g. related to plate thickness and bending stiffeners). In particular, formulations which are implemented in ISO19906 are to be considered.
3. Corresponding methods for computation of linear and non-linear load-effects and the associated structural resistance are to be highlighted. Some background to the numerical algorithms which are implemented in relevant computer software which is to be applied for the different types of calculation (e.g.Abaqus) should be given.
4. Local response calculations are performed for a particular structural component of a floating hull system. The example system is selected based on discussion with the supervisor.
5. Parametric studies are carried out to the extent that time allows. A corresponding matrix of parameter values for the different analysis cases should be established, and the matrix should be agreed upon by the supervisor before the calculations are performed.

The work scope may prove to be larger than initially anticipated. Subject to approval from the supervisor, topics may be deleted from the list above or reduced in extent. In the thesis the candidate shall present his personal contribution to the resolution of problems within the scope of the thesis work. Theories and conclusions should be based on mathematical derivations and/or logic reasoning identifying the various steps in the deduction.

The thesis should be organised in a rational manner to give a clear exposition of results, assessments, and conclusions. The text should be brief and to the point, with a clear language. Telegraphic language should be avoided.

The thesis shall contain the following elements: A text defining the scope, preface, list of contents, summary, main body of thesis, conclusions with recommendations for further work, list of symbols and acronyms, references and (optional) appendices. All figures, tables and equations shall be numbered.

The supervisor may require that the candidate, in an early stage of the work, presents a written plan for the completion of the work.

The original contribution of the candidate and material taken from other sources shall be clearly defined. Work from other sources shall be properly referenced using an acknowledged referencing system.

The thesis shall be submitted in 3 copies:

- Signed by the candidate
- The text defining the scope included
- In bound volume(s)
- Drawings and/or computer prints which cannot be bound should be organized in a separate folder.

Supervisor: Professor Bernt J. Leira

Deadline: July 16th 2019

Trondheim, January 16th 2019

Bernt J. Leira

Abstract

The interest in the Arctic has been increasing over the recent years, and there is an increase in activity in this region as the search for oil and gas continues. New challenges arise since the environment in these areas can be very harsh and challenging. Structures designed for operation in the Arctic has to be dimensioned accordingly.

The first section is a literature study that gives an introduction into the subject of ice from an engineering standpoint. A summary of ice properties, ice mechanics and ice load formulations for floating hull structures is made to increase the knowledge about the behaviour and the conditions one is faced with in the Arctic. A review of the challenges in calculating ice actions on vertical, floating, multi-legged structures, as well as a more in depth look at the local ice loads is also performed.

The main part of this master thesis is to perform a structural analysis of a section of a semi-submersible.

The analyses are performed by use of the finite element software Abaqus. The plate thickness and the stiffeners have been dimensioned according to IACS' *Requirements concerning POLAR CLASS*, using ice class PC4 to ensure sufficient ice strengthening. A convergence study was conducted in order to find what element to use and what element size would give accurate results. The convergence study resulted in the choice of S4R-elements with an element size of 100 mm, as that gave a good balance between accurate results and acceptable computational time. Another sensitivity study was performed for the boundary conditions in order to conserve conservatism. The bottom boundary was assumed to be free to rotate in vertical direction, while all other translations and rotations were kept fixed. The top boundary was assumed to be free to translate and rotate in vertical direction, while other translations and rotations were kept fixed.

Local ice pressures were calculated from three different regulations. IACS gave an average pressure of 4.74 MPa over a load patch of 7.14 m^2. Both the plating and the stiffeners were checked to see if the structural integrity had been compromised. The plate could withstand this load, with stresses being well under the yield strength for this load condition. The stiffeners exhibited some yielding, but since this formulation is based on plastic methods, some yielding is expected. The formulations by DNV and ISO 19906 was then compared, and the most conservative results were implemented. These loads were applied over design areas for plating, stiffener, stringer and bulkhead. The plating and stringer both experienced yielding

with these design loads applied. The stiffener and bulkhead on the other hand had stresses below yield strength, and was thus deemed sufficiently strengthened. Parameter studies suggested that especially the stringer needed further strengthening to withstand the large loads encountered in ice infested waters.

Sammendrag

Interessen for Arktis har vært økende de siste årene, og en økning i aktivitet i denne regionen en sett ettersom søken etter olje og gass fortsetter. Nye utfordinger oppstår siden miljøet i disse områdene er tøffe og utfordrende. Konstruksjoner designet for operasjoner i Arktis må derfor ta dette i betraktning.

Den første delen er en litteraturstudie som gir en introduksjon i forskjellige aspekter ved is fra et ingeniørsynspunkt. Et sammendrag av isegenskaper, ismekanikk og islast-formuleringer for flytende skrogkonstruksjoner er gjennomført for å øke kunnskapen om oppførselen og tilstander man står ovenfor i Arktis. En gjennomgang av utfordringer i beregninger av islaster på vertikale, flytende, flerbente konstruksjoner, såvel som en nærmere kikk på lokale islaster er også gjennomført.

Hoveddelen av masteroppgaven består av strukturanalyse av en del av en semi-submersible.

Analysene er gjennomført ved bruk av elementmetode-programvaren Abaqus. Platetykkelsen og stiverene er dimensjonert i henhold til IACS *Requirements concerning POLAR CLASS*, hvor isklassen PC4 er brukt for å sørge for tilstrekkelig isforsterkning. En konvergensstudie ble gjennomført for å finne hvilket element og elementstørrelse som ga korrekte resultater. Konvergensstudien resulterte i valget av S4R-elementer med en elementstørrelse på 100 mm, siden det ga en god balanse mellom korrekt resultat og akseptabel beregningstid. Enda en studie ble gjennomført for å finne konservative grensebetingelser. De nedre grensene ble antatt å være frie til å rotere i vertikal retning, mens alle andre translasjoner og rotasjoner ble fasthold. De øvre grensene ble antatt å være fri til å bevege seg og rotere i vertikal retning, mens alle andre translasjoner og rotasjoner ble fastholdt.

Lokale islaster ble beregnet fra tre forskjellige reguleringer. IACS ga et gjennomsnittstrykk på 4.74 MPa over et lastområde på 7.14 m^2. Både plater og stivere ble sjekket for å se om den strukturelle integriteten var kompromittert. Platen kunne stå imot denne lasten, med spenninger godt under flytspenning for denne lastbetingelsen. Stiverne viste noe flyt, men siden denne formuleringen er basert på plastiske metoder er noe flyt forventet. Formuleringene av DNV og ISO 19906 ble så sammenlignet, og de mest konservative resultatene ble implementert. Disse lastene ble anvendt over lastområder for plate, stiver, stringer og skott. Plate og stringer erfarte begge flyt med disse designlastene anvendt. Stiver og skott derimot, hadde spenninger under flytgrensen, og ble dermed ansett som sterke nok. Parameterstudier viste at spesielt stringeren behøver mer styrking for å stå imot de store lastene man møter i havområder

som inneholder is.

Preface

This report is the result of the Master's Thesis done in the field of marine structural engineering at the Department of Marine Technology at the University of Science and Technology(NTNU), Trondheim. The work has been carried out in the spring of 2019. The work is a continuation of the Project Thesis carried out in the spring of 2018, and thus some parts are kept as is since it is still relevant for the Master's Thesis.

A lot of the time devoted to the thesis has gone to getting familiar with the software Abaqus. I did not have a much experience using Abaqus to analyse complex models, so this was very challenging and more time consuming than anticipated. Thus the scope of the thesis had to be changed during the semester. Establishing the model proved challenging, as it had to be re-established several times due to small fatal errors recognized only after most of the model was already set up. This helped in learning to master the software, and it has been a great learning experience. Learning about the challenges faced in ice infested waters has also been a very interesting and educational experience.

I would like to thank my supervisor, Bernt Johan Leira, for all his help, guidance and feedback throughout the process of writing this thesis.

Mats Nilsen

Stokmarknes, July 16th 2019

Contents

List of Tables

List of Figures

Nomenclature

α	= 86400 seconds/day
α_i	Waterline angle
β	Hull slope
β_i	Normal frame angle
ϵ^e	Elastic strain
ϵ^t	Total strain
ϵ^v	Viscous strain
$\epsilon^v e$	Visco-elastic strain
μ	Viscosity
ρ_i	Density of ice
σ	Stress
σ_y	Yield stress
τ	Shear stress
CF_C	Crushing failure class factor
h_f	Floe thickness
h_i	Height of ice
H_R	Average ridge density
h_{eq}	Equivalent ice thickness
k_i	Thermal conductivity of ice

K_{IC}	Fracture toughness
l_i	Latent heat of ice
R_s	Shear resistance
S_i	Salinity of ice
T_a	Top temperature of ice sheet
T_b	Bottom temperature of ice sheet
T_i	Temperature of ice
t_t	Total freezing time
v_b	Brine volume
K	Stiffness matrix
A	Contact area
a	Height of load patch
AR	Aspect ratio
c	Cohesion factor
D	Ship displacement
E	Young's modulus
FDD	Freeing degree days of ice
G	Strain energy release rate
M	Mass
p	Ice pressure
PPF	Peak pressure factor
V	Volume
v	Poisson's ratio

w Width of load patch

x Distance from forward perpendicular

1 Introduction

There is increasing demand for floating drilling units above the Arctic circle, as large reserves of oil and gas are being discovered. The environment experienced in these regions is very challenging, with limited infrastructure, harsh weather conditions and ice actions that necessitate a lot of strengthening, which causes higher costs.

There is still a lack of research on floating structures subjected to ice actions, as most operations in the Arctic regions are in shallow waters. Deep water operations are usually preserved for the summer months when the ice coverage is minimal. New cost effective solutions must be found in order to take advantage of the vast petroleum reserves in a safe way. Most of the regulations for ice strengthening are made for ships. In this thesis these regulations will be used for an offshore platform, and an analysis will be performed to see if these regulations provide sufficient strengthening.

1.1 Outline of the Thesis

In this Master Thesis the main object is to perform a non-linear analysis of a floating offshore structure exposed to local ice loads. The structure analysed will be a part of a semi-submersible operating in Arctic regions. The following chapters presented in this master thesis are:

- **Chapter 1 - Introduction**
- **Chapter 2 - Theoretical Background**. Theoretical background on ice properties and ice mechanics used in Arctic engineering.
- **Chapter 3 - Ice Actions on Floating Structures**. Description of load conditions floating, vertical, multi-legged structures are subjected to, and the challenges that follow.
- **Chapter 4 - The Semi-Submersible Unit**. Presentation of the semi-submersible that will be analysed in this master thesis.
- **Chapter 5 - Determining Ice Actions on Floating Structures**. An overview of the existing local load formulations regarding structures subjected to ice actions.

- **Chapter 6 - Local Strength Requirements**. A review of failure modes and the existing regulations regarding local strengthening of structures subjected to ice actions.
- **Chapter 7 - The Finite Element Method**. A presentation of the finite element method, which is the algorithm implemented in the analysis tool used.
- **Capter 8 - The Computer Model**. A review of the model constructed in the analysis of the structural part.
- **Chapter 9 - Non-Linear Static Analysis**. A presentation of the results found when analysing the structure subjected to ice actions. This includes several load cases as well as parameter studies for the main parts of the model.
- **Chapter 10 - Conclusion**. Conclusion of the work.
- **Chapter 11 - Recommendations for Further Work**.

2 Theoretical Background

In order to understand ice/vessel impacts, knowledge about the Arctic region and the physical and mechanical properties of ice is necessary. This section will be divided into three subsections, namely floating ice, physical properties and lastly a review of ice mechanics will be conducted.

The material presented in this chapter will be referring to Løset et al. (2006) unless stated otherwise. Some parts of this section is gathered from the project thesis, referred to in Nilsen (2018).

2.1 The Arctic Region

The Arctic encompasses an area around the North Pole but there is no one definition of what the Arctic region is, but rather several. What definition used depends on what the definition is being used for. In general the marine Arctic is divided into three main groups. Namely the permanent ice zone, the seasonal ice zone and the marginal ice zone. The marginal ice zone includes drift ice and the ice edge. Politically the regions north of the Arctic Circle is usually defined as the Arctic, but climatically not all areas north of the Arctic Circle fulfil the criteria for being part of the Arctic. Figure 2.1 shows the Arctic north of the Polar Circle along with the Northwest and Northeast passage which are the two main sea routes through the Arctic.

The Arctic climate is diverse as the Arctic covers vast areas and stretches over several different continents. One would assume that the northernmost areas are the coldest but that is not the case. Areas far east in Russia and and west in North America, Alaska and Canada, may have warm summers but get extremely cold winters. Near the ocean the temperatures are mainly driven by the ocean. The North Atlantic Drift brings warmer water from the Gulf Stream north-east over the North Atlantic and warms up the northern part of coastal Europe and the Barents Sea. This makes the climate in the Arctic difficult to generalize as the weather conditions will be vastly different in say Northern Norway and Alaska.

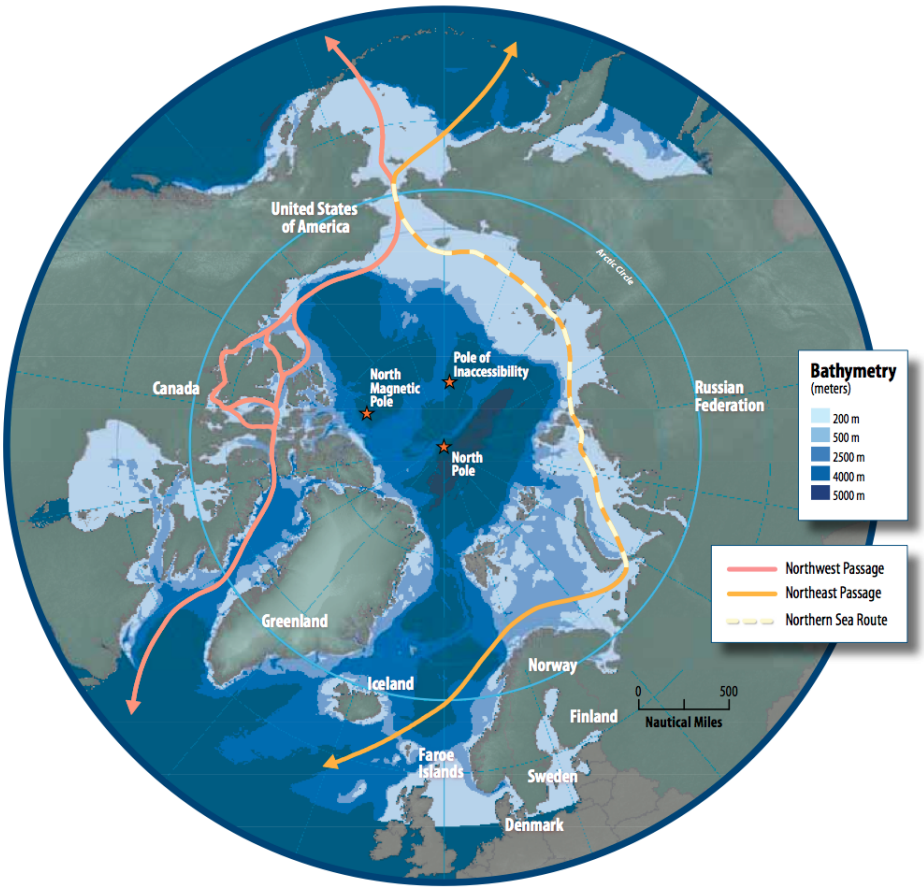

Figure 2.1: The Arctic region including northeast and northwest passage(Santos-Pedro et al. 2009)

Figure 2.2 shows the extent of sea ice in the Arctic. The extent of sea ice is of great importance for the eco-systems of the world. It is important to the dynamics of the Arctic Ocean which in turn influences the exchanges of heat with other oceans. The trend of global warming is widely accepted by climate scientists and the effects can be seen in the increased melting of the sea ice in the Arctic. Open water absorbs the majority of the solar energy while ice on the other hand reflects it. As the sea ice melts this will cause a positive feedback-loop as less heat is reflected causing further warming of the planet(Palmer and Croasdale 2013). These mechanisms will have wide consequences for both the Arctic regions and for the rest of the world.

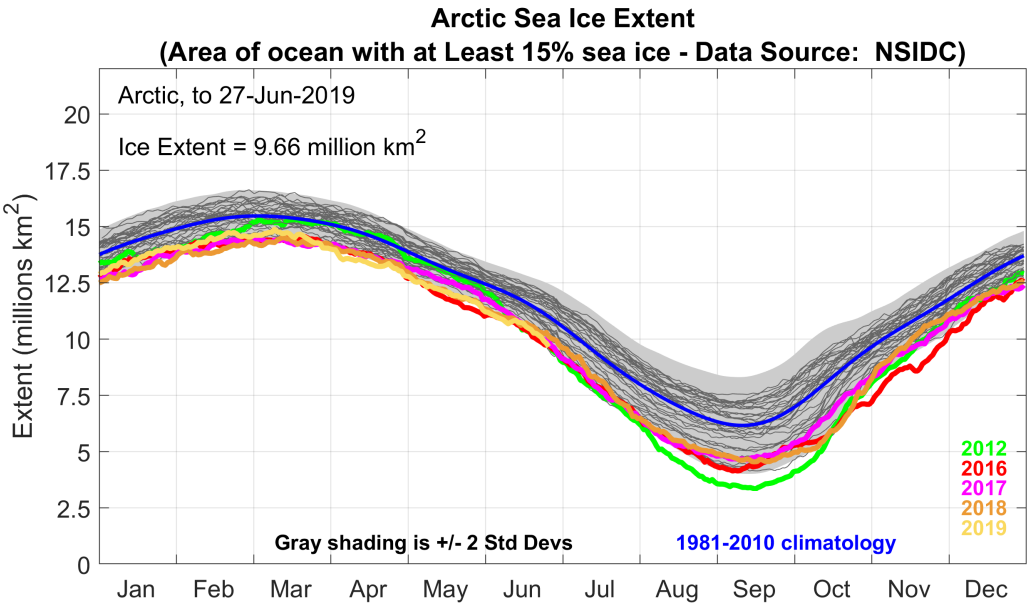

Figure 2.2: The Arctic sea ice extent since 1981(Diamond, 2019)

It is estimated that the Arctic has 145 billion barrels of oil that has not been discovered yet(CARA, 2008). That equals 6% of the total known reserves in the world. It is further estimated that the Arctic has 55 trillion cubic meters of the natural gas of the world's current known gas reserves. In total that equals 22% of the total known world reserves of oil and gas. The majority of these resources are expected to be offshore. However, the environmental conditions and the high concentration of multi-year ice has made it difficult to explore these regions for the objective of petroleum production. Ice thicknesses and the length of the seasons will however change with global warming and larger areas may be made available for further exploration. Because of this offshore platforms will be more relevant than ever.

2.2 Floating Ice

The World Meteorological Organization gives an international definition of floating ice and divides it into three main types. Sea ice which originates from the freezing of sea water and is the main kind of floating ice encountered at sea, ice of land origin which is ice formed on land and found floating in water, and river and lake ice which are formed on a lake or on a river. Ice types can also be characterized as first-year, second-year and multi-year sea ice, shelf ice and glacial ice. In this thesis multi-year ice will also include second-year ice. The appearance of first-year ice changes appearance as it transitions from black-grey for new and young ice to white when it gets thicker(Fequet, 2005). The stages of development

of floating ice is further defined by WMO(1989) as follows:

- **New ice** is recently formed ice which is subdivided into frazil ice, grease ice, slush and shuga, and are composed of ice crystals which are only weakly frozen together. New ice is usually less than 1 cm thick.
- **Nilas** has a thickness of up to 10 cm and is a thin elastic crust of ice, which easily bends with the motions of the ocean. Nilas can be subdivided into dark nilas and light nilas which comes from the color of the ice.
- **Young ice** is in the transition stage between nilas and first-year ice, and has a thickness of 10-30 cm. It can be further subdivided into grey ice and grey-white ice.
- **First-year ice** is of no more than one winter's growth and has a thickness of 30 cm - 2 m. It is subdivided into thin first-year ice/white ice, medium first-year ice and thick first-year ice.
- **Old ice** has survived at least one summer and has typically a thickness of up to 3 m or more. It is subdivided into residual first-year ice, second-year ice and multi-year ice.

First year ice and multi-year ice are of particular interest for engineering in the arctic, and will therefore be the main focus in this thesis.

Floating ice can further be classified according to forms of floating ice. Ice floe is any relative flat piece of sea ice which is 20 m or more across. Pancake ice is circular plates of ice from 30 cm to 3 m in diameter and has raised rims due to pieces striking against each other. Ice cake is a relatively flat piece of ice less than 20m across. Level ice is sea ice which has been affected by little to no deformation. Rafted ice is deformed ice formed by one piece of ice overriding another. Ridged ice is another type of deformed ice where a wall of deformed ice has been forced upwards from the pressure of the surrounding ice cover.

The motion of the water and ice makes different zones of ice. The ice stays stationary from the support of outer islands or a grounded ridge zone near the shoreline(Riska 2011) which makes the fast ice zone which can be seen in 2.3. Outside of this zone is the grounded ice zone where the ice is connected to the sea floor. In the transition zone the ice breaks and moves, and the effect of the coastline is significant. The pack ice zone comes outside of the transition zone, and signifies ice that is not landfast.

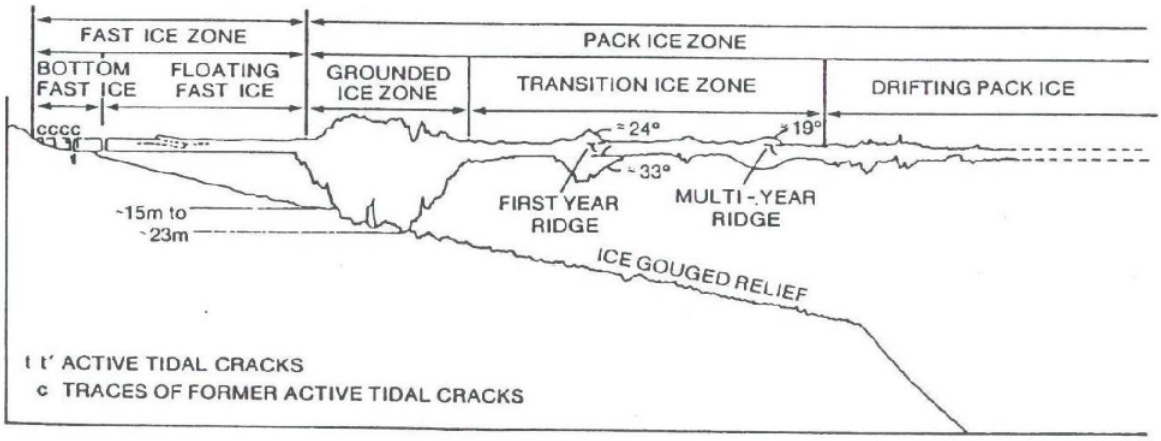

Figure 2.3: Different zones of ice(Icex 1979)

An important parameter in describing the sea coverage is the concentration of ice, and gives the portion of the surface covered by ice. The concentration of ice is given by:

$$C = \frac{A_{ice}}{A_{tot}} \tag{2.1}$$

Where A_{ice} gives the area of the ice and A_{tot} gives the total area of the surface. A typical value for the ice coverage in an ice cover is 90%.

2.3 Physical Properties

2.3.1 Microstructure of Ice

Water molecules are made up of one oxygen atom that has chemical bonds with two hydrogen atoms, and has the chemical formula H_2O. When liquid water is frozen under normal atmospheric conditions, the water molecules arrange in orderly repetitive positions to form a crystalline solid with hexagonal symmetry. At least nine different structures is possible for ice to form, but only one is observed in nature and is referred to as hexagonal ice, namely ice Ih. The other forms are only stable for higher pressures or lower temperatures than we see in nature on Earth(Palmer and Croasdale 2013). Each hydrogen atom with its partial charge is attracted to one of the lone pairs on an oxygen of a neighbouring molecule. This bond is called a hydrogen bond and is weakly ionic. The four bonds associated with each oxygen atom are arranged in six possible ways, as illustrated in figure 2.4.

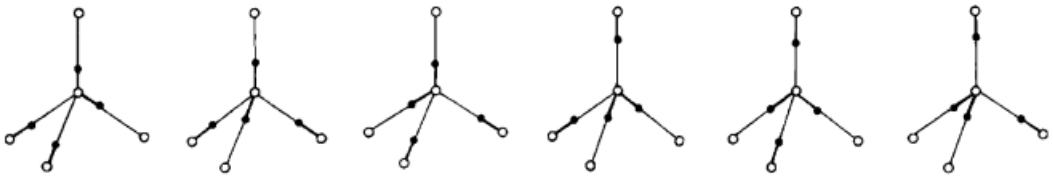

Figure 2.4: The six arrangements of hydrogen atoms around each oxygen atom (Løset et al. 2006)

The oxygen atoms are concentrated close to a series of parallel planes(basal plane) with hexagonal symmetry, which is illustrated in figure 2.5. Each oxygen atom has three hydrogen bonds withing the basal plane and just one out of the plane. Fracture along the basal plane requires the breaking of only two bonds while any plane normal to the basal plane requires the breaking of at least four bonds, which explains why ice easily glides and cleaves on the basal plane. The lattice of ice is relatively open and water molecules get closer together if they break the lattice and pack closer together, which is what happens in liquid form. This is why ice is less dense than liquid water, which is an unusual feature, as most substances are more dense in solid form than in liquid form.

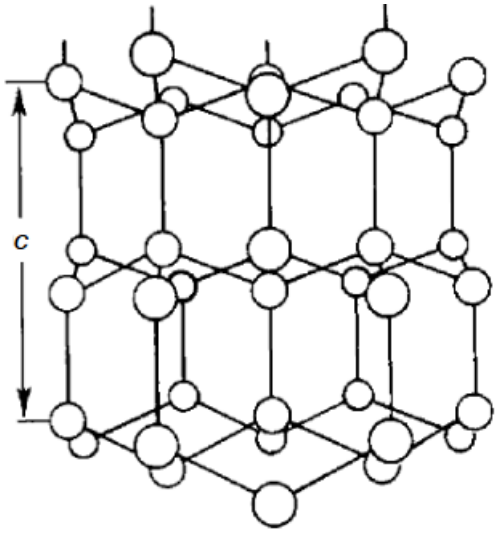

Figure 2.5: Structure of ice perpendicular to basal planes (Løset et al. 2006)

2.3.2 Sea Ice Formation

When fresh water reaches its freezing temperature the density of the surface layer is lower than the density of the water below. This causes the water to start freezing immediately. For sea water, however, the

density of the surface layer at freezing temperature is higher than the density below where the temperatures are higher. Thus the surface layer sinks down and water with higher temperature rises up. This happens continually until the whole water column has cooled down(although at some depth there is usually a density increase where the water will not move). The presence of salt in the water also causes the water to have a lower freezing temperature than fresh water(Palmer and Croasdale 2013). When the sea water freezes, the salt is expelled from the first ice plates that form. The first ice crystals start to form at a temperature of -1.9 °C due to the presence of salt. As the ice mass grows, the plates begin to bond to each other and form a highly saline slush called grease ice from its greasy appearance. As the ice grows it forms a continuous sheet called nilas(mentioned in section 2.2). If snow falls on the surface of the ice it acts as an insulator of the ice from the fluctuations of the air temperature. During growth most of the seawater is displaced, but between the platelets of pure ice a seawater concentrate called brine becomes trapped. The brine reduce the strength of the sea ice compared to freshwater ice. The brine volume of first year ice as derived by (Løset, Høyland et al. 1998):

$$\upsilon_b = S_i \left(\frac{45.917}{T_i} + 0.930 \right) \qquad -8.2^\circ C \leq T_i \leq -2.0^\circ C \tag{2.2}$$

$$\upsilon_b = S_i \left(\frac{43.795}{T_i} + 1.189 \right) \qquad -22.9^\circ C \leq T_i \leq -8.2^\circ C \tag{2.3}$$

Where υ_b is the brine volume, S_i is the salinity of ice and T_i is the ice temperature. The density of the brine is higher than that of the sea water, so if open channels form to the sea beneath, the difference in density will cause the brine to drain out.

The first ice platelets that are formed are randomly oriented, but become more and more ordered as they grow wide and stack onto each other. The first layer is denoted the primary layer and has a thickness of 0.1-0.15[m], and the vertical portion of the ice sheet where the crystal orientation has a rapid change is called the transition zone which as a thickness of 0.05-0.3[m]. The ice below the transition zone is called the columnar zone. For first-year ice the most common grain structures are granular, columnar and discontinuous columnar. The different layers are illustrated in figure 2.6. Multi-year ice can consist of a more varied microstructure, and has a lower salinity than first-year ice(due to brine drainage) and is therefore considerably stronger.

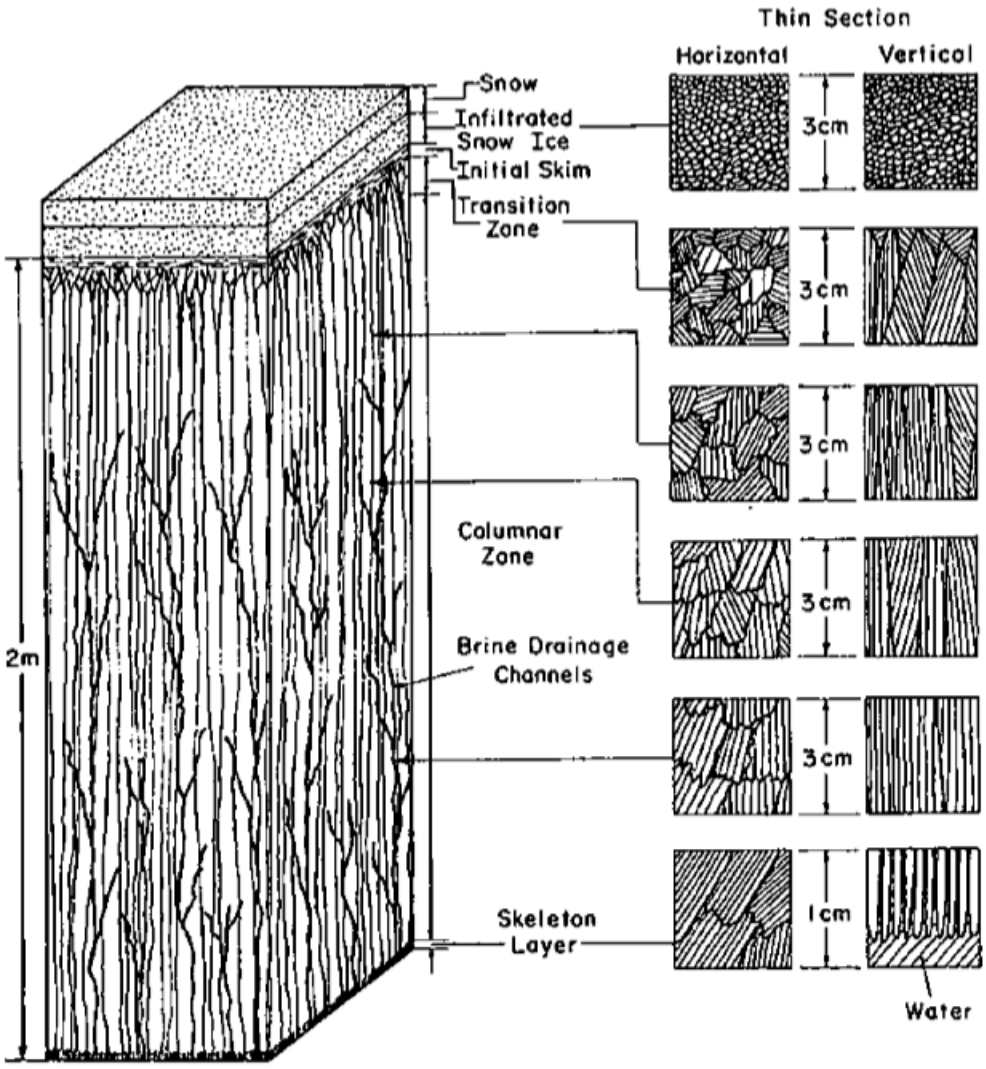

Figure 2.6: Different layers of first-year ice(Løset et al. 2006)

The ice and sea move continuously, with wind dragging on the surface of the ice and current underneath causing compression in the ice layer. If the compression forces are large enough the ice can start to fracture and break up. When the ice is pushed against each other a pressure ridge may form. Some of the fragments from the fracture gets pushed down into the sea and form a keel, while some are lifted up and form a sail. Most keels and sails are relatively small, like the sail seen in figure 2.7, but the deepest keels may reach depths of 40m and the largest sails may reach heights of 10m. The low temperatures causes the ice fragments to freeze together. As for sea ice, we have first-year ridges that only survive one summer's melt, while other consolidate and become stronger and form multi-year ridges. Also ridges become less saline as brine drains and get displaced as the fragments freeze together(Palmer and Croasdale 2013).

Ridges are of great concern for ice-going ships navigating in ice infested waters.

Figure 2.7: Typical ice ridge(Riska, 2018)

2.3.3 Ice Thickness

Ice thickness is one of the most important parameters concerning ice loads on offshore structures and vessels, since the load increase with increasing ice height. Stefan's law gives an equation for ice thickness which is derived in (Høyland), and is given as:

$$h_i^2(t) - h_{i,0}^2 = \frac{2k_i}{\rho_i l_i} FDD\alpha \tag{2.4}$$

Where h_i is the ice thickness, k_i is the thermal conductivity of ice, ρ_i is the density of the ice, l_i is the latent heat of the ice, FDD is the Freezing Degree Days and α is the the number of seconds per day. If steady state condition is assumed and the heat transfer between the water and ice is negligible, the following

equation was derived by Timco and Weeks (2010):

$$h = \sqrt{\frac{2k_i}{\rho_i L}(T_b - T_a)\,t_t} \tag{2.5}$$

Where T_a is the top temperature of the ice sheet, T_b is the bottom temperature of the ice sheet and t_t is the total freezing time. This equation will always overpredict the ice thickness.

The most important ice parameter is the existence of multi-year ice(Riska 2011). During the summer the ice will melt, and the salt will drain into the sea. The ice however, will primarily melt on the surface. When the winter comes again the ice starts freezing from the bottom. For multi-year ice this cycle of melting and freezeing reaches and equilibrium for an ice thickness of approximately 1.8m to 2.5m. The same happens for ridges, where the voids of the ridge gets filled with fresh water and the sails melt during the summer months. Multi-year ridges reaches an equilibrium thickness typically around 5m. Often the ridge thickness and level ice thickness are combined to give an equivalent level ice thickness where ridges are taken into account. Equation 2.6 gives the equivalent ice thickness for a ridge with a triangular cross section:

$$h_{eq} = (C - 4.28\mu H_R)h_i + 2.14\mu H_R^2 \tag{2.6}$$

Where h_{eq} gives the equivalent ice thickness, C is the ice concentration, μ is the average ridge density, h_i is the ice thickness and H_R is the average ridge density.

2.3.4 Temperature, Salinity and Density in Sea Ice

The temperature at the bottom of the ice cover is always equal to the temperature of the water surrounding it. In growth this temperature is equal to the freezing point of the sea water, as was mentioned earlier to be -1.9 °C. The temperature at the top of the ice cover is equal to the air temperature(or zero degrees if the air temperature is above zero degrees). For first-year ice one can usually assume a linear temperature gradient through the ice. The temperature profiles for old ice is usually more complicated, but for stable growing, not too thick, old ice will also have a linear temperature gradient from top to bottom.

The salinity profile in growing first-year ice is C-shaped, which means it's more saline in the top and

bottom of the ice, and less so in the middle. The salt do not fit the ice crystal matrix and is expelled. Most of the brine gets pushed down into the sea, while some gets stuck in brine pockets and gives the sea ice its salinity. The amount of brine is decided by the ice growth rate and the brine expulsion rate. When the ice is thin the growth rate is higher while the brine expulsion rate stays constant, so more brine gets stuck in the ice. When the ice gets thicker the growth rate decreases and the ice salinity decreases. The salinity of old ice is less than for first-year ice as some of the salt dries during the summer. Empirical equations for the salinity as a function of ice thickness is given by Kovacs (1996) for first-year ice as:

$$S_i = 4.606 + \frac{91.603}{h_i} \tag{2.7}$$

And for multi-year ice as:

$$S_i = 1.85 + \frac{80217.9}{h_F^2} \tag{2.8}$$

Where h_i is ice thickness and h_F is the floe thickness. Use of these equations assumes no salinity variation with ice depth. Typical values for first-year ice is 0.5 to 4‰and for multi-year ice 1.5 to 5‰(Timco and Weeks, 2010).

The most common technique to measure the density of ice is to cut out a standard sized ice block from a sheet of ice, which gives the volume. Then weighing the ice block gives the mass. This is called the mass/volume technique(ISO 19906) and the resulting density is given by:

$$\rho_i = \frac{M}{V} \tag{2.9}$$

Where M is the mass and V is the volume. Measurements given by Timco and Frederking(1996) tells that the sea ice density ranges between 720 kg/m^3 and 920 kg/m^3. The densities differ above and below the waterline. The density of sea ice above the waterline ranges from 840 kg/m^3 to 910 kg/m^3 for first-year ice and from 720 kg/m^3 to 910 kg/m^3 for multi-year ice. The density of sea ice below the waterline ranges from 900 kg/m^3 to 920 kg/m^3 for both first-year and multi-year ice.

2.4 Ice Mechanics

Ice engineering calculations do not generally start with the microstructure of ice, but rather see the ice as a continuum with mechanical properties described by constitutive equations. Ice is a crystalline material which in principle behaves much like metals, with ductile and brittle behaviour. Two characteristics about ice makes it more complicated from an engineering standpoint than the ordinary approach to metals, and those are that the grains are relatively large and ice exists close to its freezing point in its natural state. It is also a multiphase material consisting of pure ice, brine, air and sometimes solid salts. Therefore a full mechanical model of ice would need to include linear and non-linear aspects of elasticity, visco-elasticity, visco-plasticity and fracture, since there is both a solid part and a fluid part.

2.4.1 Sea Ice Behaviour

As mentioned earlier sea ice exhibits both solid and fluid behaviour. For a solid there is no time dependence, and the load is only a function of the displacements. Fluids however are time-dependent, and specifically depend on the velocity. The total strain is often decomposed as follows:

$$\epsilon^t = \epsilon^e + \epsilon^{ve} + \epsilon^v \tag{2.10}$$

Where ϵ^e is the elastic strain, ϵ^{ve} is the visco-elastic strain and ϵ^v is the viscous strain. Figure 2.8 illustrates a creep test performed on ice, where a load is applied and kept constant for a while before being released. The resulting strain-displacement diagram shows the different regions of strain experienced by the material.

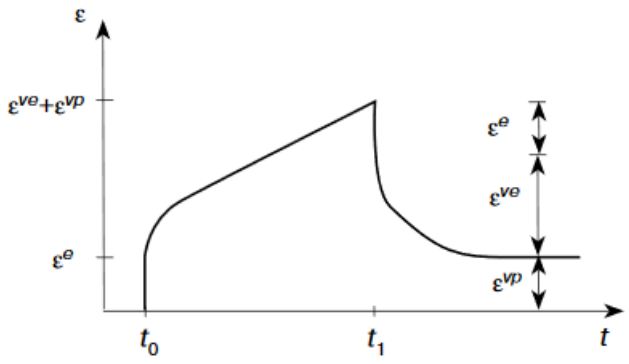

Figure 2.8: Decomposition of strain for a creep test(Løset et al. 2006)

For a time-independent, one-dimensional case the stress-strain relationship can be expressed by Hooke's law, where the stresses are given as a function of the strains:

$$\sigma = E \cdot \epsilon \tag{2.11}$$

Where σ is the stress, E is the elastic(Young's)-modulus and ϵ is the strain.

If the load is applied slowly, the ice responds in a viscous or plastic manner. If the load is removed the deformations will be permanent, opposite of elastic behaviour where the deformations returns to how it was before the load was applied. The time-dependent relation between the stress and the strain-rate for a viscous or a viscous-plastic material is given by:

$$\sigma = \mu \cdot \dot{\epsilon} \tag{2.12}$$

Where μ gives the viscosity.

For time-dependent elasticity where the energy is gradually recovered after the load is removed, the following relationship between stresses, strains and strain-rate is given as:

$$\sigma = E \cdot \epsilon + \mu \cdot \dot{\epsilon} \tag{2.13}$$

For short-term loading the visco-elastic and visco-plastic strains will have little time to develop, and can be assumed to be negligible. What is left is the elastic-plastic behaviour, and can be described as three different phases, namely elastic deformation up to first yield, plastic strain hardening until the peak stress is reached and softening after the peak stress. This behaviour can be seen in figure 2.9.

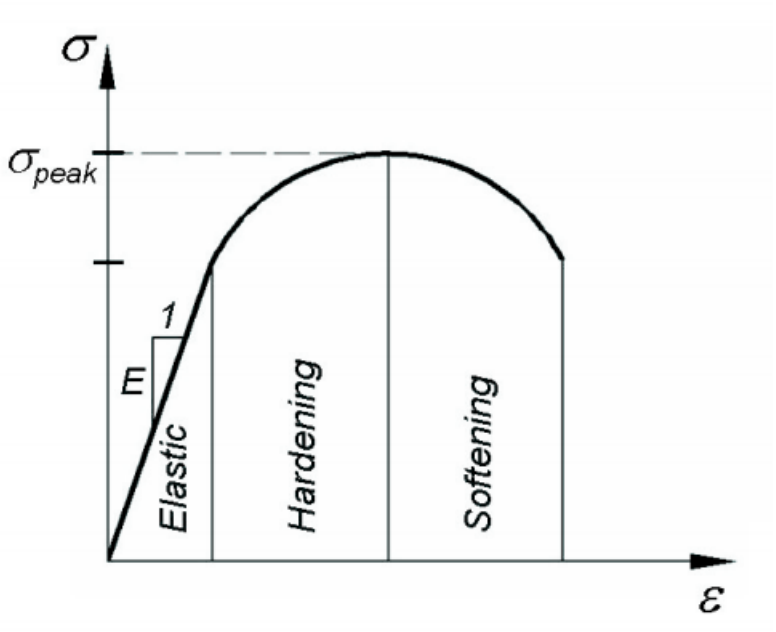

Figure 2.9: Stress-strain plot for an elastic-plastic material (Løset et al. 2006)

2.4.2 Failure Models of Ice

Two common failure models to describe the failure stress will be presented in this section. These models are Tresca and von-Mises models, and they only need one material property. The Tresca criterion assumes that the material is behaving elastically as long as the shear stress is below a certain stress limit R_s. This is formulated mathematically as:

$$\tau \leq R_s \tag{2.14}$$

Where τ is the shear stress limit and R_s is the shear resistance of the material. Figure 2.10 shows how the failure takes place on the plane where the maximum shear stress acts(which is at an angle of 45° to the principal stresses). The von Mises criterion assumes failure for a critical combination of normal stresses which is also shown in the same picture.

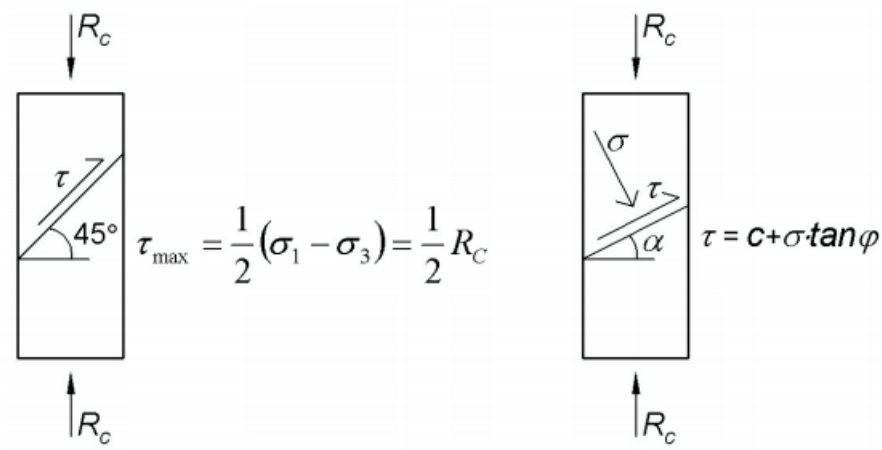

Figure 2.10: Failure criteria according to Tresca/von-Mises model and the Coulomb-Mohr failure criteria (Løset et al. 2006)

The Tresca and von-Mises models works well for metals that exist far from their melting temperature, but that is not the case for ice. Ice is weaker in tension so pressure dependent behaviour has to be accounted for. The Coulomb-Mohr model is the simples model where a critical combination of the shear and normal stresses on a plane gives failure. It is expressed as follows:

$$\tau \leq c + \sigma \cdot \tan\phi \tag{2.15}$$

Where τ and σ are the shear and normal stresses, c is the cohesion and ϕ is the angle of internal friction. Figure 2.11 shows the two criterias in the $\tau - \sigma$ plane, where it is observed that if the angle of internal friction ϕ is 45° the Tresca criterion can be used.

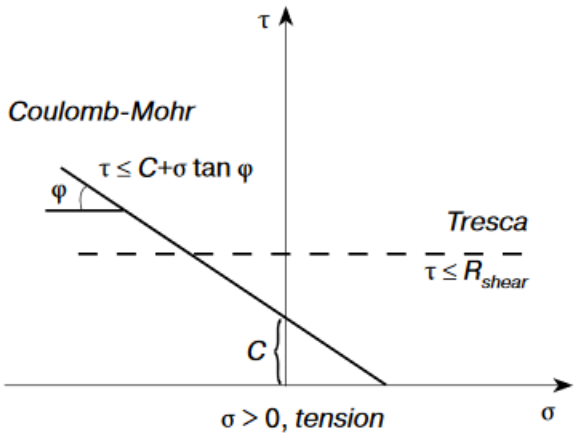

Figure 2.11: Comparison of Tresca and Coulomb-Mohr models(Løset et al. 2006)

Modelling the ice as a Coloumb-Mohr material is a big simplification, but alternative approaches that are more appropriate are difficult to find as this is an area that needs more research. The conditions for the simulations run in a laboratory with procured ice from fresh water are very different from real life conditions.

2.4.3 Material Properties of Ice

The mechanical behaviour of ice depends on several parameters. State variables and type of material is usually distinguished between, where state variables are parameters such as stress, strain, loading rate and temperature. For ice the most important parameters are the temperature and the strain rate. The type of material, or ice in this case, is usually defined by grain size and orientation and the size and shape of the pores.

The main parameters that govern the mechanical behaviour of ice are the temperature, the porosity, the grain size and the strain rate. Generally the ice becomes weaker and softer with increasing temperature, porosity and grain size. The temperature of the ice along with the salinity of ice affects the brine volume which in turn also affects the porosity. The effect of strain rate is shown in figure 2.12. It is seen that the strength increases with increasing strain rate until brittle failure occurs and the strength decreases. This is called brittle-to-ductile transition, where the ice transforms from almost purely ductile behaviour into brittle behaviour as the stress increases.

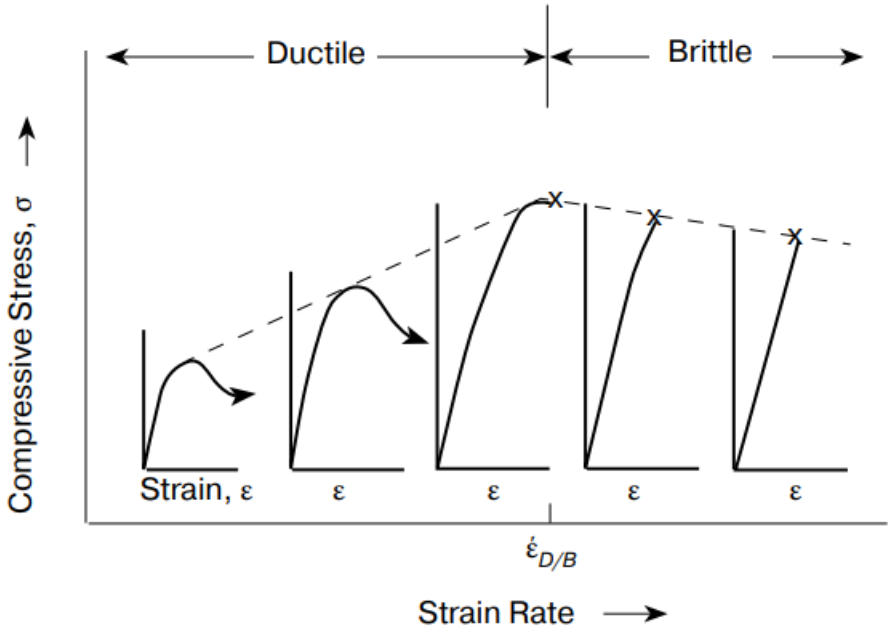

Figure 2.12: Ice strenght as a function of strain rate (Løset et al. 2006)

Elastic properties of ice can be difficult to measure, but Kämärainen(1993) gives approximate values given in table 2.1.

Table 2.1: Elastic properties of Ice

	Pure Ice	Sea Ice	Brackish Ice
E [GPa]	9	4-6	4-6
v [-]	0.3		

An equation for ice is given in ISO 19906 and is given as:

$$E = E_{fi}\left(1 - \sqrt{v_t}\right)^4 \tag{2.16}$$

Where E_{fi} is the elastic modulues of freshwater ice, and has a value that ranges between 9 GPa to 10 GPa, and v_t is the total brine void volume factor.

Compressive Strength

Sea ice failure due to compression can become a significant design criterion for interaction with thick ice. The compressive strength is dependant on brine volume, the content of air bubbles, the load direction, the grain size, strain rate, temperature and the ice type(ISO 19906). Columnar ice is an anisotropic material, and the mechanical behaviour of samples in uniaxial compression taken horizontally and vertically varies due to the grain structures and growth directions. Uniaxial tensile and compression experiments on ice is conducted as shown in figure 2.13.

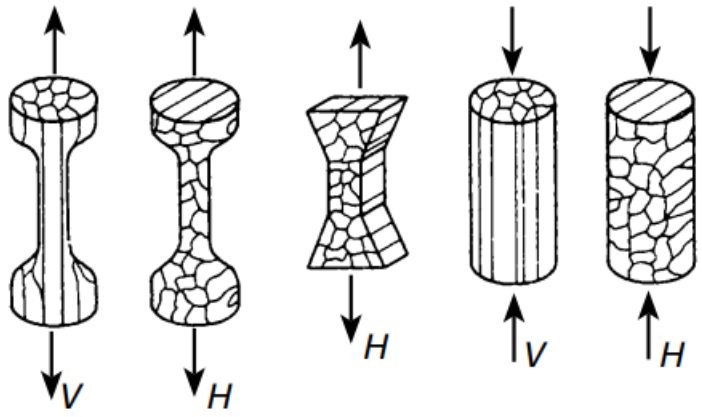

Figure 2.13: Uniaxial tensile and compression on ice with different orientation(Løset et al. 2006)

When the ice fails at the transition between ductile to brittle deformation the compressive strength has a maximum. For first-year ice the uniaxial strength, σ_c, of respectively horizontal, vertical and granular ice is given by Timco and Frederking(1990) as:

$$\sigma_{c,h} = 37\dot{\epsilon}^{0.22}\left(1-\sqrt{\frac{v_t}{0.27}}\right) \tag{2.17}$$

$$\sigma_{c,v} = 160\dot{\epsilon}^{0.22}\left(1-\sqrt{\frac{v_t}{0.20}}\right) \tag{2.18}$$

$$\sigma_{c,g} = 49\dot{\epsilon}^{0.22}\left(1-\sqrt{\frac{v_t}{0.28}}\right) \tag{2.19}$$

Where v_t gives the porosity or the void volume fraction of brine and air and $\dot{\epsilon}$ gives the strain rate per

second. The strength is found to be between 1.2 and 5 times higher for vertical loading than horizontal loading. For horizontal loading with a porosity range of about 0.001 to 0.15 the strength is found to be between 2-5 MPa, and for vertical loading 5-15 MPa, i.e. around 3 times higher for vertical loading. For multi-year ice the strength values range from 4-12 MPa depending on the strain rate. When the ice is very cold, the strength is similar as for first-year ice, but multi-year ice is considerably stronger when the ice is warmer(ISO 19906).

When loaded multi-axially in compression, ice can take substantially higher stresses before failure occurs than in the uniaxial case.

Flexural Strength

The tensile and flexural strengths should be equal during a flexural failure, but the experiments done for the calculations are usually different. Tensile strength is derived from experiments as the one shown inn figure 2.13, while the flexural strength is derived from beam bending tests as shown in figure 2.14. The flexural strength is defined as extreme fiber stress in tension, and decreases with increasing brine volume(which includes effects of ice temperature). An expression for the flexural strength is given by Timco and O'Brien(1994) and is based on a large number of small-scale tests, and the equation is given by:

$$\sigma_f = 1.76e^{-5.88\sqrt{v_b}} \tag{2.20}$$

Typical values for the flexural strength are between 0.3 MPa and 0.5 MPa for winter conditions and values around 0.2 MPa for warmer conditions(Vershinin et al., 2006).

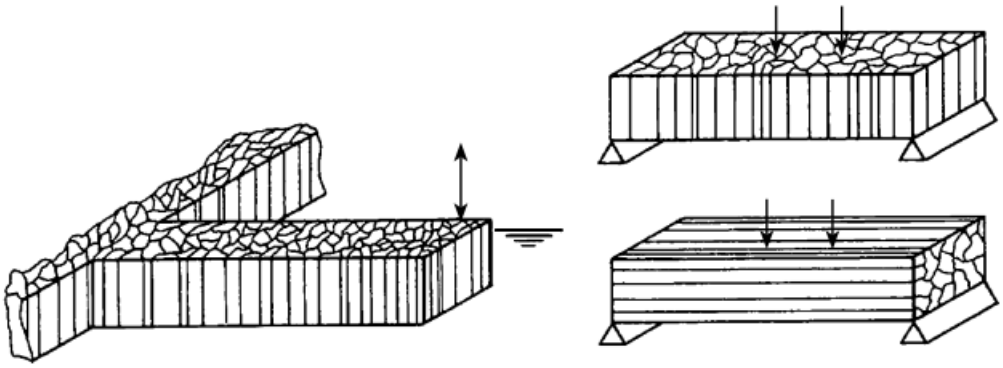

Figure 2.14: Flexural bending experiment setup (Løset et al. 2006)

Tensile Strength

The tensile strength of ice is an important property when structures interact with ice. As for compressive strength, the tensile strength differs with loading direction due to grain structures, brine volume and the growth directions. The tensile strength in the vertical direction of columnar-grained ice is around twice as high as for horizontal direction. Equations for horizontal and vertical tensile strength respectively is given in ISO 19906 as:

$$\sigma_{t,h} = 1.0\left(1 - \sqrt{\frac{v_b}{0.31}}\right) \tag{2.21}$$

$$\sigma_{t,v} = 2.2\left(1 - \sqrt{\frac{v_b}{0.14}}\right) \tag{2.22}$$

Where v_b is the brine volume fraction. Typical values tensile strength in horizontal direction for first-year ice range from 0.2 MPa to 0.8 MPa, and in vertical direction the tensile strength goes up to 2 MPa. Multi-year ice ranges from 0.5 MPa to 1.5 MPa in both horizontal and vertical direction Timco and Weeks (2010).

Shear Strength

Ice tends to fail in tension rather than shear. However, ice is rarely in a state of pure shear when acting on a structure. Shear strength ranges from 0.2 MPa to 2.5 MPa which is a wide range due to difficulty excluding

other stress states from the shear strength values. Some data indicate that shear strength varies from 0.4 MPa to 1.3 MPa(ISO 19906). Based on small-scale tests by Frederking and Timco(1984) the shear strength can be expressed by:

$$\tau = 1.5\left(1 - \sqrt{\frac{v_t}{3.9}}\right) \tag{2.23}$$

Where v_t is the total void volume fraction including brine and air, and τ is the shear strength.

Fracture Toughness

Fracture toughness is another material property, and it describes the stress required to make a crack of a known size propagate(Timco and Weeks, 2010). It is dependant on the size of the ice that is being fractured, the length of the crack, the temperature, the composition of the ice and the action rate(ISO 19906). For plain strain condition the expression for the fracture toughness is given as:

$$K_{Ic}^2 = \frac{GE}{1 - \nu^2} \tag{2.24}$$

Where K_{1c} gives the fracture toughness, G is the strain energy release rate, E is the elastic modulus(Young's modulus) and v is the Poison's ratio. Dempsey et al. (1999) have shown that for fracture tests on sea ice samples larger than 3 m(thick first-year ice) the fracture toughness is around 250 kPa $m^{1/2}$.

3 Ice Actions on Floating Structures

For deep water operations floating structures are usually utilized. The general principles of ice mechanics are still valid for floating structures, but ice forces are usually more complex than for a fixed platform. Figure 3.1 shows some of the most common concepts used for floating structures. Figure 3.1 a shows a SPAR floating vertically, b is a semi-submersible, c is a ship-shaped floater(FPSO e.g.), and d is a circular floating vessel with conical sides. For floating structures in ice infested waters, there will be interactions with floating sea ice. This will result in both global and local forces acting on the structures. Interaction between structure and global loads describes the total response of the structure with an ice feature, while interaction with local loads describes the response of a single structural part of the structure. This thesis will analyse a local part of a semi-submersible subjected to local ice actions. The material in this section is gathered from Palmer and Croasdale (2013) and Løset et al. (2006) unless stated otherwise.

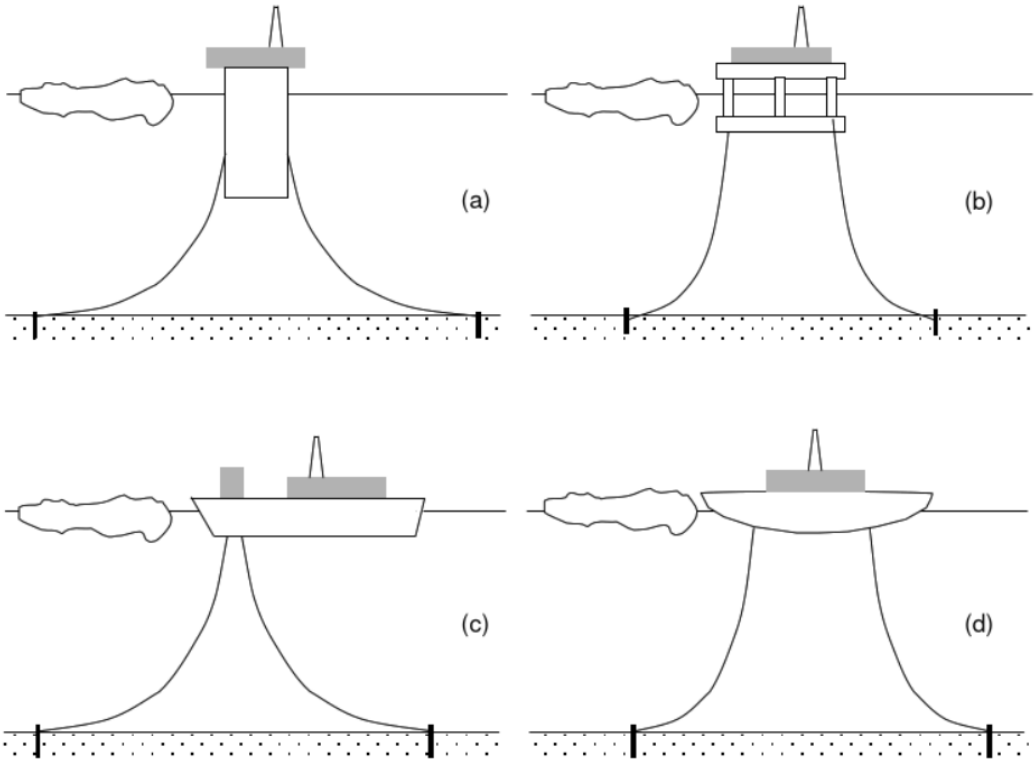

Figure 3.1: Several floating concepts(Palmer and Croasdale 2013)

3.1 Ice Actions on Vertical Structures

Ice moves with the wind and currents and will push against structures located in ice infested waters. These structure-ice interactions may move or damage the structure. Because of this ice actions will be of the utmost concern for engineering of structures in these locations. If the structure is held in place Palmer and Croasdale (2013) proposes three possible scenarios for a vertical structure which is illustrated in figure 3.2, along with the notation of limits for ice interaction. Mode (a) is called limit stress and occurs when the ice fails upon interaction with the structure. This makes the strength of the ice the determining factor of the force the ice applies to the structure. The driving force on the ice is the wind and current acting on the top and bottom of the ice cover respectively. Mode (b) is called limit stress and occurs when the driving force and not the strength of the local ice acting governs the force applied to the structure. This is illustrated with an ice ridge that acts on the structure by smaller ice floes upstream "pushing" on the ridge, i.e. the total force acting is limited by the force of the ice floes on the ridge instead of the strength of the ridge itself. Mode (c) is called limit momentum and occurs when a larger ice mass drifts towards the structure, hits it and subsequently slows down as the momentum of the mass is used up.

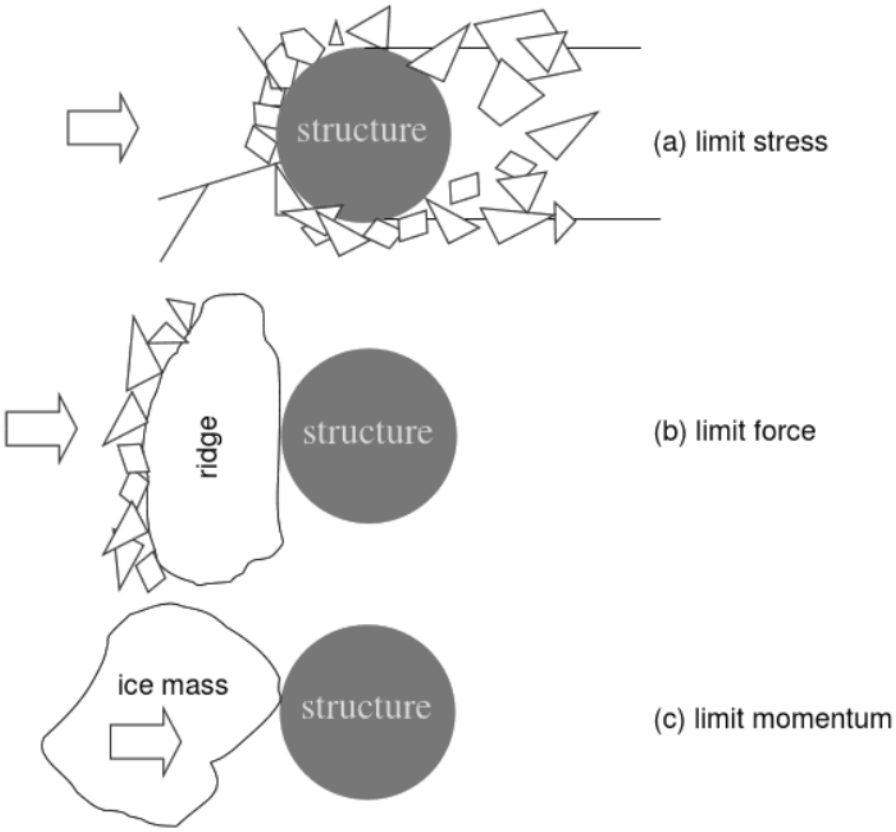

Figure 3.2: Ice load limits(Palmer and Croasdale 2013)

Ice can deform in several different ways, but most common is ice breaking. Some common failure modes gathered from Palmer and Croasdale (2013) and Løset et al. (2006) will be referenced in the following. The principle mechanisms observed in laboratory experiments are shown in figure 3.3.

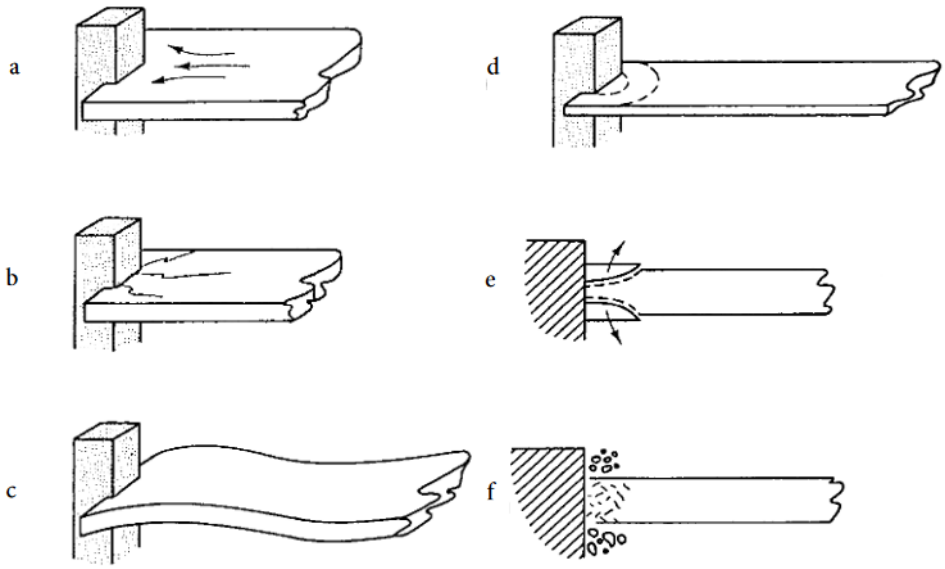

Figure 3.3: The main failure modes of ice(Sanderson, 1988)

Creep

When the ice moves very slowly against a structure it is said to deform in creep. This is illustrated in figure 3.3 a. Creep occurs when the ice has been moving at a higher velocity but has slowed down due to a diminishing driving force. This kind of deformation is not very common and is usually short-lived. The force acting on the structure is approximately proportional to the 1/3 power of the relative velocity between the ice and the structure.

Radial Cracking

Radial cracking occurs when the ice fails in tension. This failure mode is illustrated in figure 3.3 b. For structures with cylindrical cross-sections cracks form in front of the structure and at the sides. A certain stress level has to be reached for radial cracks to occur.

Buckling

For thin ice covers the ice buckles from the edge loads acting upon contact with the structure, see figure 3.3 c. Sanderson(1988) concludes that elastic buckling is most likely the governing mode when the ice is thinner than 0.4 m.

Circumferential cracking

Circumferential cracks as seen in figure 3.3 d, may form when the ice buckles elastically, or for out-of-plane bending caused by eccentric action conditions.

Spalling

Figure 3.3 e shows spalling failure, and occurs when out-of-plane cracks form and grow away from the contact area and the sheet gets divided into layers. The velocity of the ice sheet influences the length of the spalling, where higher velocities cause smaller spalling lengths.

Crushing

For thicker ice, the dominating ice action for vertical structures is crushing failure which is illustrated in figure 3.3 f. The maximum ice force is dependant on the ice strength, an indentation factor and the contact area it is acting upon. This dependency on the contact area is commonly called a size effect. For vertical structures two failure modes are possible. Brittle crushing occurs for high velocities, where the ice crushes continually in a brittle manner against the structure. This causes a non-uniform pressure over the contact area. For lower velocities, alternating creep and brittle failure is another possible failure mode. The interaction between the ice and the structure still cause brittle crushing, while at the same time the moving ice sheet will undergo creep deformation. This gives a saw tooth form of action.

3.2 Ice Actions on Multileg Structures

Three distinctive features are observed for ice actions of multilegged structures, namely a mutual influence of legs, sheltering and jamming effects, and non-simultaneous maximal actions on legs. The subsequent discussion is based on material from Løset et al. (2006).

Mutual Influence of Legs

For legs that are far apart there is not much influence on the loads acting, but as the distance decreases the stress fields around the legs mutually affect each other. This influence is shown in figure 3.4, where the maximum load shows to form a linear dependence on the leg spacing. The abscissa gives the non-dimensional distance between the legs(distance divided by diameter of the leg), while the ordinate gives the non-dimensional maximum load acting(maximum load divided by the load on one single leg). The ice moves perpendicular to the line connecting the legs. The left side of figure 3.4 shows the force in normal direction while the right side shows the force in transversal direction. It is observed that the force in normal direction decreases as the legs get closer together, while the opposite is true for transversal forces. The magnitude, however, does not change, only the direction of the total forces.

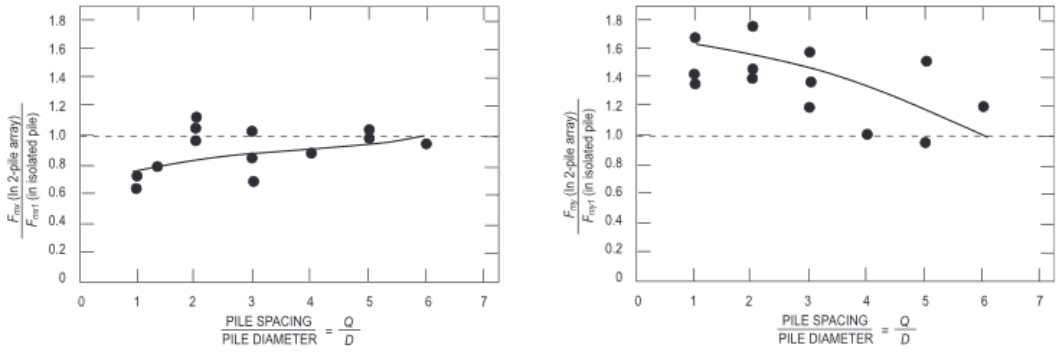

Figure 3.4: Maximum load on legs vs. leg spacing(Timco and Pratte, 1985)

Sheltering Effects

Legs that are placed in parallel in the direction of the ice motion may be sheltered and only interact with broken ice, i.e. the leg in front of them breaks the ice first. This leads to a reduction in forces on the sheltered legs. Figure 3.5 shows this effect. The abscissa gives the direction of the ice motion relative to the

line connecting the front legs. The ordinate gives the force on the whole structure divided with the force on one leg(the 4 in brackets indicates that this is for a structure with four legs). K is the dimensionless distance between the legs. It is seen that there is a sheltering effect as long as the spacing between the legs in parallel are not to big, i.e. less than 18, and the angles are not in the range of 15-30°. For a K of 2 the total maximum force is only in the range of 2.5 to 2.6 of the force on the front leg.

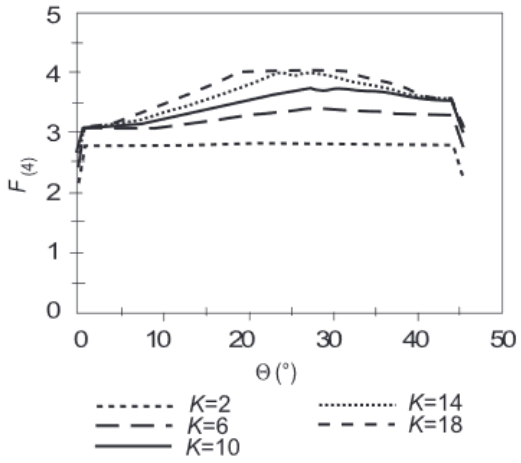

Figure 3.5: Total force on structure vs. angle of ice motion(Takeuchi et al., 1993)

Non-Simultaneous Maximal Actions on Legs

Studies have shown that the maximum load is rarely reached simultaneously on all platform legs at the same time. The dynamics are not necessarily synchronized between several legs. This means that the maximum loads on each leg and the total load have a different probability of occurrence. This is, however, based on a restricted set of studies .

Total Action

From the discussion above an equation for the total force acting on a multi-legged structure can be expressed as:

$$F_{tot} = F_1 F_i K_{ns} K_j \tag{3.1}$$

Where F_1 is the force acting on a single leg, F_i is the sheltering factor, K_{ns} is the factor of a non-simultaneous

failure and K_j is a jamming factor(if the legs are close together ice may jam between them).

3.3 Ice Actions on Floating Structures in Managed Ice

Floating structures are usually not designed for interaction with the worst-case ice conditions, since the mooring lines have limited load capacity. It is therefore important to utilize some kind of ice management to avoid collapse of the mooring lines and the structure. Ice management includes detection and monitoring of the ice, breaking of ice features, towing of ice bergs and disconnection of the structure to avoid the ice altogether. The material in this section is gathered from Palmer and Croasdale (2013).

Floating structures in ice infested waters are very unlikely to be deployed without some type of ice management, actions on structures in unmanaged ice will therefore not be considered here. Methods for determining the ice actions on structures in managed ice are derived using bounding approaches based on simplified scenarios. The model for the ice load is derived under the assumption that the managed ice consists of broken ice features surrounded by ice rubble with ambient level ice. The force from the ice loads in this case is mostly due to the clearing of broken ice. The model used is seen in figure 3.6. The moving ice causes pressure on the wedge composed of broken ice, causing loads on the platform.

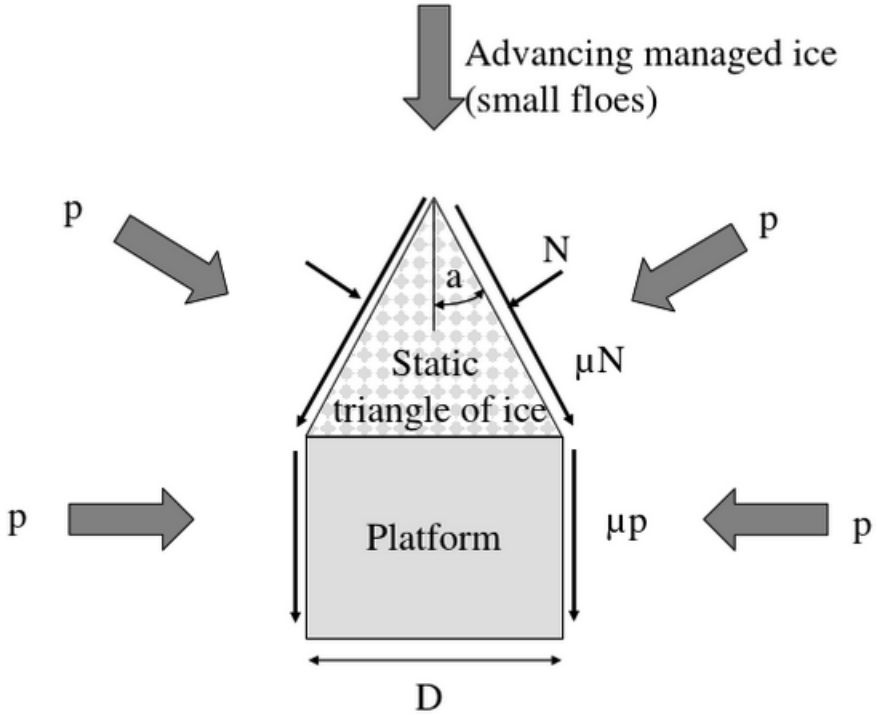

Figure 3.6: Model for calculating ice load in managed ice(Palmer and Croasdale, 2013)

The ice load acting on the ice wedge is given as:

$$F_w = pDh\left(1 + \frac{\mu}{tan(a)}\right) + 2pDh\mu + 2Lh\left(p\mu + c\right) \tag{3.2}$$

Where the parameters are as given in figure 3.6, h is the ice thickness, μ is a coefficient of friction and c is the cohesion. The second part of the equation is due to friction on the side of the platform and the third term is due to cohesion along the sliding surfaces.

Some influencing factors should be considered before applying this method, namely ice concentration, ice strength and thickness, pressured ice and floe size. The ice concentration has a big influence on the ice loads, the actions on the mooring lines may rise fast for increasing concentration. The ice strength is not of high importance for the platform itself, but rather for the ice breakers breaking the ice. Ice thickness rubble thickness is of importance since it is used in the equation derived above. The mooring lines are very sensitive to pressured ice since this is the most important term in equation 3.2. Floe size should be sufficiently small for high ice concentration, while it is less important for low concentrations as the ice can divert the platform.

3.4 Load Patch Area

Information in this chapter is gathered from Riska(2011) and Riska(2018).

In this thesis an analysis of a local part of the structure is performed. This is done by applying a local pressure on the model. In interaction with ice it is assumed that the load acts on a load patch when the local part interacts with an ice edge. The load patch is idealized, and the height of the load patch is narrow while the width is long, as seen in figure 3.7. The load patch is varied according to what structural part is being analysed, e.g. plating, stiffener or stringer. The total area of the load patch is described by the length and height as:

$$A = L \cdot h_c \tag{3.3}$$

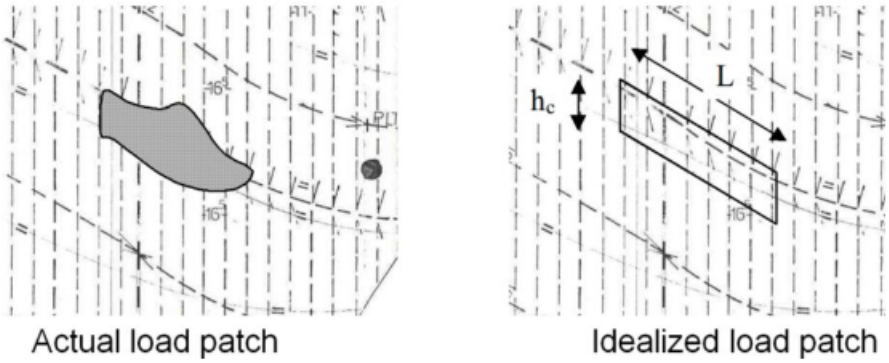

Figure 3.7: Actual and idealized load patch for design(Riska, 2011)

The concept of load height has developed over the years, and Riska(2011) discusses this based on figure 3.8. To the left, which was the original concept, the load height is defined as the full thickness of the ice. This caused an underestimation of the loads acting. Thus the load height was decreased to the height seen in the middle of figure 3.8, while the line load was kept constant. This caused higher pressures on the load patch. New studies suggest that the load acts along a narrow line, as seen to the right in the figure, which suggests decreasing the load height further and thus a further increase in the pressure. This is discussed in the next subsection. In general the load height should be chosen such that it gives the largest response on the structure.

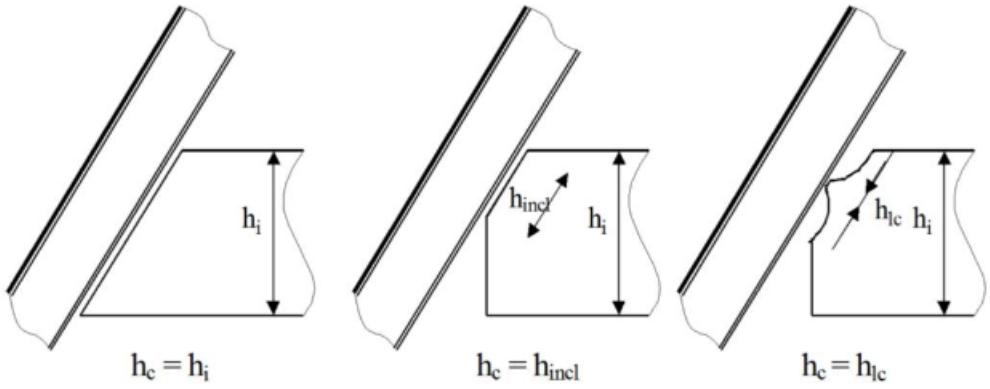

Figure 3.8: Change of load height over the years(Riska, 2011)

3.5 Local Ice Pressure Model

A common formulation used in e.g. ISO 19906 for ice pressure(see section 5.1.2) is based on observation that the average ice pressure is dependant on the magnitude of the area(Riska, 2018). This is the size

effect which was mentioned in section 3.1. The pressure-area relationship has been observed from small areas to very large areas. The drawback of this method is that it is empirical and has little basis in physics. One possible explanation is based on the observation of a line-like feature on the ice where the pressure is transmitted, which can be observed in figure 3.9. The line in the ice is produced by flaking under high pressure, where the line is directed towards the corners of the contact area.

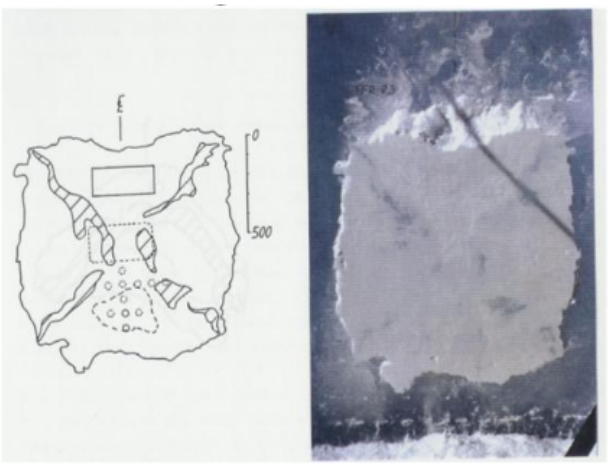

Figure 3.9: Line-like feature in the ice(Muhonen 1991)

When the average pressure over an area is calculated, the normal force can be found as:

$$F_n = A \cdot p_c \tag{3.4}$$

Where A is as defined in equation 3.3 and p_c is the pressure acting on the area.

4 The Semi-Submersible Unit

With the focus turning to Arctic regions for future offshore operations, ice strengthened semi-submersible units will be increasingly relevant. Semi-submersibles are able to operate at large water depths, they offer large deck space, great stability and sea keeping properties, can withstand rough waters, they are flexible and efficient and offer mobility, i.e. they can be moved if their services are required elsewhere. All of which are important capabilities to have operating under the environmental conditions prevalent in the Arctic regions.

In this thesis a semi-submersible exposed to ice loads will be analysed. The model is based on drawings of a column stringer of the aft port side column of Odfjell Drilling's semi-submersible drilling rig Deepsea Stavanger. Deepsea Stavanger is a harh environment deepwater unit, and is built by Daewo Shipbuilding and Marine Engineering Co in South Korea. It has been in operation since 2010 on the west coast of Africa and in British waters, but is now operating in the North Sea. In this thesis it is further strengthened for the ice actions that it would be exposed to under operational conditions in the Arctic. Figure 4.1 shows Deepsea Stavanger under operation.

Figure 4.1: Deepsea Stavanger(Petroleumtilsynet)

The main dimensions of the Deepsea Stavanger model including the main dimensions of the semi-submersible is given in table 4.1, modified from Skjetne(2015). The stringer model has a length and width of 19.5m and 15.1m respectively and a height of 5.5m. The operational draught of the unit is 25m, and the stringer analysed in this thesis is located 22.5m above the bottom of the pontoons. Figure 4.2 shows the stringer plate modelled in this thesis. Some details connected to the mooring system(shown in the top of the drawing in figure 4.2) is ignored in this thesis for simplicity, and would probably need to be re-designed for ice interactions. The displacement at operational draught is 52000 tons, and must be taken into account when calculating the forces acting on the column.

Table 4.1: Main Dimensions of the Deepsea Stavanger Model

Parameter	Value	Unit
Length	19.5	m
Width	15.1	m
Height	5.5	m
Corner Radius	3.2	m
Operational Draught	25	m
Displacement	52000	tons
Length deck	78	m
Breadth deck	38	m

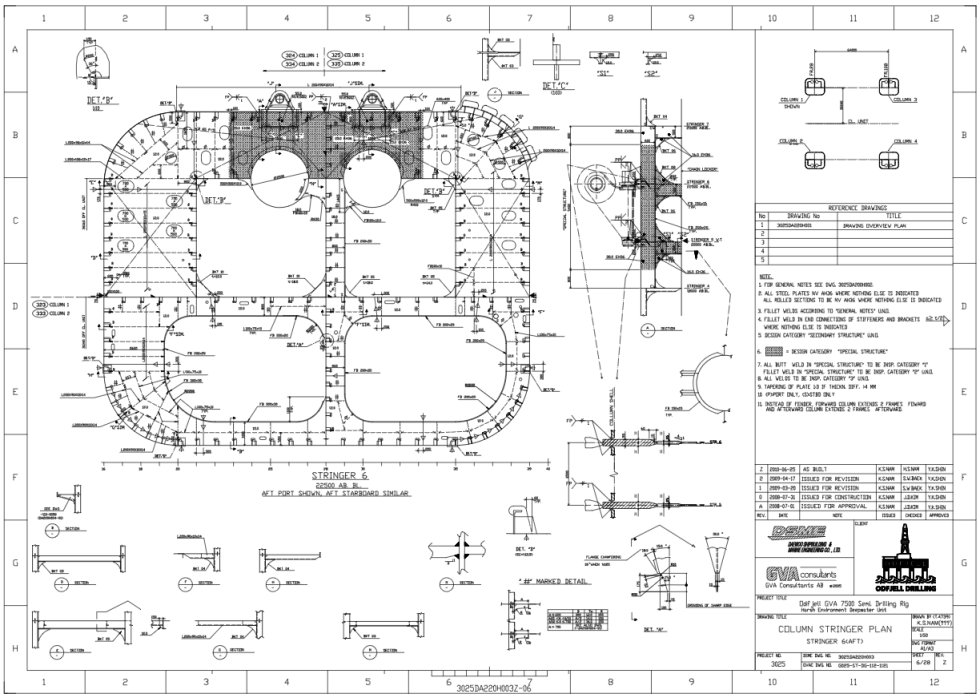

Figure 4.2: Drawing of the Stringer modelled(Skjetne, 2015)

5 Determining Ice Actions on Floating Structures

This chapter will give a review of different ice classes and their corresponding loads for vessels operating in the arctic. *ISO 19906*, IACS' *Requirements Concerning POLAR CLASS* and DVN GL's *Ships for Navigation in Ice* are presented along with methods for calculating ice pressures for floating offshore structures. This chapter is modified from the project thesis done on a similar subject, found in reference Nilsen(2018).

5.1 ISO 19906

ISO stands for the International Organization for Standardization, and is an independent, non-governmental inernational organization with a membership of 162 national standard bodies. It is the world's largest developer of voluntary international standards. Publication of an international standard requires the approval of 75% of the members attending. The aim of ISO is that products and services are safe, reliable and of high quality.

ISO 19906 is the International Standard for Arctic offshore structures, and is one of a series of International Standards for offshore structures. It specifies requirements and provides recommendations and guidance for the design, construction, transportation, installation and removal of offshore structures which are related to activities of petroleum and gas industries in the arctic and in cold regions. The objective is to ensure that offshore structures provide an appropriate level of reliability with respect to personal safety, environmental protection and asset value to the owner, to the industry and to society. In this thesis the focus will be on local ice actions and local strength requirements. All material in this section is found in (ISO 19906).

5.1.1 Local Ice Actions

Local ice pressure calculations are used in the design of plates and stiffeners on a structure. Global actions are calculated from average pressures over a nominal area, while local actions are calculated from smaller areas which are subjected to higher local pressures. The load patch areas are illustrated in figure 5.1, where it is shown how the local pressures should be used in the design of plating or stiffeners.

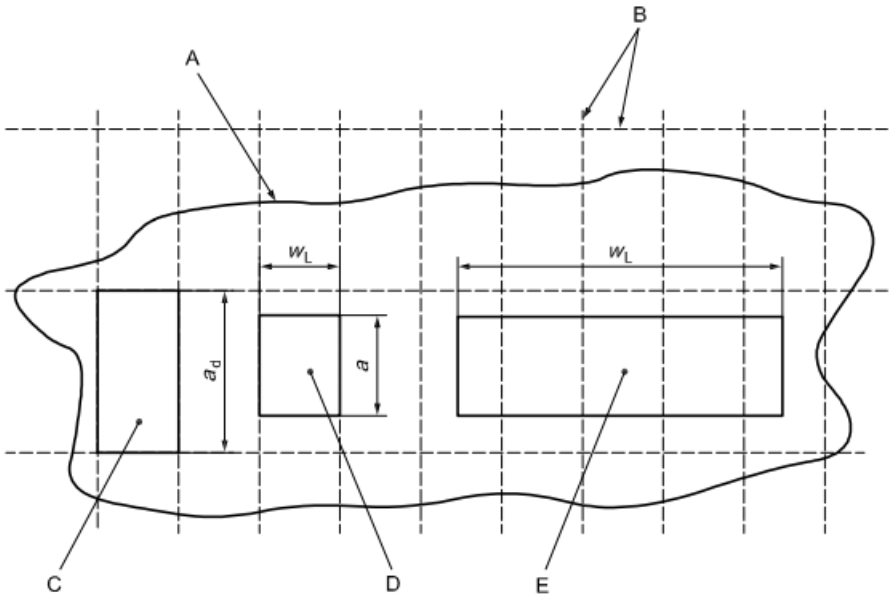

Key

A	global interaction area (grows as interaction proceeds)	a	loaded height
B	frames and stiffeners	a_d	frame spacing
C	local area for plate design	w_L	loaded width
D	loaded area for plate design		
E	loaded area for stiffener design		

Figure 5.1: Definition of loaded areas for local ice actions (ISO 19906)

Local ice pressures can be considered constant over an area given by:

$$A = a \cdot w_l \tag{5.1}$$

Where A is the area of the load patch as illustrated in figure 5.1, a is the height of the loaded area, and w_l is the width. Maximum action effects occur when the height of the load patch a is equal to the height of the local design area.

5.1.2 Local Ice Action from Thin First-year Ice

The formulas used in this subsection refers to determining local pressure from level ice, rafted ice and consolidated layers of first-year ice ridges. They are valid for ice thicknesses up to 1 m, and are based on data from the Gulf of Bothnia. Its derivation is based on an upper bound value for the full thickness pressure, and is given as:

$$p_f = 2.35h^{-0.50} \qquad for h > 0.35m \tag{5.2}$$

$$p_f = 4.0 \qquad for h \leq 0.35m \tag{5.3}$$

Where p_f is the full ice thickness pressure and h is the ice thickness. The local pressure acting on the loaded area is given by:

$$p_L = \gamma_l \cdot p_f \tag{5.4}$$

Where p_l is the local pressure and γ_l is a coefficient that reflects a simplified vertical distribution of the full thickness pressure on the loaded area, and is set equal to 2.5.

5.1.3 Local Pressures for Thick, Massive Ice Features

For thick, massive ice features in excess of 1.5 m, local pressures can be determined using data that has been derived from indentation tests in the Beaufort Sea and from measurements on ice pressure panels on the Molikpaq structure. These data are shown in figure 5.2.

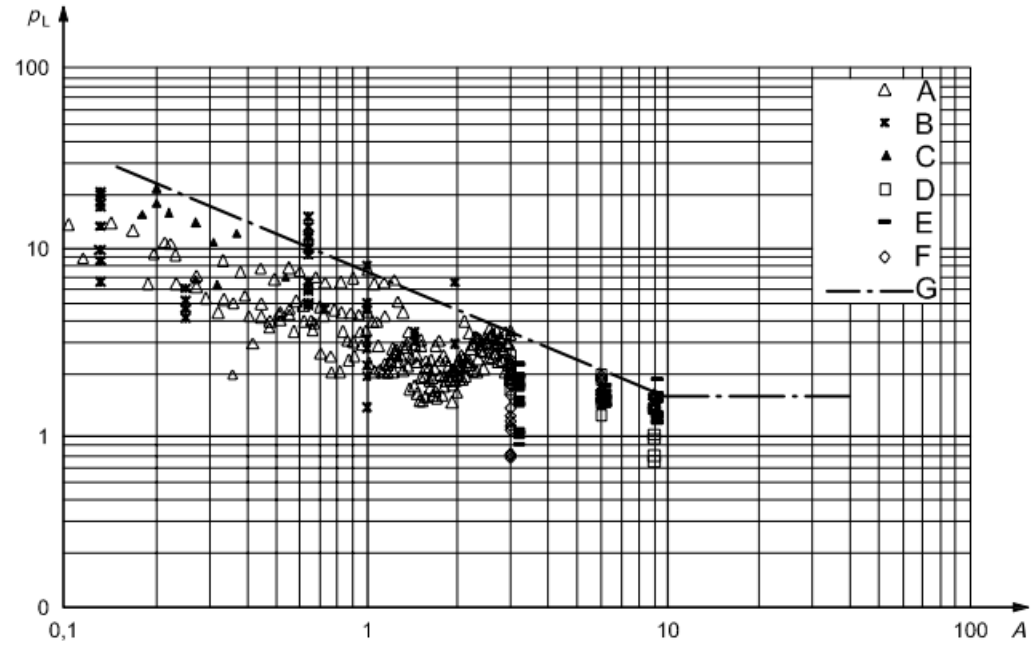

Key

A 3 m² Pond Inlet test data
B flat jack test data
C 1989 Hobson's Choice test data
D Molikpaq BW data
E Molikpaq N face data
F Molikpaq E face data
G $p_L = 7{,}40A^{-0{,}70}$ (mean plus three times the standard deviation), $A \cup 10$ m²; $p_L = 1{,}48$, $A > 10$ m²
p_L local ice pressure, expressed in megapascals
A contact area, expressed in square metres

Figure 5.2: Pressure as function of loaded area (ISO 19906)

The fitted function from these data gives the following ice pressure for thick, massive ice features:

$$p_L = 7.40A^{-0.70} \qquad for A \leq 10m^2 \tag{5.5}$$

$$p_L = 1.48 \qquad for A > 10m^2 \tag{5.6}$$

5.2 IACS

IACS stands for the International Association of Classification Societies, and is a technically based non-governmental organization. It currently consists of twelve member marine societies. IACS was founded in 1968 in Hamburg. Today IACS contributes to maritime safety and regulation through technical sup-

port, compliance verification and research and development.

Requirements concerning POLAR CLASS is the IACS unified requirements for polar ships constructed of steel and intended for navigation in ice-infested polar waters. It contains requirements to both the structural strength of hulls and machinery. The requirements for local dimensioning covered in the code will be further discussed in chapter 4.

5.2.1 Polar Classes

IACS divides ships after their operational requirements into seven classes. These classes can be seen in table 5.1. In this thesis the operation area, period of operation and ice management system is not specifically defined, therefore Polar Class 4 is chosen as a flexible class.

Table 5.1: Polar Class Descriptions

Polar Class	Ice Description
PC 1	Year-round operation in all Polar waters
PC 2	Year-round operation in moderate multi-year ice conditions
PC 3	Year-round operation in second-year ice which may include multi-year ice inclusions
PC 4	Year-round operation in thick first-year ice which may include old ice inclusions
PC 5	Year-round operation in medium first-year ice which may include old ice inclusions
PC 6	Summer/autumn operation in medium first-year ice which may include old ice inclusions
PC 7	Summer/autumn operation in thin first-year ice which may include old ice inclusions

5.2.2 Design Ice Loads

The design scenario for determining the ice pressure for ships of all polar classes is a glancing impact on the bow. This may overestimate the loads calculated, since a bow impact on a ship with forward speed likely is higher than that of an impact for a floating offshore unit. The design ice load will be characterized by an average pressure which is uniformly distributed over a rectangular load patch area.

The influence of hull angles is calculated through a bow shape coefficient, which is given as the minimum of the following three functions:

$$fa_{i,1} = \left(0.097 - 0.68 \cdot \left(\frac{x}{L} - 0.15\right)^2\right) \cdot \frac{\alpha_i}{(\beta_i')^{0.5}} \quad [-] \tag{5.7}$$

$$fa_{i,2} = \frac{1.2 \cdot CF_F}{(sin(\beta_i^{'}) \cdot CF_C \cdot D^{0.64})} \quad [-] \tag{5.8}$$

$$fa_{i,3} = 0.60 \quad [-] \tag{5.9}$$

Where i denotes the sub-region considered, L is the ship length measured on the upper ice waterline, x is the distance from the forward perpendicular, α is the waterline angle, $\beta^{'}$ is the normal frame angle and D is the ship displacement. CF_C and CF_D are failure class factors. The force is found as:

$$F_i = fa_i \cdot CF_C \cdot D^{0.64} \quad [MN] \tag{5.10}$$

Where F_i denotes the force and the rest is as described before. The load patch aspect ratio is given as:

$$AR_i = 7.46 \cdot sin(\beta_i^{'}) \geq 1.3 \quad [-] \tag{5.11}$$

The angles α and $\beta^{'}$ are defined in figure 5.3.

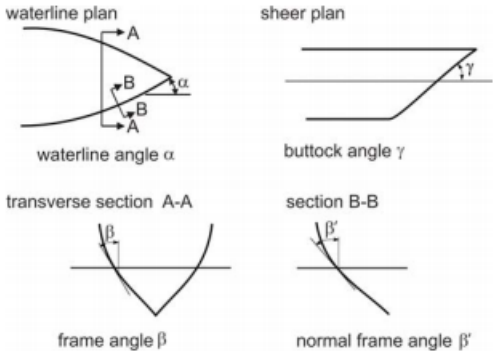

Figure 5.3: Definition of hull angles provided by IACS

The line load is given by:

$$Q_i = \frac{F_i^{0.61} \cdot CF_D}{AR_i^{0.35}} \quad [MN/m] \tag{5.12}$$

The pressure is then found by:

$$P_i = F_i^{0.22} \cdot CF_i^2 \cdot AR_i^{0.3} \quad [MPa] \tag{5.13}$$

For the bow area the design load patch has width and height defined as:

$$w_{bow} = \frac{F_{bow}}{Q_{bow}} \quad [m] \tag{5.14}$$

$$b_{bow} = \frac{Q_{bow}}{P_{bow}} \quad [m] \tag{5.15}$$

Finally the average pressure within a design load patch is given as:

$$P_{avg} = \frac{F}{b \cdot w} \quad [MPa] \tag{5.16}$$

The ice loads inside this load patch can be quite peaked, i.e. there are areas of higher, more concentrated pressures within the load patch. This is accounted for by using peak pressure factors. The magnitude of these peak pressure factors depends on the member under consideration. Figure 5.4 shows how the pressure is magnified over an area with a length of the stiffener spacing.

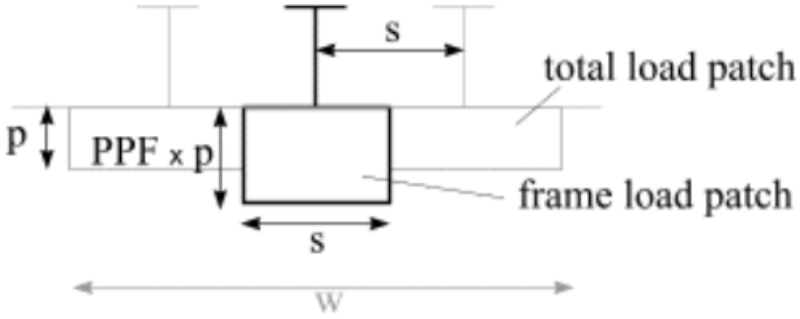

Figure 5.4: Illustration of the use of peak pressure factor(Daley, 2000)

For a transversely-framed structure the peak pressure factor is given by:

$$PPF = (1.8 - s) \geq 1.2 \tag{5.17}$$

5.3 DNV GL - Ships for Navigation in Ice

DNV GL, or Det Norske Veritas Germanischer Lloyd is an international accredited registrar and classification society. It provides services for several industries including maritime, renewable energy, oil and gas, electrification, food and beverage, and healthcare. DNV GL is the largest classification society in the world.

DNV GL - Ships for navigation in ice applies to vessels occasionally or primarily intended for navigation in waters with ice conditions. Requirements for local dimensioning will be covered in chapter 4.

5.3.1 Class Notations

DNV GL provides several classes depending on their intended use and the degree of exposure to ice and area of operation. For vessels that are intended for service in waters with light ice conditions the class notations ICE-C and ICE-E is given, and are intended for light localised drift ice in mouths of rivers and coastal areas. These are the lowest ice classes provided by DNV GL. Vessels that are intended for service in the northern Baltic in winter or areas with similar ice conditions are given class notations ICE-1A*, ICE-1A, ICE-1B or ICE-1C. Icebreakers, passenger and cargo vessels intended to operate unassisted in ice-infested waters of sub-Arctic, Arctic or Antarctic regions may be given class notations Icebreaker ICE-05(or -10 or -15) or Icebreaker POLAR-10(or -20 or -30). The Sealer class concerns vessels built for catching in cold regions. The WINTERIZATION class is given to vessels designed for service in cold climate environment. The DAT(-X°) class is for materials in ships who operate for longer periods in areas with low air temperatures. For this thesis POLAR-30 class is used to ensure conservatism. The table of ice conditions as given by DNV GL is given in table 5.2.

Table 5.2: Ice Conditions

Class notation	Nominal ice strength [MPa]	Nominal ice thickness [mm]	Ramming condition
ICE-05	4.2	0.5	No ramming anticipated
ICE-10	5.6	1.0	No ramming anticipated
ICE-15	7.0	1.5	No ramming anticipated
POLAR-10	7.0	1.0	Occasional ramming
POLAR-20	8.5	2.0	Occasional ramming
POLAR-30	10.0	3.0	Occasional ramming

5.3.2 Design Ice Loads

DNV GL states that all vessels shall withstand local ice pressure as defined for the different class notations. Further it shall be applied over a contact area reflecting the type of load in question. The basic ice pressure is given as:

$$p_0 = 1000 \cdot F_A \cdot \sigma_{ice} \quad [kPa] \tag{5.18}$$

Where F_A is a correction factor for the reinforced area. It is taken as 1.0 for the bow and stem area. The design pressure can then be taken as:

$$p = F_B \cdot p_0 \quad [kPa] \tag{5.19}$$

Where F_B is a correction factor for the size of the load patch area. The formula is given as:

$$F_B = \frac{0.58}{(A_C)^{0.5}} \qquad A_C \leq 1.0m^2 \tag{5.20}$$

$$F_B = \frac{0.58}{(A_C)^{0.15}} \qquad A_C > 1.0m^2 \tag{5.21}$$

Where A_C is the load patch area.

6 Local Strength Requirements

Vessels operating in arctic regions must be able to resist the large ice actions that they are subjected to in addition to the loads they are subjected to in warmer regions. For the engineer it is important to design and dimension the construction so that it is strong enough to withstand these loads but also not over dimension the structure since that can lead to a heavy and expensive structure. Safety is however always most important, therefore it is necessary to be conservative in the dimensioning process. In this chapter a review of the local ice strengthening practices of IACS and DNV GL will be looked into as well as the most important failure modes of local parts of structures operating in ice. This chapter is modified from the project thesis done on a similar subject, found in reference Nilsen(2018).

6.1 Failure Modes

This chapter will present a short summary of common failure modes with respect to local strength. Capacity checks of this form is important to ensure that the structure is well dimensioned to withstand the actions that it is subjected to.

6.1.1 Yielding of materials

Yielding is one of the most important failure modes to dimension any local part against. The yield point is the point on the stress-strain curve that gives the point of transition from elastic behaviour to plastic behaviour, i.e. where the material starts to exhibit permanent deformations. Generally no yielding is allowed anywhere in the material, unless special considerations needs to be made e.g. where large stress concentrations appear. The yield point can be seen in figure 2.9 as the point where the material goes from the elastic zone to the hardening zone. Dimensioning against yielding is generally done by making sure that the stress peaks are kept low, which is done by dimensioning plate and stiffeners solid enough to withstand the loads acting on them.

One of the most common design criterions used against yielding is the von Mises yield criterion, which is also the criterion that will be used in this thesis. The von Mises yield criterion can be expressed mathematically as:

$$\sigma_y < \sigma_v = \sqrt{\frac{(\sigma_1 - \sigma_2)^2 + (\sigma_2 - \sigma_3)^2 + (\sigma_3 - \sigma_1)^2}{2}} \tag{6.1}$$

Where σ_1, σ_2 and σ_3 represents the principal stresses acting.

6.1.2 Buckling

Buckling is a mathematically instability that leads to failure. The plate field examined in this thesis will be subjected to pressures which causes membrane stresses in the plate field. If these membrane stresses are compressive in nature, they can cause buckling of the part or any of its components if the forces are large enough. A buckling check is therefore important to do on the most exposed parts, and should include global buckling(column buckling), plate buckling between stiffeners, stiffener buckling with associated plate flange, as well as local buckling of the web and/or flange. These buckling checks will be done according to the standards presented, but will not be pursued in depth.

6.1.3 Fatigue

Fatigue is the weakening of a material onset by cyclic and repeatedly applied loads. If the loads are above a certain threshold, microscopic cracks will begin to form where stress concentrations appear. If the crack reaches a certain critical size, the crack will suddenly propagate and the structure will finally fracture. Fatigue checks will however not be pursued in this thesis.

6.2 Local Strength Requirements for Plate Field according to IACS

Several standards for local strength requirements of ship hulls in ice exist for various classification societies, but none such standard exist yet for floating offshore units. In this thesis standards used for ship hulls will therefore be used, and as long as conservatism is applied the results should be applicable. Shell plate thickness will first be examined, before stiffener requirements will be looked into.

6.2.1 Shell Plate Requirements

The required minimum plate thickness according to IACS is given as:

$$t = t_{net} + t_s \qquad [mm] \tag{6.2}$$

Where t_{net} is the plate thickness required to resist ice loads according to equation 27 of section 3.2.2. t_s is an added thickness to account for corrosion and abrasion due to ice interaction. For longitudinally-framed plating the net thickness is given as:

$$t_{net} = 500 \cdot s \cdot \frac{\sqrt{\frac{AF \cdot PPF_p \cdot P_{avg}}{\sigma_y}}}{1 + \frac{s}{2 \cdot l}} \qquad [mm] \tag{6.3}$$

Where s is the stiffener spacing, AF is a hull area factor, PPF_p is a peak pressure factor, P_{avg} is the average patch pressure as found by equation 27, σ_y is the yield stress of the material and l is the length of the stiffener.

6.2.2 Stiffener Requirements

The dimensioning process of the stiffeners according to IACS is divided into four parts, namely: calculation of the actual net effective capacity, calculation of capacity needed to withstand the load conditions, comparison of the two to ensure the actual capacity is greater than the capacity needed to withstand the load, and finally a structural stability check to prevent local buckling. The dimensioning proess is therefore a trial and error process, where several iterations may be needed to ensure all conditions are met. The stiffener geometry and parameters used is illustrated in figure 6.1.

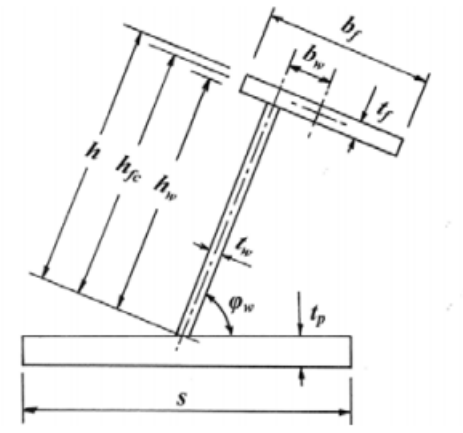

Figure 6.1: Stiffener geometry provided by IACS

The actual net effective shear area of the stiffener is found by:

$$A_w = \frac{h \cdot t_{wn} \cdot sin(\phi_w)}{100} \qquad [cm^2] \tag{6.4}$$

Where h is the height of the stiffener, t_{wn} is the net web thickness which implies the total thickness of the web minus the corrosion addition and ϕ_w is the angle between the stiffener and the plate, which is 90° in this case. The stiffener dimensions are based on plastic methods, and therefore plastic section moduli will be calculated. The actual net effective plastic section modulus is calculated as:

$$Z_p = \frac{A_{pn} \cdot t_{pn}}{20} + \frac{h_w^2 \cdot t_{wn} \cdot sin(\phi_w)}{2000} + A_{fn} \cdot \frac{h_{fc} \cdot sin(\phi_w) - b_w \cdot cos(\phi_w)}{10} \qquad [cm^3] \tag{6.5}$$

Where A_{pn} is the net cross-sectional area of the stiffener, t_{pn} is the net shell plate thickness, h_w is the height of the web, A_{fn} is the net cross-sectional area of the plate flange, h_{fc} is the height of the stiffener measure to the centre of the flange area and b_w is the distance from the middle of the web to the centre of the flange area. The stiffener is to be dimensioned such that the combined effects of shear and bending does not exceed the plastic strength of the member. The shear area due to the load effects is given as:

$$A_t = \frac{100^2 \cdot 0.5 \cdot LL \cdot s \cdot (AF \cdot PPF_t \cdot P_{avg})}{0.577 \cdot \sigma_y} \qquad [cm^2] \tag{6.6}$$

Where LL is the length of the loaded portion of the span and the rest is as before. The shear section modulus due to the load effects is given as:

$$Z_{pt} = \frac{100^3 \cdot LL \cdot Y \cdot s \cdot (AF \cdot PPF_t \cdot P_{avg}) \cdot a \cdot A_1}{4 \cdot \sigma_y} \qquad [cm^3] \tag{6.7}$$

Where a is the frame span, and Y and A_1 are coefficients given in section l2.6.3 in the IACS Polar Code. The other parameters are as given before. The shear area and the shear section modulus are to comply with the following conditions: $A_w \geq A_t$ and $Z_p \geq Z_{pt}$ in order to withstand the loads acting on the platefield. To prevent local buckling in the web and in the flange the following three conditions must be satisfied:

$$\frac{h_w}{t_{wn}} \leq \frac{805}{\sqrt{\sigma_y}} \tag{6.8}$$

$$b_f \geq 5 \cdot t_{wn} \tag{6.9}$$

$$t_{wn} = 0.35 \cdot t_{pn} \cdot \sqrt{\frac{\sigma_y}{235}} \tag{6.10}$$

6.3 Local Strength Requirements for Plate Field according to DNV GL

The requirements given by DNV GL for ships navigating in ice will be further investigated in this section. The requirements in this section apply to stiffeners and plating directly exposed to local ice pressure.

6.3.1 Shell Plate Requirements

The thickness of the plating exposed to the local patch load should not be less than:

$$t = 23 \cdot k_a \cdot \frac{s^{0.75}}{h_0^{0.25}} \sqrt{\frac{k_w p_0}{m_p \sigma_f}} + t_k \qquad [mm] \tag{6.11}$$

Where k_a is an aspect ratio factor of the plate field, s is the stiffener spacing, h_0 is the height of the ice load patch, k_w is an influence factor for narrow strip of load, p_0 is the basic ice pressure found by equation 28, m_p is a bending moment factor and lastly σ_f is the ice strength.

6.3.2 Stiffener Requirements

DNV GL gives requirements for web sectional area, web thickness and section modulus. The web sectional area shall not be less than:

$$A_W = \frac{3.7 \cdot (l - 0.5s) \cdot h_0^{1-\alpha} \cdot p_o}{\tau \cdot sin\beta l^{\alpha}} + A_K \tag{6.12}$$

Where l is the stiffener span, τ is equal to 45% of the ice strength, α is 0.15 for a load patch area of over 1 m^2 and β is the angle of the web with the shell plating. The requirement for minimum web thickness is given as:

$$t_w = 1.5 \cdot \left(\frac{p_0}{\sigma_f \cdot sin(\beta)}\right)^{0.67} \left(\frac{h_w \cdot h_0}{t_s}\right)^{0.33} + t_k \qquad [mm] \tag{6.13}$$

Where h_w is the height of the web, t_s is the plate thickness and t_k is a corrosion addition. The requirement for minimum section modulus is given as:

$$Z = \frac{41 \cdot h_0^{1-\alpha} \cdot l^{2-\alpha} \cdot p_o \cdot w_k}{\sigma \cdot sin\beta} \qquad [cm^3] \tag{6.14}$$

Where w_k is a section modulus corrosion factor and σ is equal to 90% of the ice strength. The rest of the parameters are as given before.

7 The Finite Element Method

This chapter will contain an overview of the finite element method(FEM), which is used to calculate the load effects and the structural requirements of the structural part. There will also be taken a closer look at the theory behind the software Abaqus which is the software used to model the part. The following linear and non-linear theory is based on Moan(2013) unless otherwise is specified. This chapter is modified from the project thesis done on a similar subject, found in reference Nilsen(2018).

7.1 Outline of the Method

The finite element method is a numerical procedure for analysing structures and continua. Analytical methods can usually not be used for such problems, due to the complexity of the problem. The results are usually not exact, but the error decreases by utilizing more equations. The problem is split into several smaller problems, which are then assembled and put together into a total solution. This makes the finite element method so practical, since it can be used for a wide variety of structures. FEM is based on the three principles of equilibrium in stresses, kinematic compatibility of strains and the stress-strain relationship. The steps of this method will be further outlined in this section.

The first step is to discretize the model. The geometry of the structure is divided into small pieces or elements where each element is connected at points along the edges of each element. The smaller the element size, the more accurate the results will be usually, but at the cost of needing more processing power and time consumption. The engineer needs to show good judgement as to how big he can allow the elements to be in order to get sufficiently accurate results.

The next step is the element analysis. The key components of this part is expressing the displacements withing the elements and maintaining equilibrium of the elements. The result of this is the element stiffness relationship, which can be expressed as:

$$\mathbf{S} = \mathbf{k} \cdot \mathbf{v} + \mathbf{S}^0 \tag{7.1}$$

Where $\mathbf{S}$ are the generalised nodal points forces, $\mathbf{k}$ is the element stiffness matrix, $\mathbf{v}$ are the nodal point displacements and $\mathbf{S}^0$ are the nodal point forces for external loads. The displacements are expressed by

shape functions which are assumed expressions, and gets more accurate for higher order shape functions. The choice of element is done by the engineer, and is a crucial step in order to get accurate results.

The third step is the system analysis, where a relationship is established between the load and the nodal point displacements by requiring equilibrium for all nodal points in the structure. The equations governing this is given by:

$$\mathbf{R} = \mathbf{K} \cdot \mathbf{r} + \mathbf{R}^0 \tag{7.2}$$

$$\mathbf{K} = \sum_j \mathbf{a}_j^T \, \mathbf{k}_j \, \mathbf{a}_j \tag{7.3}$$

$$\mathbf{R}^0 = \sum_j \mathbf{a}_j^T \, \mathbf{S}_j^0 \tag{7.4}$$

Where **R** is the system load vector, **K** is the system stiffness matrix, **r** are the global displacements, $\mathbf{R}^0$ are the external loads on the system and **a** is the topology matrix.

The fourth step is introducing boundary conditions by setting nodal displacements or rotations to known values, or adding spring stiffness.

The fifth step is finding the global displacements. This is done by solving the linear set of equations from equation 5.2, i.e.:

$$\mathbf{r} = \mathbf{K}^{-1} \cdot (\mathbf{R} - \mathbf{R}^0) \tag{7.5}$$

The fifth and final step is calculation of stresses. The stresses are determined from the strains given by Hooke's law. Generally this can be expressed as:

$$\sigma(x, y, z) = \mathbf{D} \cdot \mathbf{B}(x, y, z) \cdot \mathbf{v} \tag{7.6}$$

$$\mathbf{v} = \mathbf{a} \cdot \mathbf{r} \tag{7.7}$$

Where **D** is Hooke's law on matrix form and **B** is derived from **u**(x,y,z).

7.2 Shell Elements

Shell structures are curved surfaces, and they are characterized by by carrying the loads by a combination of membrane forces and bending moments. A lateral pressure load causes bending of the plate, as well as overall bending with the stiffeners acting as beams with the plate contributing to an effective flange. The overall bending causes membrane stresses in the plates which are well modeled by shell elements. Plate elements can only carry loads by bending moments, and is thus not very well suited for these types of problems.

Depending on the ratio between the thickness and the characteristic length of the plate, the theory used is usually distinguished between thin plate theory, thick plate theory and three-dimensional theory of elasticity. Abaqus(2014) differentiates between thin and thick shell elements. Thin plate theory corresponds to Kirchhoff theory, while thick plate theory corresponds to Mindlin-Reissner theory, both of which will be further elaborated on in the following. The limits given by Abaqus is that thin plate theory is to be used when the ratio between the thickness of the plate and the characteristic length of the plate is less than 1/15, and thick plate theory is to be used when the ratio is greater than 1/15.

7.2.1 Kirchhoff Theory

Kirchhoff theory is based on the assumption that the deformation work according to Kirchhoff-Navier's hypothesis which states that straight lines normal to the mid-surface remain straight after deformation. This implies that that transverse shear stresses are not accounted for. The stress-strain relationship is given by:

$$\sigma = \begin{bmatrix} \sigma_x \\ \sigma_y \\ \tau_{xy} \end{bmatrix} = \frac{E}{1-\nu^2} \begin{bmatrix} 1 & \nu & 0 \\ \nu & 1 & 0 \\ 0 & 0 & \frac{1}{2}(1-\nu) \end{bmatrix} \begin{bmatrix} \epsilon_x \\ \epsilon_y \\ \gamma_{xy} \end{bmatrix} = \mathbf{D}\boldsymbol{\epsilon} \tag{7.8}$$

Where σ and τ are the stresses, E is the elastic modulus, v is the Poisson number and ϵ and γ are the strains.

7.2.2 Mindlin-Reissner Theory

The main difference between Kirchhoff theory and Mindlin-Reissner theory is the assumed deformation pattern. Thick plate theory is based on the assumption that straight lines normal to the mid-surface remain straight, but not necessarily perpendicular to the mid surface after deformations. This implies that transverse shear deformation is accounted for by Mindlin-Reissner theory as opposed to Kirchhoff theory. However, when used for thin plates the results may still be less accurate than thin plate elements. This gives the following stress-strain relationship:

$$\sigma = \begin{bmatrix} \sigma_x \\ \sigma_y \\ \tau_{xy} \\ \tau_{xz} \\ \tau_{yz} \end{bmatrix} = \frac{E}{1-\nu^2} \begin{bmatrix} 1 & \nu & 0 & 0 & 0 \\ \nu & 1 & 0 & 0 & 0 \\ 0 & 0 & \frac{1}{2}(1-\nu) & 0 & 0 \\ 0 & 0 & 0 & \frac{1}{2k}(1-\nu) & 0 \\ 0 & 0 & 0 & 0 & \frac{1}{2k}(1-\nu) \end{bmatrix} \begin{bmatrix} \epsilon_x \\ \epsilon_y \\ \gamma_{xy} \\ \gamma_{xz} \\ \gamma_{yz} \end{bmatrix} = \mathbf{D}_{MI}\epsilon \tag{7.9}$$

Where k is a correction factor set to 1.2 to ensure that the shear strain energy is correctly represented by a uniform shear stress.

7.2.3 Numerical Integration

Determining the stiffness matrix and the load vector requires integrations over the region of interest. This is because, apart from 1D or 2D problems or for some simple geometrical configurations, the integrations required to achieve the FE equations become so complex that exact analytical integration cannot be obtained. And even if an exact analytical integrations is possible, it may hinder the establishment of an efficient FE program. That is why numerical integration techniques are needed. In some instances it can even improve the FEM solutions, even if it is an approximate method.

Abaqus solves such integrals either by the use of the Gaussian quadrature rule or by the use of Simpson's quadrature rule. The Gauss integration scheme is an optimal method for use in finite element analysis, and will be the preferred rule in this thesis. The two dimensional integral can be expressed by:

$$I = \int_{-1}^{1}\int_{-1}^{1} f(\xi,\eta)d\eta = \sum_i \sum_j w_i w_j f(\xi_i,\eta_j) \tag{7.10}$$

The number of integration points for finite element analysis is usually 2 by 2 or 3 by 3. The ξ and the η denotes the coordinates in the natural coordinate system, and corresponds to the locations showed in figure 7.1. These coordinates are used for mapped isoparametric elements. f gives the value of the integrand at the integration point, while w_i and w_j denotes weight functions.

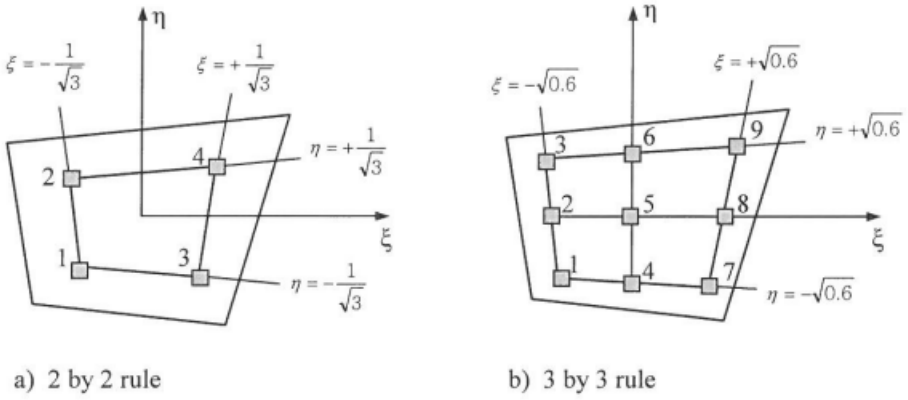

a) 2 by 2 rule b) 3 by 3 rule

Figure 7.1: Gauss integration points (Moan 2003)

Abaqus offers both full and reduced integration. Full integration is defined as a quadrature rule that provides exact integration of the polynomial as long as the element is undistorted. Gauss integration provides an exact integration of a polynomial of the order $2n-1$. However, exact integration does also provide a structure that is too stiff, therefore a lower-order integration rule called reduced integration may be desirable. Reduced integration means that the order of integration is one lower than that of a full integration. Using fewer integration points will also lower the cost of computation as well as "softening" the structure. This increased accuracy occures because it negates the effects of shear locking, which happens when spurious shear strains appear and makes the element overly stiff. One pitfall associated with the use of reduced integration is the existence of so-called spurious zero-energy modes. This happens when the model exhibits no stress or strain when undergoing displacements of some particular modes, i.e. no elastic energy is created by these modes. Abaqus deals with this by introducing artificial stiffnesses which limits these effects, and the effects will also decrease with increased mesh refinement.

7.2.4 Shell Elements in Abaqus

Abaqus offers many different shell elements depending on the properties and the number of nodes desired. In this thesis general-purpose, conventional elements which are suitable for modelling of thin and

thick shells will be further elaborated on. These elements allow transverse shear deformation, and use thick and thin shell elements depending on the thickness of the element. Non-linear geometry may be induced, which will be further elaborated on in the next section. The information in this section is all gathered from ABAQUS(2016).

The naming convention used by Abaqus is fairly intuitive to understand. The first letter denotes the type of element, e.g. S stands for shell-element. The type of element is followed by a number indicating the number of nodes used for the element. The third letter is optional and indicates that the element uses reduced integration if R is added. To illustrate this, S4R would denote a four noded shell element which utilizes reduced integration. Below a presentation of the relevant element types for the structure modelled in this thesis will be illustrated.

S3/S3R elements are three noded, triangular shell elements, and are a degenerate version of S3-elements. These elements uses constant bending and membrane strain approximations and may require high mesh refinement to capture pure bending deformations or accurate results to problems that involve high strain gradients. These elements are fully compatible with S4-elements and may be useful to model the transition between small and large stress gradients areas.

S4/S4R elements are four noded, quadrilatural shell elements. S4-elements gives accurate solutions to in-plane bending problems, they are not sensitive to element distortion and avoid shear locking. Since full integration is used in both the membrane and the bending terms, hourglass modes are avoided. They are more computationally expensive than S4R-elements since it has four integration points compared to one for S4R-elements. The S4R-elements applies reduced integration in order to avoid locking. In order to avoid hourglass modes, hourglass control is used. This is done by adding an artificial stiffness to the element. S4R-elements are recommended when high strain gradients or large strains are expected. S4 and S4R-elements can be used both for thin and thick shell problems.

S8R elements are eight noded, quadrilateral thick shell elements that utilizes reduced integration. The S8R-elements are only to be used for thick shell problems. They are small-strain shell elements and the change in thickness with deformation is ignored. Locking is avoided by reduced integration, and hourglass control is not utilized.

7.3 Non-linear Finite Element Theory

Linear finite element theory is based on the assumptions of small displacements and that the material is linear elastic. This is however often not the case. When the yield strength is reached and exceeded, plastic deformations occur. Linear theory is then no longer valid. Large displacements may also occur when this happens, and the equilibrium equations need to account for the change in geometry. Non-linear theory is applied to account for geometry, material and boundary condition non-linear behaviour, all of which will be discussed further in this section.

7.3.1 Geometry Effects

For linear theory the stiffness matrix is kept constant throughout the analysis, but when a structural member is subjected to increased loading the initial shape of the member will change as the displacements increase. This is accounted for in non-linear theory by changing the stiffness matrix throughout the analysis. Figure 7.2 shows the load-displacement relationship for a pretension cable with lateral load, and shows the non-linear response. Abaqus accounts for such non-linear geometry effects by updating the stiffness matrix.

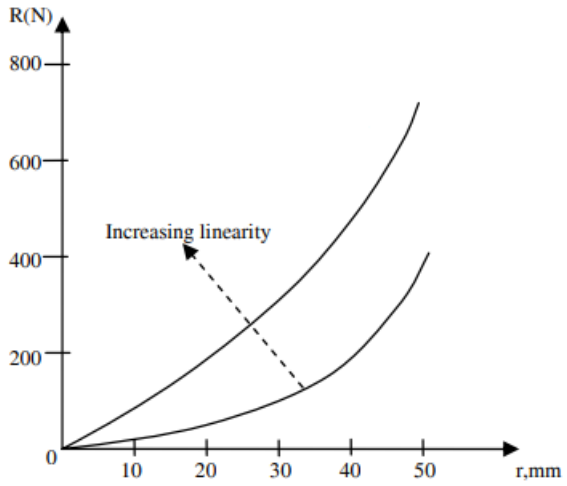

Figure 7.2: Non-linear load-displacement relationship (Moan 2003)

7.3.2 Material Effects

When the stress exceeds a certain limit, σ_P the proportionality limit, the linearity relationship between the strains and the stresses are no longer valid. Above this threshold the material goes from behaving linear elastic to behaving non-linear. Unloading from a stress condition above the proportionality limit occurs along a line parallel to the initial linear elastic line. The model does not return to its initial state post loading, but rather a residual plastic strain, ϵ_p remains. When the yield stress is reached the stresses suddenly increase without any more increase of the strain. The stress then increases again and the material experiences strain hardening until it reaches the ultimate stress and unloading occurs as the material fails.

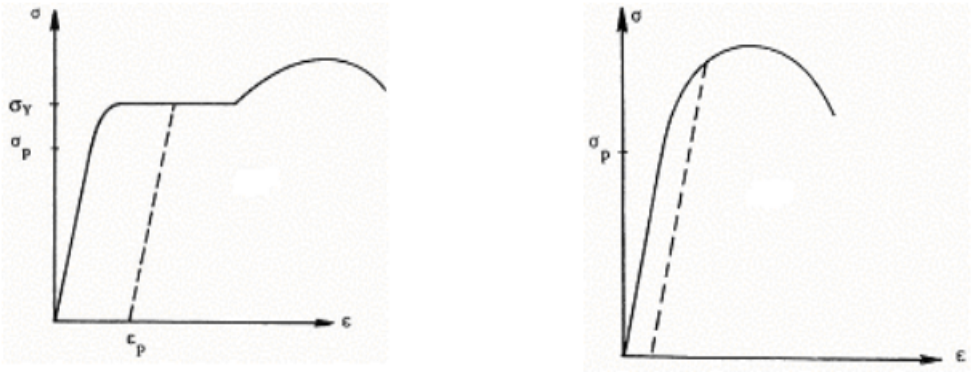

Figure 7.3: Non-linear stress-strain curves for mild steel and high-strength aluminium (Moan 2003)

7.3.3 Boundary Conditions

Effects of non-linearity by boundary conditions occur due to contact because of large displacements. If two surfaces come into contact, the displacements and stresses of the contacting bodies are not a linear function of the loads.

7.3.4 Solution Methods

In non-linear theory the stiffness matrix is dependent on the displacement, the solution can therefore not be found by solving a single system of equations as is done for linear theory. The solution must therefore be found by using a step wise approach to solving the equations. Many solution methods exist, and a few

of them will be discussed further. Since the stiffness depends on the displacements, equation 5.2 can be rewritten to account for non-linearity as:

$$\mathbf{K}_I(\mathbf{r})d\mathbf{r} = d\mathbf{R} \tag{7.11}$$

7.3.4.1 Load Incremental Methods

By use of incremental methods the solution is found by step wise applicating the external loading. For each load step, the displacement step is found by use of equation 5.11. The total displacement is found by adding each displacement increment. The incremental stiffness matrix is found from the known displacement before a new load increment is applied. The Euler-Cauchy method is one such load incremental method, and can be expressed by the following equations:

$$\Delta\mathbf{R}_{m+1} = \mathbf{R}_{m+1} - \mathbf{R}_m \tag{7.12}$$

$$\Delta\mathbf{r}_{m+1} = \mathbf{K}_I(\mathbf{r}_m)^{-1}\Delta\mathbf{R}_{m+1} \tag{7.13}$$

$$\mathbf{r}_{m+1} = \mathbf{r}_m + \Delta\mathbf{r}_{m+1} \tag{7.14}$$

With the initial condition of $r_0 = 0$. The Euler-Cauchy-method is illustrated in figure 7.4. It is seen from the figure that the result deviates from the exact solution. Total equilibrium is thus not fulfilled for this method. The accuracy increases by reducing the load increments.

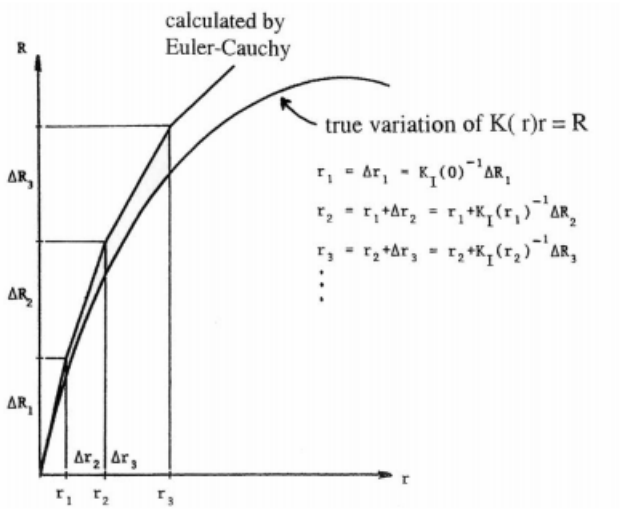

Figure 7.4: Euler-Cauchy method (Moan 2003)

An improvement on the Euler-Cauchy method can be achieved by an equilibrium correction. This is done by adding the unbalanced forces to the next increment. This restores the global equilibrium by reducing the external forces. This is expressed by the following equations:

$$\Delta \mathbf{R}_{m+1} = \mathbf{R}_{m+1} - \mathbf{R}_m \tag{7.15}$$

$$\mathbf{R}_{eq} = \mathbf{R}_m - \mathbf{R}_{int}(\mathbf{r}_m) \tag{7.16}$$

$$\Delta \mathbf{r}_{m+1} = \mathbf{K}_I(\mathbf{r}_m)^{-1}[\Delta \mathbf{R}_{m+1} + \mathbf{R}_{eq}] \tag{7.17}$$

$$\mathbf{r}_{m+1} = \mathbf{r}_m + \Delta \mathbf{r}_{m+1} \tag{7.18}$$

Figure 7.5 shows that total equilibrium is now fulfilled after the correction.

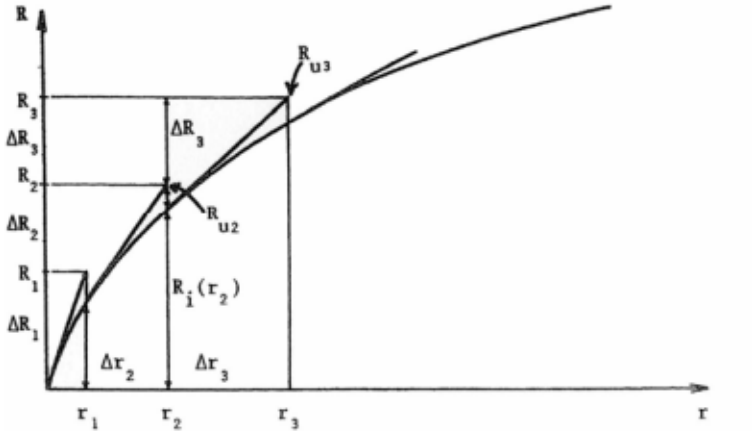

Figure 7.5: Euler-Cauchy method with equilibrium correction (Moan 2003)

7.3.4.2 Iterative Methods

Load incremental methods utilize step wise application of the loads, while iterative methods utilize step wise application of the displacements. The stiffness term is kept constant for each step and is updated throughout the analysis. The most frequently used iterative method is the Newton-Raphson method. The displacements are found by the iteration formula:

$$\mathbf{r}_{n+1} = \mathbf{r}_n - \mathbf{K}_I^{-1}(\mathbf{r}_n)(\mathbf{R}_{int} - \mathbf{R}) \tag{7.19}$$

The displacement increment for the next iteration is found from:

$$\mathbf{R} \text{ - } \mathbf{R}_{int} = \mathbf{K}_{I(n)} \Delta \mathbf{r}_{n+1} \tag{7.20}$$

For each iteration. This is however very time consuming, so a modified Newton-Raphson method where the stiffness matrix is updated less frequently can be utilized, but with more iterations. The iteration process is stopped when the error is sufficiently small by checking the change of displacement from one iteration to the next. Figure 7.6 illustrates the principle of the Newton-Raphson method.

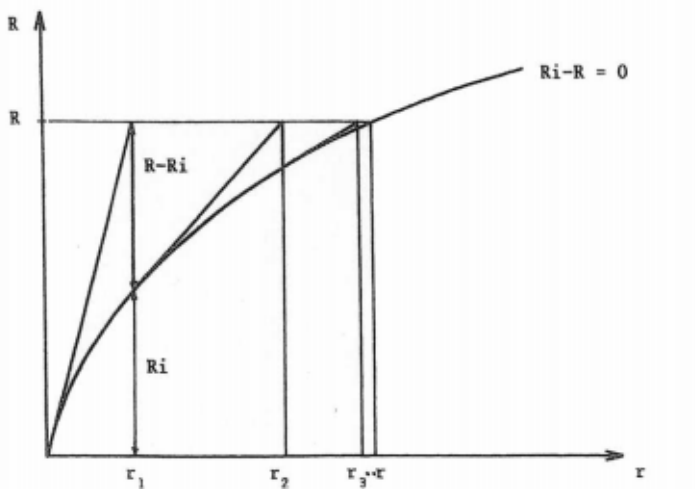

Figure 7.6: Newton-Raphson method (Moan 2003)

7.3.4.3 Combined Methods

Abaqus utilizes a combination of the Euler-Cauchy method and the Newton-Raphson method. This is done by applying the loads in increments, and for every increment equilibrium is achieved by iteration. Figure 7.7 illustrates the combined method. A modified Newton-Raphson is commonly used, by keeping the incremental stiffness matrix constant for several iterations.

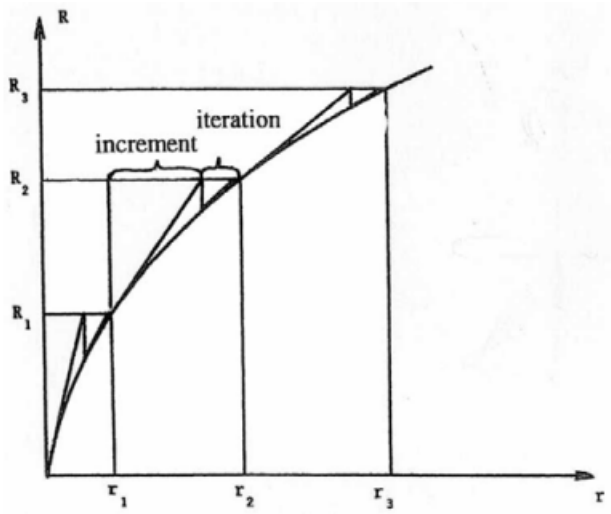

Figure 7.7: Combined method (Moan 2003)

8 The Computer Model

This section describes how the structural part subjected to ice actions is set up using Abaqus 6.14. A presentation of the model, the material selection, meshing and boundary conditions will be given. The structural part is both modelled and analysed in Abaqus. This proved to be very challenging, and a design software should have been considered, as it was very time consuming modelling.

8.1 Model

The model is based on the semi-submersible drilling unit presented in chapter 4, and is modelled from the drawings provided in Appendix A. The final model is shown in figure 8.1. The model is mirrored from how it is supposed to be, as what is seen in figure 8.1 is modelled as the topside, but in the analysis it will be used as the bottom side. There is no easy way to correct this without making the model from the start, but as it has no impact on the analyses it will be used as is.

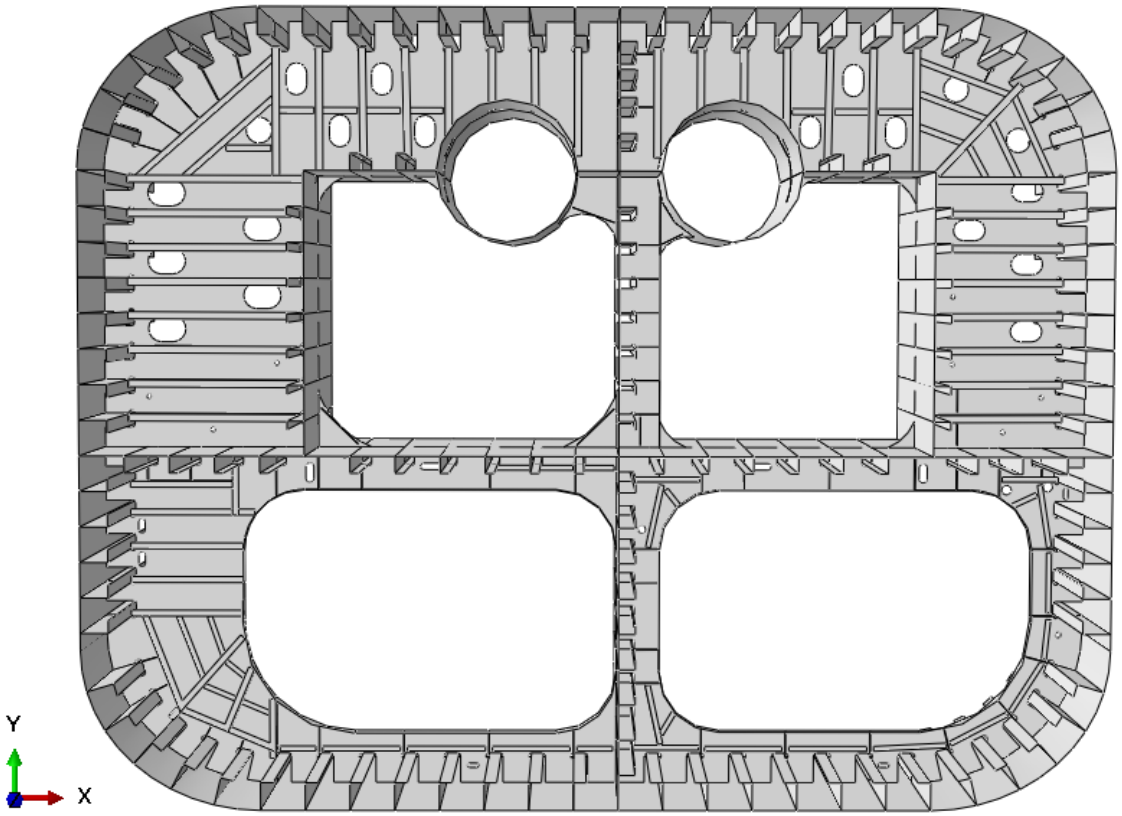

Figure 8.1: Model Designed in Abaqus

The model is made up of two parts, a frame and a stringer, which are assembled into one model. Several features are added to the stringer, which makes up the various stiffeners. The main dimensions of the frame are a length of 19.5m, a width of 15.1m and a height of 5.5m. The stiffener spacing of the frame is different for different sections, but the stiffener spacing used in the calculations is shown in table 8.1. Each of the lower corners of the frame have one stiffener less than the drawings indicate because the author at the time of modelling assumed the number of stiffeners were the same for top and bottom corners. Apart from that all local details have been modelled as closely as possible to the drawings provided, but some strengthening has been done to all stringer stiffeners due to the ice loading. Some dimensions are not included in the drawings and thus dimensions for those parts are assumed. The section modulus and the plate thickness of the frame is established by use of IACS Polar Code(see section 5.2). Verification of these results is done using DNV, but this formulation is not made for offshore platforms. The plating according to DNV gives a plate thickness of 46 mm, so compared to IACS there is not a big difference. The section modulus found by use of DNV's formulation is 2073000 mm^3, i.e. the IACS' formulation causes more conservative stiffener dimensions. The stiffeners used in the model are designed according to Polar Class PC4. The calculations done to find the dimensions can be found in Appendix B, where the matlab code for calculation of the section modulus is given. This, along with the conditions to prevent local buckling, gave the following dimensions to the outer stiffeners of the frame:

Table 8.1: Plate and Stiffener Dimensions

Parameter	Value	Unit
Stiffener Span	848	mm
Plate Thickness	48	mm
Section Modulus	3122131	mm^3
Web Height	530	mm
Web Thickness	50	mm
Flange Width	240	mm
Flange Thickness	50	mm

Figure 8.2 shows the different thicknesses of the different sections. The frame consists of outer stiffeners with dimensions L530x240x50 while the inner stiffeners have dimensions L320x160x13x18. The mooring system shown in the drawings are not modelled. For the stringer the largest stiffeners have dimensions L420x140x14x20. The other stiffeners have smaller dimensions with thicknesses as shown in the figure below.

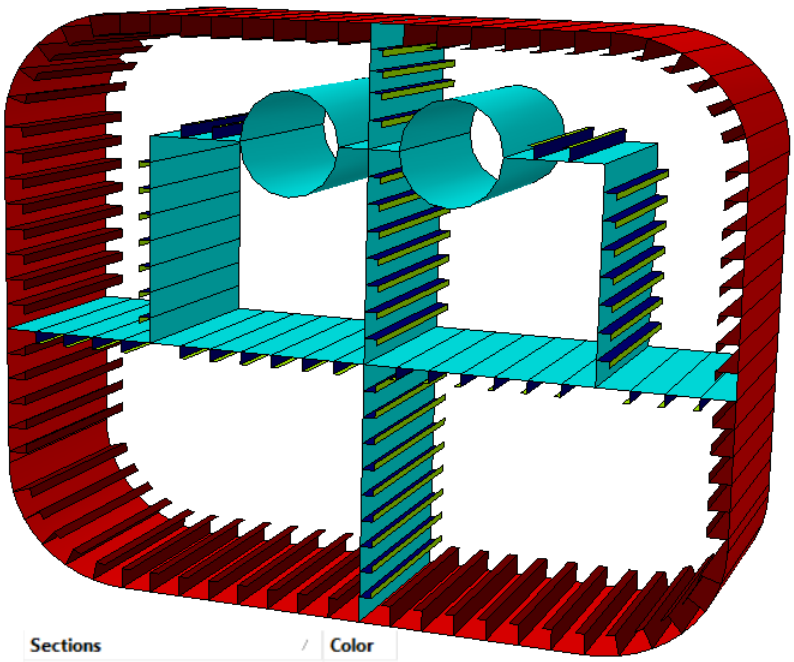

Sections	Color
thickness 12mm	
thickness 13mm	
thickness 14mm	
thickness 16mm	
thickness 18mm	
thickness 20mm	
thickness 24mm	
thickness 36mm	
thickness 48mm	
thickness 50mm	

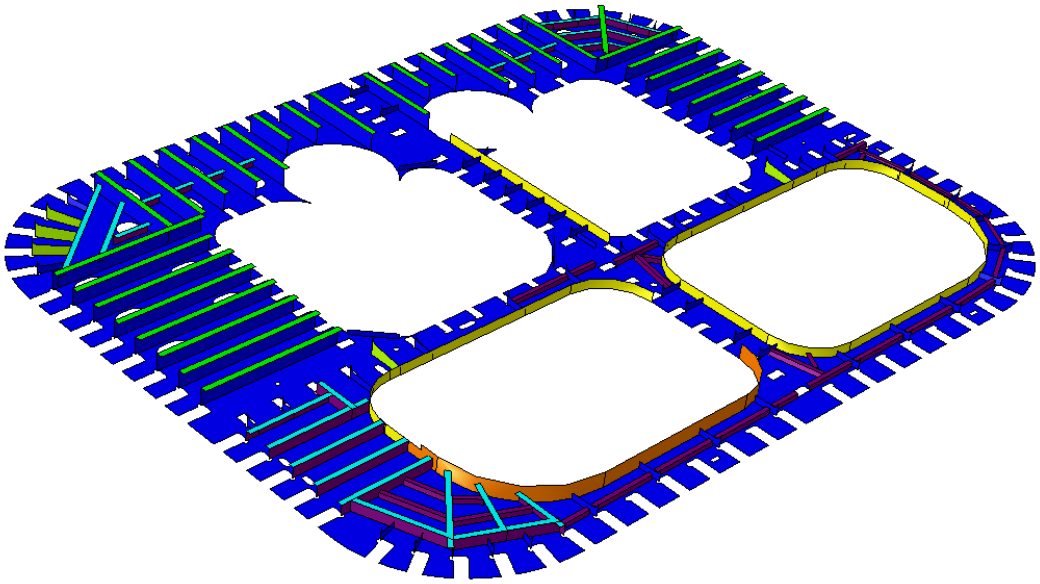

Figure 8.2: Frame and stringer with different colors for different thicknesses

8.2 Material Properties

The material used in the computer model is S355 carbon steel due to the high load actions from ice. S355 carbon steel is also a frequently used steel in the marine industry, and has its designation from the fact that the yield strength is 355 MPa. Several material behaviours are possible in Abauqs, such as linear, nonlinear, isotropic, anisotropic and ortothropic. In this thesis both elastic and plastic behaviours are modelled. The material properties assigned in Abaqus is shown in table 8.2:

Table 8.2: Material Properties

Parameter	Value	Unit
Density	7850	kg/m^3
Young's Modulus	210	GPa
Yield Stress	355	MPa
Poisson's Ratio	0.3	-

The material is modelled in Abaqus as being elasto-plastic, i.e. non-linear. DNV GL(2016) recommends thickness dependent non-linear stress-strain curves according to European Standards(EN) for use in modelling of material properties. The material is modelled as a combination of a stepwise linear and a power law with a yield plateu as shown in figure 8.3, where the stresses and strains used are true stresses and true strains.

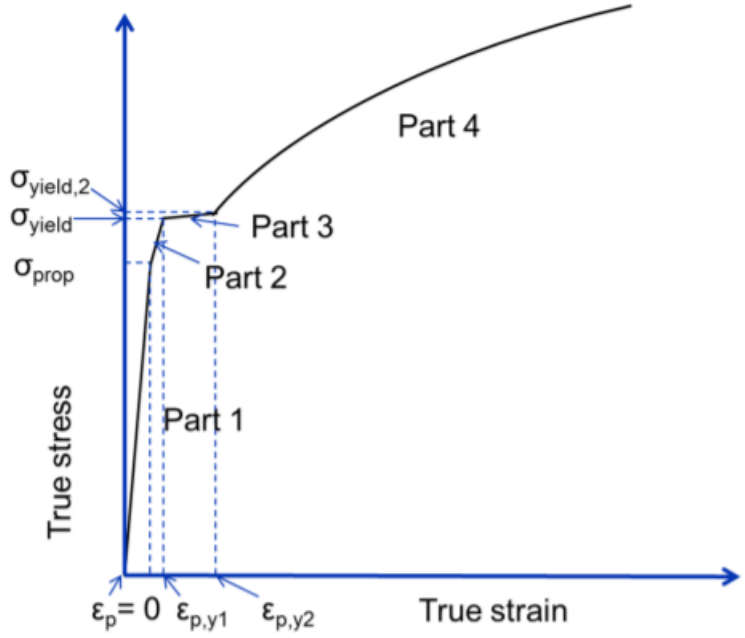

Figure 8.3: Non-linear stress-strain curve (DNV GL, 2016)

The stresses and strains up to $\epsilon_{p,y2}$ are given as linear. Beyond this point the relation between stress and strain is given as shown in equation 8.1:

$$\sigma = K\left(\epsilon_p + \left(\frac{\sigma_{yield2}}{K}\right)^{\frac{1}{n}} - \epsilon_{p,y2}\right)^n \qquad \epsilon_p > \epsilon_{p,y2} \tag{8.1}$$

The stress-strain curve is thickness dependent, and in this model three different curves are used. The parameters and properties used for calculating the stress strain curves for the different thicknesses are given in table 8.3:

Table 8.3: Properties for S355 steel

Thickness [mm]	t ≤ 16	16 < t ≤ 40	t > 40
σ_{prop} [MPa]	320.0	311.0	301.9
σ_{yield} [MPa]	357.0	346.9	336.9
σ_{yield2} [MPa]	366.1	355.9	345.7
$\epsilon_{p,y1}$ [-]	0.004	0.004	0.004
$\epsilon_{p,y2}$ [-]	0.015	0.015	0.015
K [MPa]	740	740	725
n [-]	0.166	0.166	0.166

To use this in Abaqus we can construct stepwise linear stress-strain curves by inserting several different strains above σ_{yield2} according to equation 8.1. The resulting points on the stress-strain curve is seen in table 8.4:

Table 8.4: Plastic Strain Model

Plastic Strain [-]	Stress_{t16} [MPa]	Stress_{t16-40} [MPa]	Stress_{t40} [MPa]
0.000	320.0	311.0	301.9
0.004	357.0	346.9	336.9
0.015	366.1	355.9	345.7
0.030	412.1	406.7	396.9
0.045	441.3	437.5	427.6
0.060	463.1	460.2	450.0
0.075	480.8	478.3	467.9
0.090	495.6	493.5	483.0
0.105	508.6	506.7	496.0
0.120	520.0	518.4	507.4
0.135	530.3	528.9	517.7
0.150	539.7	538.4	527.1

No ultimate stress is given in DNV GL(2016), so an ultimate strength for a true strain of 0.15 is here as-

sumed. The stress-strain curves plotted can be seen in figure 8.4:

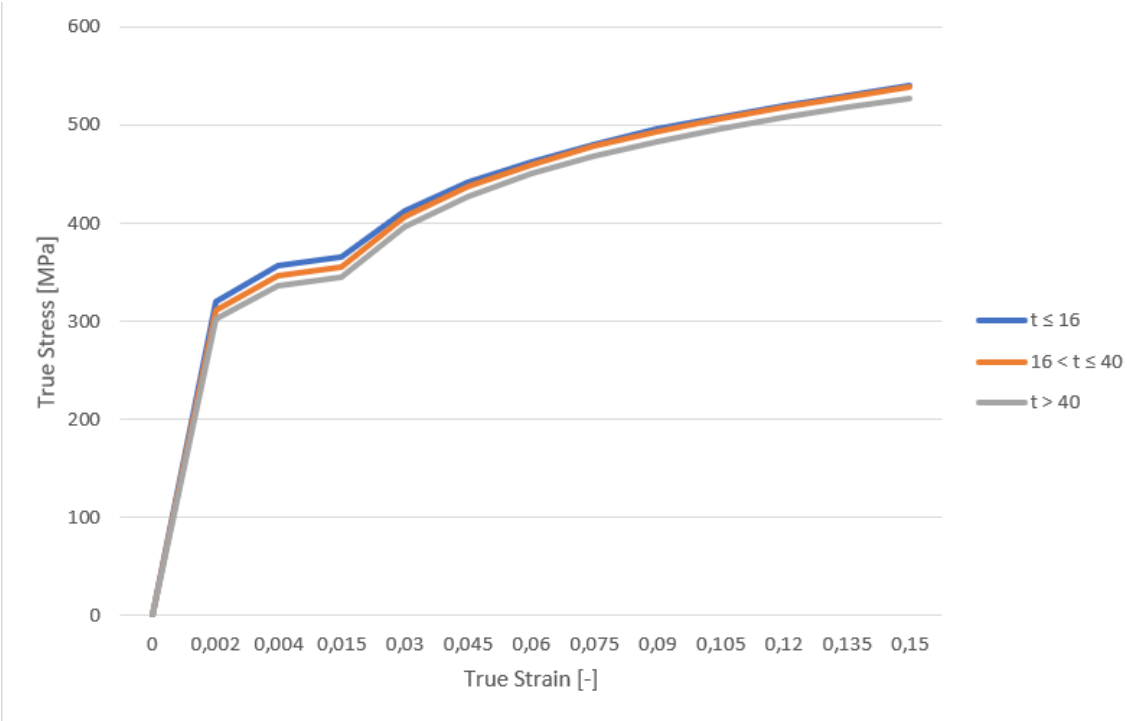

Figure 8.4: Stress-strain curve used in Abaqus

8.3 Boundary Conditions

The choice of boundary conditions is essential to get accurate results. According to DNV GL(2016), the model boundary conditions should represent the real condition so that it leads to results that are accurate or on the safe side. If there is uncertainty as to what would be realistic boundary conditions, conservatism should be ensured. In this thesis a local model is analysed, and thus how much stiffness the adjacent structure provides should be considered. According to Moan(2003), it is advised to extend the model to locations where boundary conditions are easy to predict and apply. The best way to find suitable boundary conditions is to first perform a global analysis of the structure and then model the local part by using boundary conditions obtained by the global analysis, or increasing the size of the model. However, the same problem with unknown boundary conditions will occur at the bigger model unless the whole model is modelled. Since only the local part is provided in this thesis that is not a feasible way to obtain realistic boundary conditions.

If the boundaries are all assumed to be fixed against both translations and rotations on both edges of

the model, this will produce high stresses along the edges close to the ice loads and thus ensuring conservatism. However, the boundaries will give a stiffness higher than the adjacent structure in reality can provide. The opposite is true away from the boundaries, where the deflections and stresses are smaller than they in reality would be. Another problem with fixing the edges is that singularities will occur in corners along the boundary, such as in stiffener flanges. A singularity in a point has the implication that stresses do not stop rising for increased mesh refinement. Introducing spring stiffnesses is another possibility, but it will not be elaborated on in this thesis.

Three alternative boundary conditions will be investigated herein. The natural structural restraints will in reality be stringers as in the middle part of the model and upper and lower bounds of these restraints will be looked at so that sufficient conservatism is ensured. Fixed boundary conditions on both sides will give the boundary of the structure a stiffness that the stringers in reality can not provide. This will act as a lower bound. Letting the boundaries rotate freely while keeping all the translations fixed will give the boundaries more freedom than they have in reality. This will give an upper bound of the stresses out in the plate field. A third alternative is keeping the bottom part fixed against all translations, and all rotations except for in z-direction. Keeping the structure fixed against translation in z-direction is required in order to let the structure carry the axial loads it is subjected to. The top part of the structure will be fixed against horizontal translations and rotations, while it is allowed to translate and rotate in z-direction. This is the boundary condition that is expected to give the most conservative results. The structure will be subjected to IACS' design pressure given in section 7.4.3 over an area of 7.14 m^2 on the upper right side of the structure. The von Mises-stress is checked at the elements shown in figure 8.5. The displacements are checked at the same or similar locations for different boundary conditions.

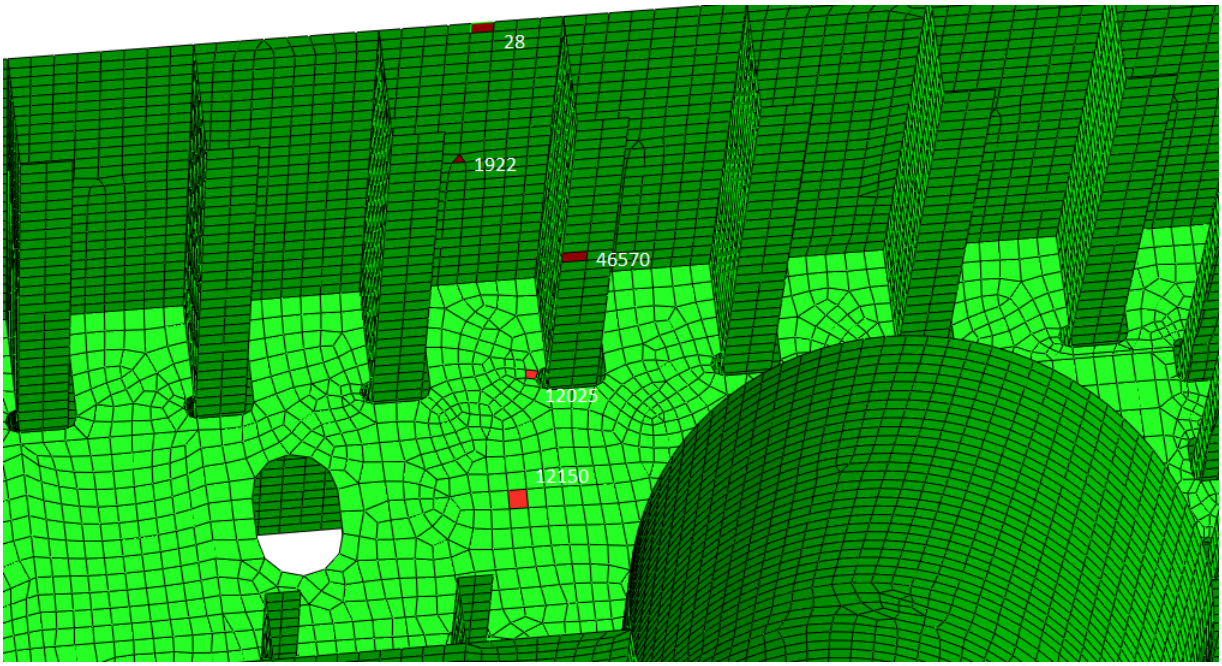

Figure 8.5: Elements checked for different boundary conditions

Table 8.5 and table 8.6 shows the von Mises-stress and the displacements at the points indicated in figure 8.5. We see that the stress is low at the boundary when the edges are free to rotate, with stresses at 111.4 MPa compared to 306.2 MPa for fixed boundaries. However, the stresses are larger for all other elements indicated for rotation free boundaries, even if the differences are not very large. For displacements we see that the magnitude is larger for all points for rotation free boundaries than for the fixed boundaries. This indicates that fixed boundaries are a true lower bound for stresses and displacements out in the field away from the boundaries. However, it is seen that mixed boundaries, i.e. the upper edge is free to rotate and translate in z-direction and the lower edge is free to rotate in z-direction gives both the largest stresses and the largest displacements for all elements investigated. This confirms that these boundary conditions will give the most conservative results, and they are therefore chosen for the analyses in this thesis. The model with the boundary conditions applied are shown in figure 8.6.

Table 8.5: von Mises-stress for different boundary conditions

Element number	Fixed Boundaries [MPa]	Translations fixed [MPa]	Mixed boundaries [MPa]
28	306.2	111.4	316.5
1922	308.9	310.3	315.8
46570	302.7	304.8	317.0
12025	359.8	362.2	364.0
12150	164.2	177.2	188.4

Table 8.6: Displacements for different boundary conditions

Element number	Fixed Boundaries [mm]	Translations fixed [mm]	Mixed boundaries [mm]
1922	14.0	15.7	18.0
46570	14.4	16.6	18.6
12025	17.5	19.7	22.5
12150	4.5	4.9	6.0

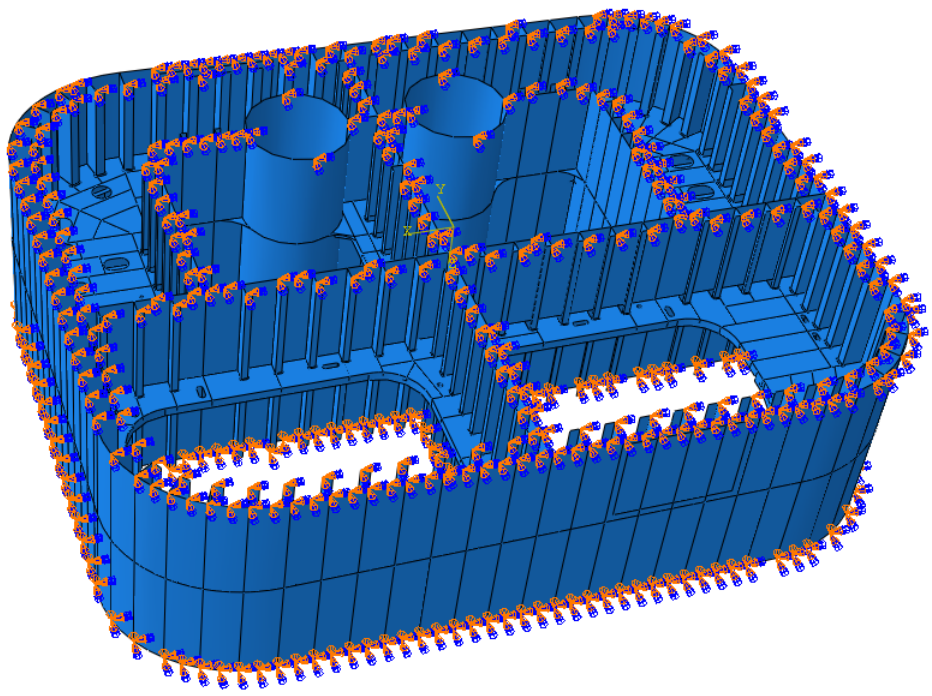

Figure 8.6: Boundary conditions for model

8.4 Load Cases

Three load cases are considered in this thesis, namely; the weight of the platform, a hydrostatic load from the water column and a local ice load acting on the column.

8.4.1 Weight of Platform

In Chapter 3 it was mentioned that Deepsea Stavanger has a displacement of 52000 tons at operational draught. This weight is shared between the four columns supporting the deck structure. In this thesis, dynamics is neglected and the structure is modelled with static forces acting. It is assumed that the weight therefore is carried equally by the four columns. The force is applied as a shell edge load acting over the top part of the model with a magnitude of 1.0 MN/m which is on the conservative side. The force on the model is shown in figure 8.7.

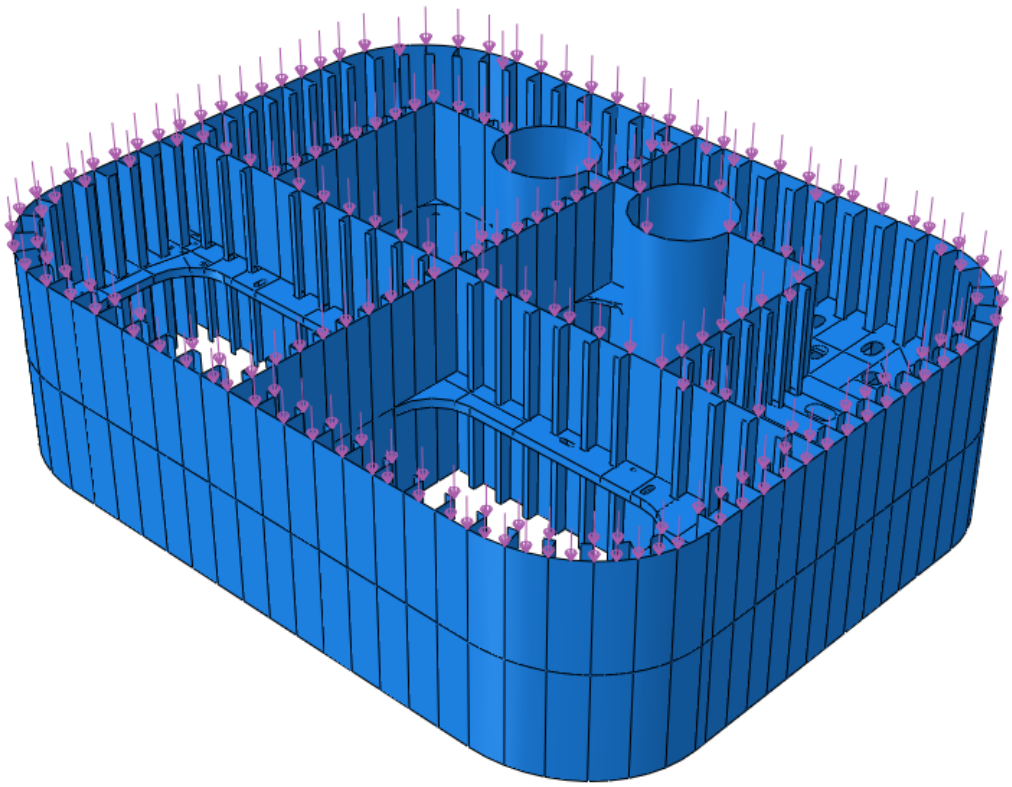

Figure 8.7: Shell axial edge load

8.4.2 Hydrostatic Load

The pressure due to the water column has to be accounted for as well. The waterline is assumed to be at the location of the stringer plate. This give a water height of 2.75m. The formula for the hydrostatic pressure is given by:

$$p_w = \rho_w \cdot g \cdot h \tag{8.2}$$

Where p_w is the hydrostatic pressure due to the water column, ρ_w is the density of sea water which is given as 1025 kg/m^3, g is the acceleration of gravity and is given as 9.81 m/s^2 and h is the height of the water column. Insertion into this equation gives a hydrostatic pressure of 27652 Pa. The model is designed mirrored to how it is supposed to be, thus not making it possible to use a hydrostatic pressure in Abaqus. Thus an evenly distributed pressure of half of the hydrostatic pressure is applied to the model. The hydrostatic pressure is small compared to the other loads, so this will not have any significant effect on the results. The equivalent hydrostatic pressure applied to the model is seen in figure 8.8.

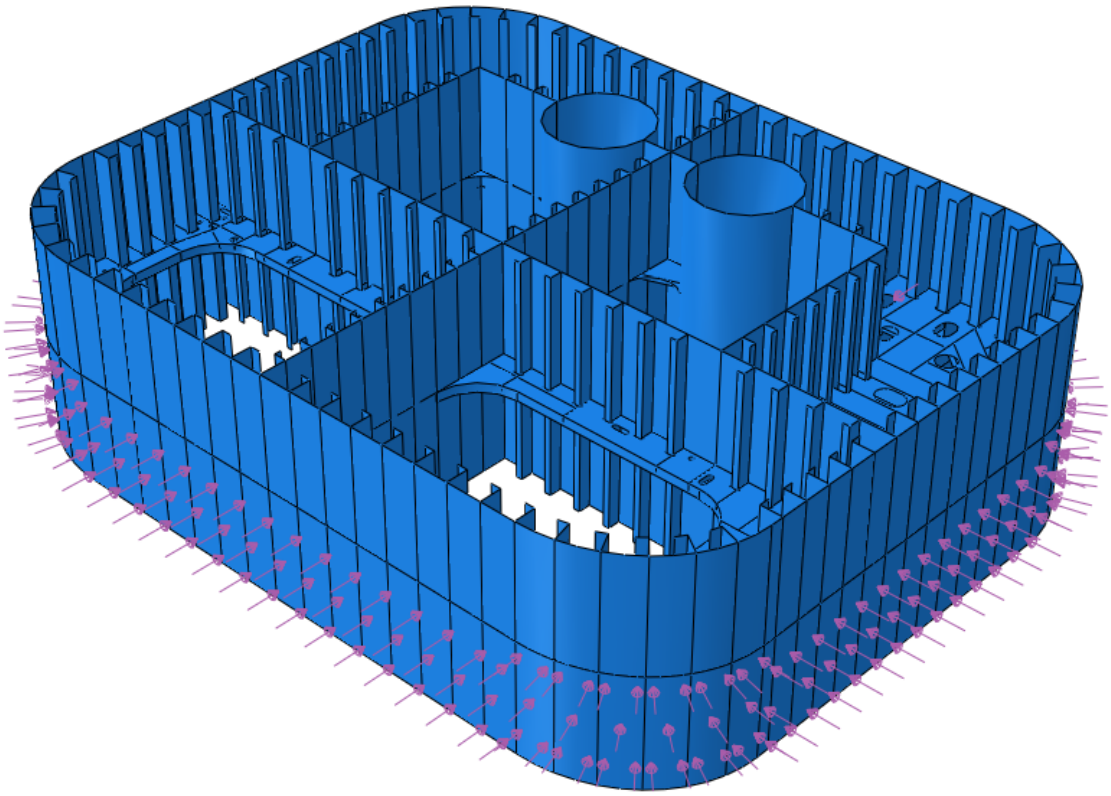

Figure 8.8: Equivalent hydrostatic pressure applied to model

8.4.3 Local Ice Loads

Several load conditions will be examined in this thesis. First IACS procedure for determining the ice pressure for ships of a glancing impact on the bow will be investigated. Further DNV and ISO.

IACS PC4 for Glancing Impact on the Bow

The outer stiffeners are dimensioned according to IACS PC4 which is described in section 5.2.2. These dimensions was found based on calculations of the ice pressure by use of the procedure described in section 4.2. The hull geometry is described by the minimum bow coefficient of three equations(see equation 4.7 to 4.9) and was found the be 0.6[-]. The total force on the bow is then found by multiplying the bow coefficient with the crushing failure class factor CF_C and the ship displacement in kilotons, giving:

$$F_b = 0.6 \cdot 4.5 \cdot 52^{0.64} = 33.9MN \tag{8.3}$$

Further following the procedure given in section 4.2.2 gives a a design load patch with a width of 3.04m and a height of 2.35m, i.e. the pressure will act over an area of 7.14 m^2. The average pressure can then be found from the following equation:

$$P_{avg} = \frac{F_b}{b_b \cdot w_b} = \frac{33.9MN}{7.14m^2} = 4.74MPa \tag{8.4}$$

A peak pressure factor is applied for the stiffener design load. Using equation 5.17 from section 5.2.2, with a stiffener spacing of 0.85, which gives a PPF of 1.2, results in an average pressure of:

$$P_{avg,stiffener} = 4.74MPa \cdot 1.2 = 5.69MPa \tag{8.5}$$

In general the average pressure is supposed to be calculated at several locations along the bow of a ship, and then the maximum average pressure is taken as the design pressure and the corresponding load patch is calculated(Daley, 2000). But here we are not looking at a ship bow and thus a single average pressure is calculated. Thus the load patch must be placed at an unfavourable location on the model. A study is therefore performed to find the location on the model that produces the largest response to use

throughout all of the analyses.

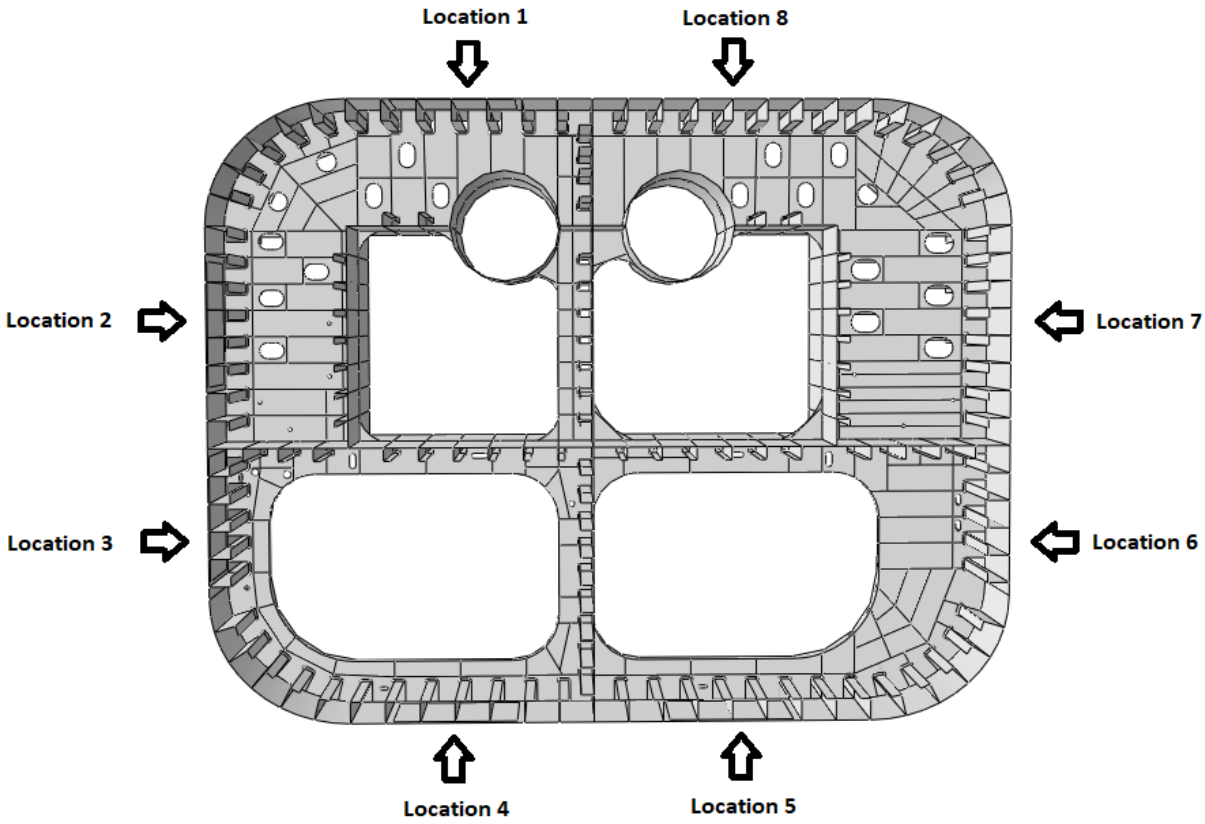

Figure 8.9: Locations studied to find maximum response

Figure 8.9 shows the locations that are being studied. Only one location is considered on the right side of the model. This is because the loads are assumed to be largest on the left side since these are that areas that have the least amount of support an area to carry the loads. Location 5 is still considered since it is still assumed to be one of the weakest parts of the structure, and also for comparison.

Table 8.7: Response for various load cases

Load case	Max stiffener stress [MPa]	Max S11 [MPa]	Max S22 [MPa]	Max displacement [mm]
Location 1	321.6	343.2	378.1	22.5
Location 2	305.9	340.3	298.6	13.2
Location 3	313.9	322.2	331.4	18.0
Location 4	339.9	394.6	393.2	34.3
Location 5	340.0	354.1	385.4	32.8

Table 8.7 shows that location 4 has the highest response for all stresses and for the displacement, except for maximum von Mises-stress in the stiffeners which occurs at location 5 but this is only by 0.1 MPa. This

means that location 4 will govern the response for the lower part of the model, and will therefore be used in the analyses. Location 1 has the highest response for the upper part of the model, and will therefore be used for comparison in the analyses.

Comparison between DNV GL - Ships for Navigation in Ice and ISO 19906

It is not easy to compare the ice classes from various ice rules. In this thesis the polar class PC4 is assumed to be equivalent to DNV GL's Polar-30 to ensure conservatism. This class is supposed to be used for vessels intended to operate unassisted in ice-infested waters in Arctic regions. By use of table 5.2 in section 5.3.1, this gives a nominal ice strength of 10 MPa and a nominal ice thickness of 3.0 m. Using a correction factor, F_A, of 1.0, a basic ice pressure is obtained as:

$$P_0 = 1.0 \cdot 10MPa = 10MPa \tag{8.6}$$

Using equation 5.19 and combining this result with the correction factor for the size of the load patch we get the following area dependent equations for the design pressure:

$$p = \frac{5.8}{(A_C)^{0.5}} \qquad A_C \leq 1.0m^2 \tag{8.7}$$

$$p = \frac{5.8}{(A_C)^{0.15}} \qquad A_C > 1.0m^2 \tag{8.8}$$

The area dependent equations for the design pressure for thick, massive ice features by ISO 19906 is given in section 5.1.3, equation 5.5 and 5.6. The design pressure as a function of the load patch area is sketched in figure 8.10. It is seen that for small areas, i.e. areas smaller than 1.6 m^2, the ISO 19906 design pressure is largest. For values larger than 1.6 m^2 the DNV GL design pressure is governing. It is also observed that for small values the ISO-loads are very large, while the difference is not very big for larger pressures. From these results it is decided that ISO 19906's design pressure will be used for areas smaller than 1.6 m^2, while DNV GL's design pressure will be used for values equal to 1.6 m^2 and above in order to ensure conservatism in the analyses.

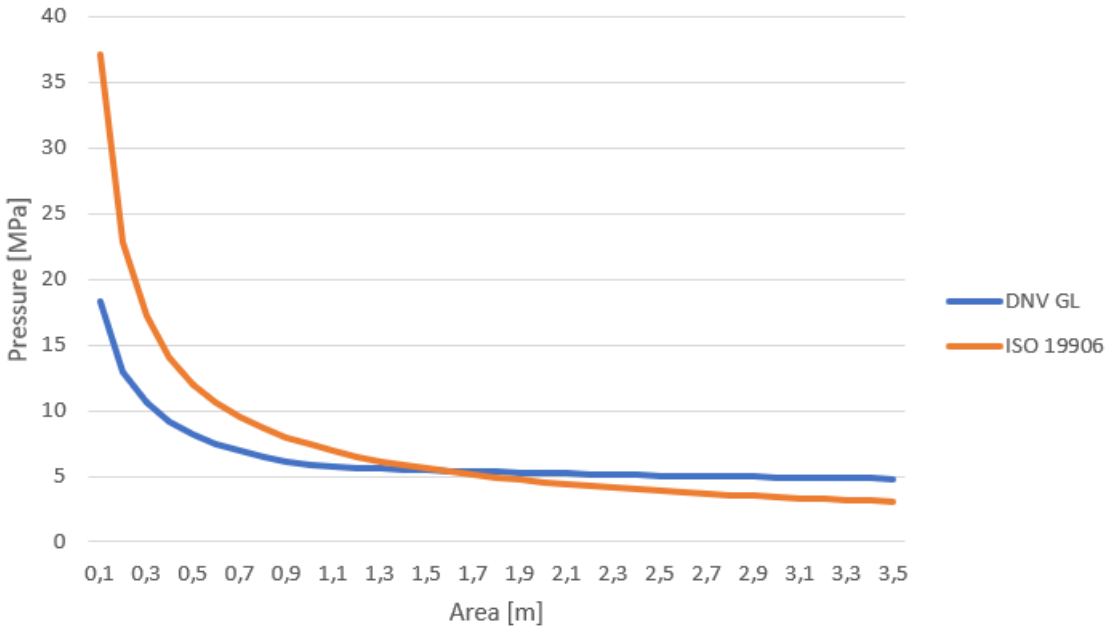

Figure 8.10: Design pressure by DNV GL vs ISO 19906

In order to calculate the forces acting on the model, the area of the load patch has to be defined. Several checks will be performed, so the load patch has to be defined for each structural part considered. It is assumed that the areas should be chosen such that it gives the most conservative results possible also here.

For the plating DNV GL(2009) specifies that the area should be chosen such that the width is the length between two transverse stiffeners and the height is the length between two stringer plates. This pressure load will be acting along the top boundary which will further amplify the importance of conservative boundary conditions. The plating will be checked at several locations. With reference to figure 8.9, the plating will be checked in the critical location 4, in the corner between location 3 and 4, and in location 1 and 2. Following the calculation procedure for the design loads, this gives the design loads(all using DNV GL design load because of large areas) shown in table 8.8.

Table 8.8: Design loads for plating

Load case	Area [m^2]	Design Load [MPa]
Location 1, 4	2.33	5.11
Location 2	1.84	5.29
Corner 3/4	2.35	5.10

We see that the design loads are very similar in magnitude. This is due to the fact that the design loads are slowly decreasing for large load patch areas. For the stiffener design load, a load width equal to the stiffener span is used in the calculations. To find the height of the load patch a study has to be performed to see what load height gives the largest response. Here a combination of design loads using DNV GL and ISO 19906 will be used, and the results are seen in table 8.9.

Table 8.9: Response in stiffener for various load cases

Load height [m]	Design load [MPa]	Max S11 [MPa]	Max S22 [MPa]	Max displacement [mm]
0.4	15.78	307.5	303.6	8.1
0.8	9.71	313.6	315.6	9.9
1.2	7.31	314.4	315.6	10.6
1.6	5.98	312.4	314.0	10.8
2.0	5.36	312.0	313.6	11.2

It is seen from table 8.9 that the largest response from the stress in both x- and y-direction is largest for a load height of 1.2 m. The displacement is monotonically rising, but the stresses will be governing in this case. The stiffeners will be checked, again with reference to figure 8.9, in the corner between location 1 and 2, at location 3, at the critical location 4 and at location 5 where the test was performed. This gives the following load cases(ISO 19906 will be used here):

Table 8.10: Design loads for stiffener

Load case	Area [m^2]	Design Load [MPa]
Corner 1/2	1.46	5.68
Location 3	0.80	8.65
Location 4, 5	1.01	7.31

Finding the stringer design load and load patch area is very challenging due to the changing geometry in the different parts of the stringer. Therefore a load width corresponding to the length of the stiffener spacing times three is chosen. The height of the load patch is chosen in the same manner as for the stiffeners:

Two points are chosen on the stringer. One in a low stress area, and another in a high stress area. From table 8.11 it is seen that the stresses are largest in the low stress area in x-direction and in both the high and low stress area for y-direction(low stress area not included in the table) for a load height of 2.0 m. The stresses in x-direction continue to rise for higher load height, but a load height of 2.0 m is chosen for further analyses. The stringers will be checked in location 4, 6 and 8. This gives the following load cases:

Table 8.11: Response in stringer for various load cases

Load height [m]	Design load [MPa]	S11 high stress [MPa]	S11 low stress	S22 high stress [MPa]
0.4	7.31	41.3	-16.4	-80.0
0.8	5.21	57.2	-21.5	-109.9
1.2	4.91	78.1	-28.3	-149.2
1.6	4.70	94.6	-39.5	-183.1
2.0	4.54	101.2	-53.0	-215.8
2.4	4.42	118.8	-12.1	-186.7
2.75	4.33	120.2	-5.3	-178.1

Table 8.12: Design loads for stringer

Load case	Area [m^2]	Design Load [MPa]
Location 4, 8	5.09	4.54
Location 6	4.02	4.71

The bulkheads will be checked for a for a width equal to the stiffener span. The height assumed to give the largest response is the stringer span. The bulkhead will be checked between location 2 and 3, and between location 4 and 5. This gives the following load cases for the bulkheads:

Table 8.13: Design loads for bulkhead

Load case	Area [m^2]	Design Load [MPa]
Location 2/3	1.84	5.29
Location 4/5	2.33	5.11

Figure 8.11 shows the load patches for the 4 load cases being considered in location 4.

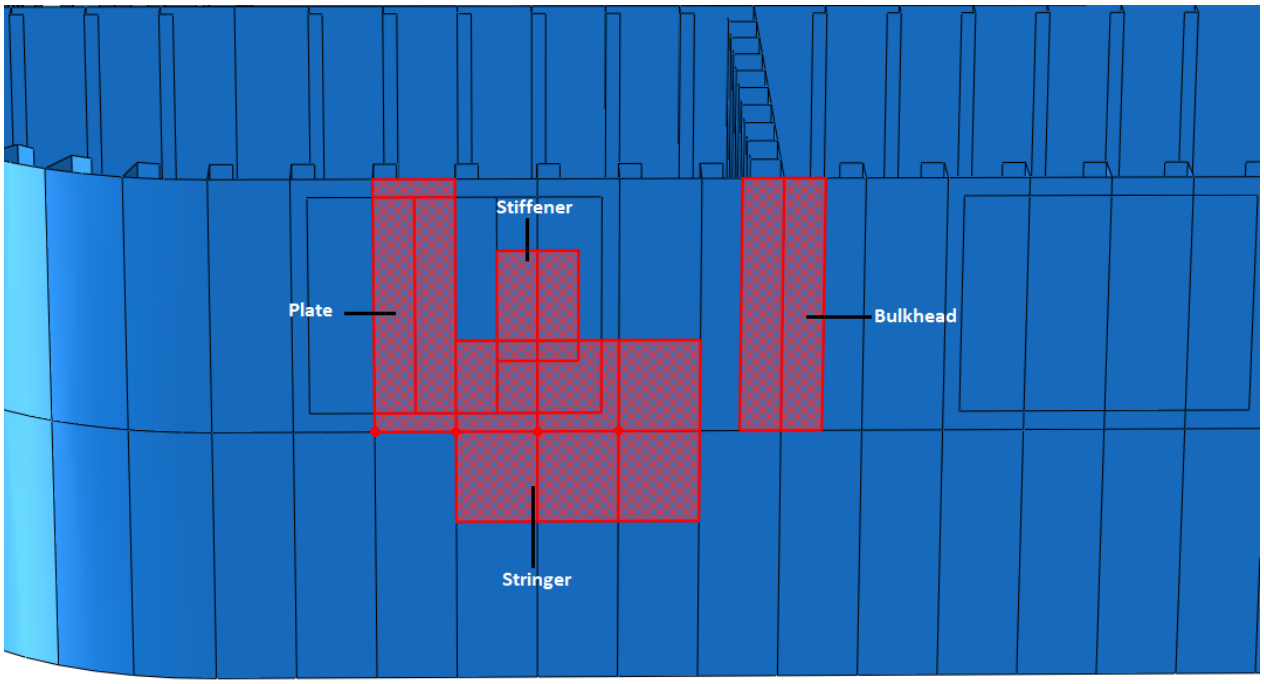

Figure 8.11: Design load patches for various load cases

8.5 Convergence Analysis and Choice of Elements

In order to get accurate results it is important to chose the right elements to use during the analysis, as well as make sure that the stresses and displacements converge towards the correct solution. This section will further elaborate on the considerations made on the choice of elements and meshing. The selection of elements are largely dependent on the problem at hand. DNV GL(2016) notes several points that are important to consider when choosing which elements to use, notably:

- Shell elements or solid elements
- Elements based on constant, liner or higher-order shape functions
- Full vs reduced, vs hybrid integration formulations
- Number of through thickness integration points(shell)
- Volumetric locking, membrane locking and transverse shear locking
- Hourglass control/artificial strain energy(for reduced integration elements)

The main objective is to find a combination of element type and mesh size that solves the problem to a satisfactory degree at the same time as being economic in terms of computational effort. For marine structures shell elements are usually preferred, and is thus chosen as the preferred element type in this thesis. Higher-order elements are preferred for accurate stress estimates, but these elements will also require more computational effort. Both linear and higher-ordered elements will be investigated in the convergence analysis. ABAQUS gives the choice of full and reduced integration. The advantage of using reduced integration is that they are less prone to shear locking than full integration, but they may, however, produce zero energy modes. It is possible to use hourglass control to prevent this from happening. Both full and reduced integration will be investigated, but reduced integration is assumed to perform better.

The model contains many different sections, and the geometry is very complex. It is therefore important to ensure that the different parts are partitioned correctly to make sure that the quality of the mesh is sufficient. Figure 8.12 shows the model after partitioning. Abaqus gives several options for meshing controls. Since the geometry is complex the element shape chosen is quad-dominated, i.e. quad elements is mainly used but triangles are allowed in transition regions. The are also several options for technique to be used during the meshing. The relevant ones are free and structured meshes. In figure 8.12 the green areas uses structured meshing while the pink areas uses free meshing. Free meshing is used for the areas that are especially complex.

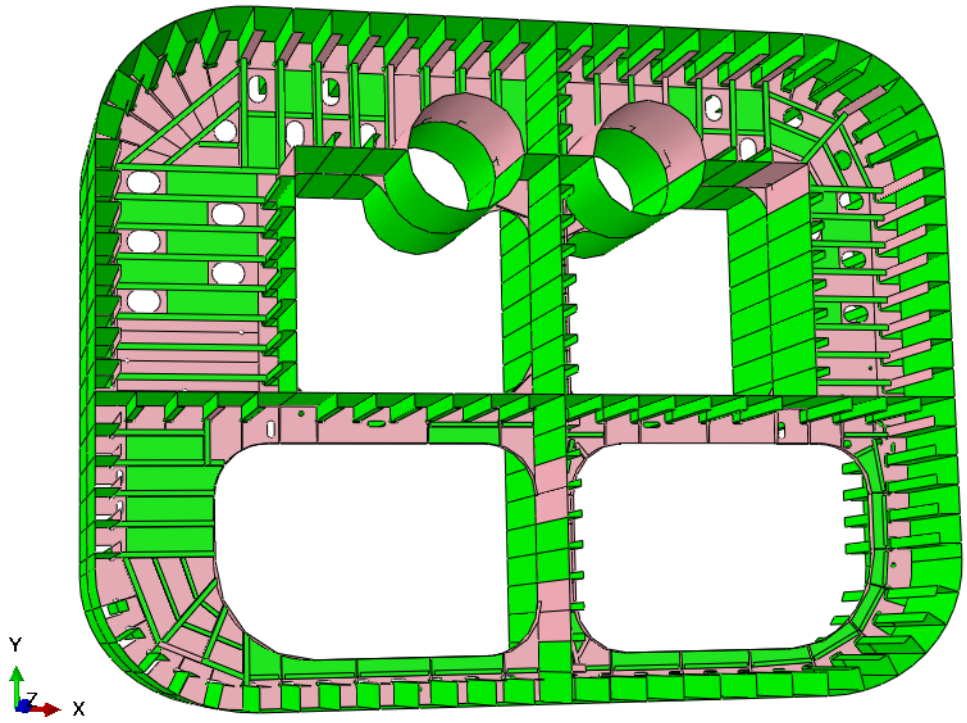

Figure 8.12: Partitioned model to be meshed

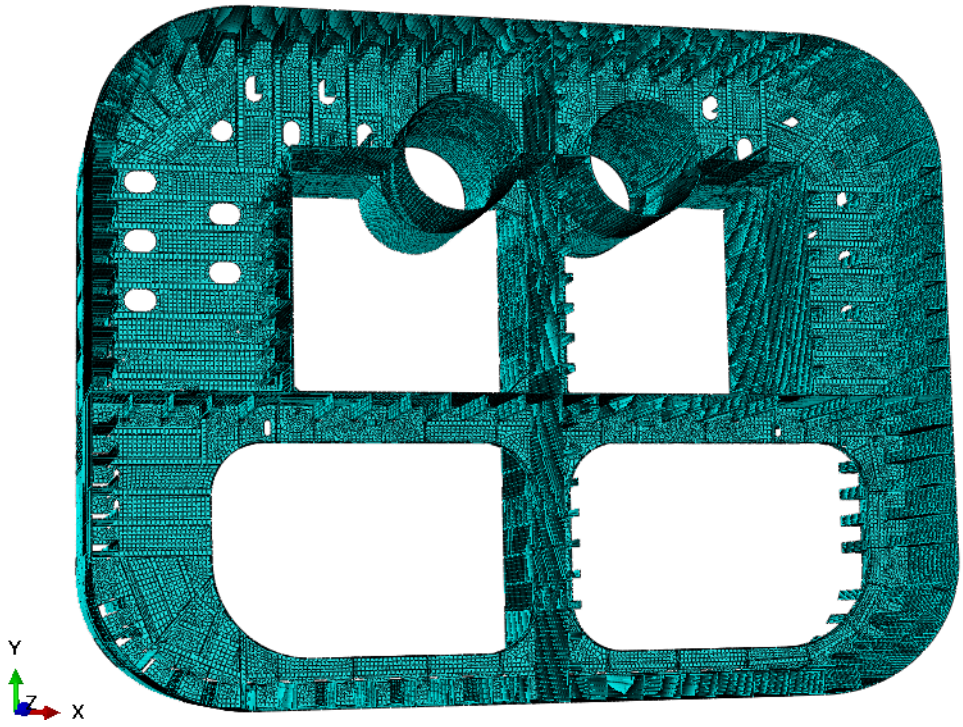

Figure 8.13: Meshed model with a mesh size of 100mm

The meshed model for a mesh size of 100mm is shown in figure 8.13. It is seen that some parts of the

mesh are still not perfect, especially around holes, intersecting stiffeners and other small details. They are deemed to be sufficiently accurate as it is both time consuming and difficult to get every part meshed perfectly.

For the choice of mesh size, DNV GL(2016) suggests using a mesh that is detailed enough to capture the relevant failure mode. The general rule is that the results get more accurate as the mesh size is reduced, but at the same time the computational time increases drastically. So the goal is to find a balance between computational time and acceptable results. We will here look at several different elements with regards to integration rules, element shapes(i.e. order of shape function) and element sizes. Below a convergence analysis is performed using IACS design load of 4.74 MPa over an area of 7.14 m^2 which encompasses both plate and stiffeners. The load is applied at the top left corner of the model. The sampling points are for the maximum von Mises-stress in the ice loaded area which occurs in the middle of the flange, for the maximum displacement which occurs in the middle of the plate between two stiffeners and one point in the stringer where it is expected to be a lower stress area. The locations of the checks are highlighted in figure 8.14.

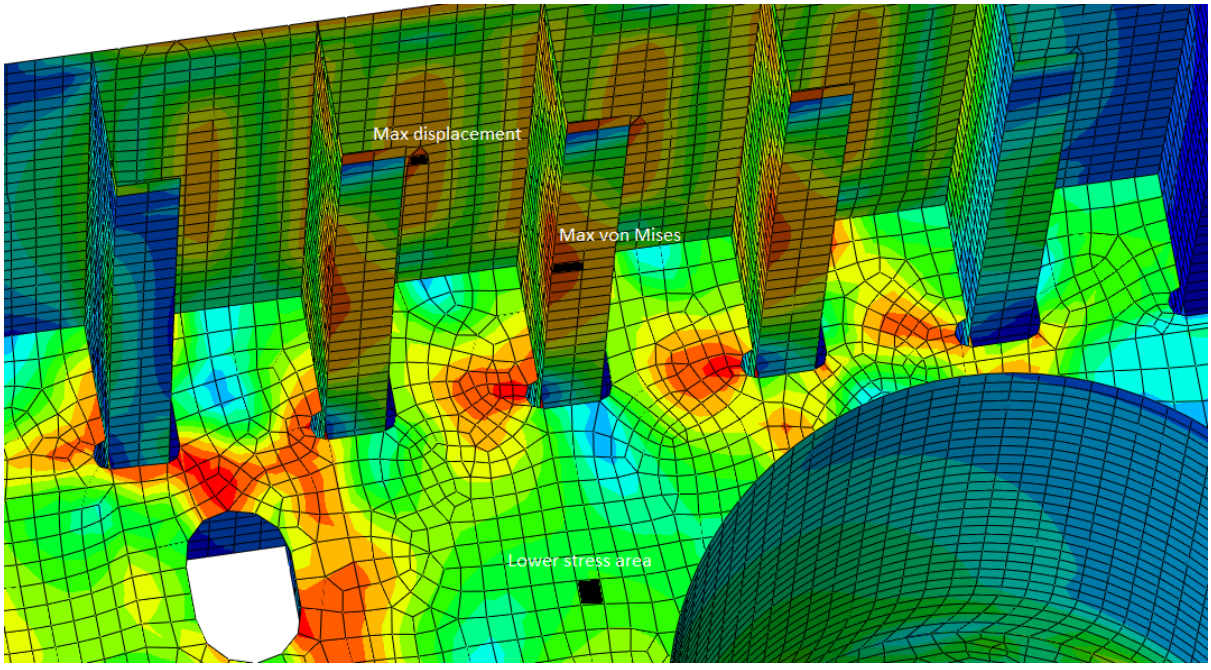

Figure 8.14: Locations for convergence check

Four element types are analysed, namely S3R-, S4-, S4R- and S8R-elements(see section 7.2.4). The mesh size ranges from 200 mm to 75 mm. Because of the size of the model, element sizes smaller than this

was not feasible, as it would have gone many days for the calculations to be done, especially for the S8R-elements which proved to be very computationally expensive. The element size to be used in analysis is expected to be larger than 75 mm, so this should not cause any problems as the solution should have converged by this point.

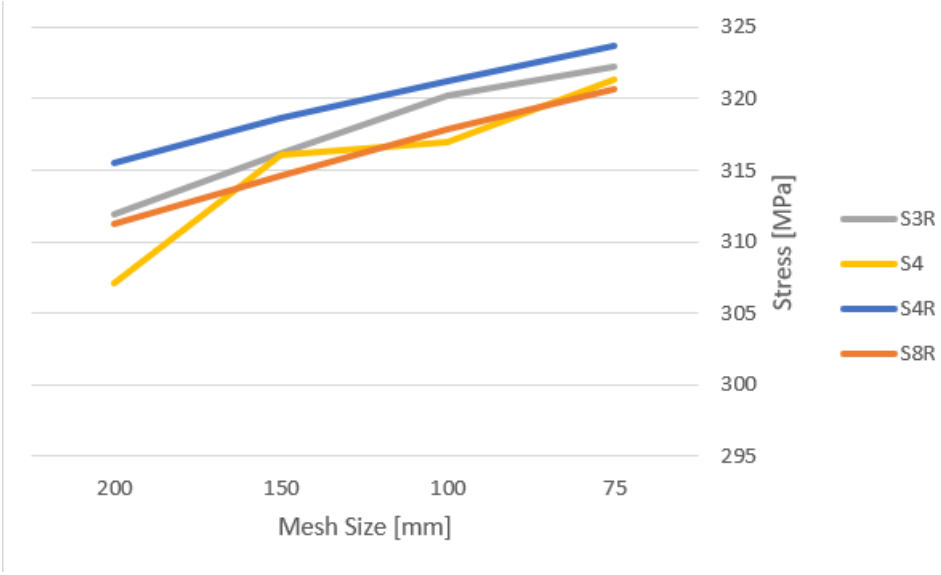

Figure 8.15: Convergence of stresses at point of maximum von Mises-stress

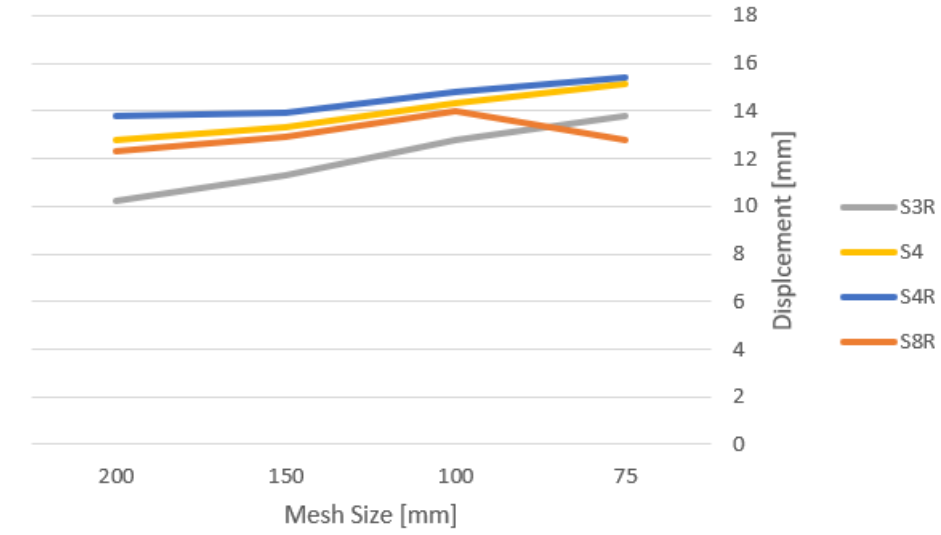

Figure 8.16: Convergence of displacement at point of maximum von Mises-stress

It is seen from figure 8.15 that the stresses for the different elements converge at a similar rate. The S4R-elements gives the most conservative stresses for the whole range of mesh-sizes. The S4-elements

converge at the slowest rate. From figure 8.16 the S4- and the S4R-elements seem to converge at the same rate, and also in this case S4R gives the most conservative results, but this is by a very small margin. In general the displacement converges faster than the stress. This implies that if the stress has converged the displacement can be assumed to have converged as well. The S3R-elements converge slower for displacements, but are similar to S4R-elements for stresses. At the point of maximum displacement, which can be found in the appendix in figure C.1 and C.2, the S8R-elements has already converged for an element size of 200 mm, while the other elements converges around and element size of 100 mm. Similar results are observed in figures C.3 and C.4. In general it seems like the results are converged for an element size of 100 mm, and through all the convergence tests the S4R-elements seems to consequently behave most conservatively and is therefore chosen as the element size and type to use in the analyses. For some of the checks the stresses do get a little bit higher for the 75 mm elements, but the computational time is long so 100 mm seems like the best compromise regarding accuracy and computational efforts.

8.6 Setup of Analysis Step

The analysis is performed using steps. In the step-module the type of load is chosen, in this case a static analysis is performed. It is also possible to include or ignore nonlinear effects of large deformations and displacements. In this thesis a non-linear analysis is performed, and a large deformation formulation is therefore applied. Full Newton solution technique is used to solve the nonlinear equations. The loads are applied in automatic increments, i.e. Abaqus chooses the appropriate size of the increments. The increments are slowly increased until equilibrium is no longer achieved, whereas the increment size is decreased. The input used in this thesis was changed from the initial input, using is a maximum increment size of 100, an initial increment size of 0.25 since increment sizes larger than this usually do not reach equilibrium, a minimum increment size of $1*10^{-6}$ and a maximum increment size of 1(when the total increment is 1 the analysis is finished).

9 Non-Linear Static Analysis

In this section the different results obtained from the non-linear static analysis of the local model for the different load cases will be presented. The analysis is conducted to check the structural integrity of the different structural components that make up the model. The following cases will be analysed:

- **9.1** IACS design load with plate and stiffener design load conditions
- **9.2** Response in Plating due to Local Ice Pressure
- **9.3** Response in Stiffener due to Local Ice Pressure
- **9.4** Response in Stringer due to Local Ice Pressure
- **9.5** Response in Bulkhead due to Local Ice Pressure

9.1 Response due to IACS Design Load

From the calculations shown in section 8.4.3 using IACS polar class PC4, a design load of 4.74 MPa was found to act over an area of 7.14 m^2. The outer stiffeners are dimensioned according to Polar Code PC4 class. The design criterion chosen is the von Mises yield criterion, which states that the maximum von Mises stress anywhere on the structure should not behigher than the yield stress of the material. In this case we have a yield strength that ranges from 336.9 MPa for the thickest components to 357 MPa for thinner members. A safety factor should also be added, and the safety factor present will be investigated as long as the material does not reach yield stress.

Figure 9.1 shows the von Mises-stress of the model where the load has been applied. The maximum stress is 450 MPa. The location of the maximum stress can be seen in figure 9.2, i.e. at the underside of the stringer where the bracket connects with the stringer plate. At corners or cut outs, such as here, stress singularities appear with the implication that the stresses do not stop rising for increased mesh refinement. In reality such sharp corners do not exist, there will always be some area for the stresses to spread over. A finer mesh at such complex areas may give more correct results, as this is a limitation with the finite element method. If the singularities are ignored the maximum von Mises-stress in the outer plate is found to be 321 MPa. This is under the yield strength and gives a safety factor of 1.04.

The maximum von Mises-stress in the stiffeners is 340 MPa which is just over the yield strength. The largest von Mises-stress on the topside of the model occurs in the stringer plate. In the orange areas in the stringer in figure 9.1 there is significant yielding, but the magnitude of the stresses is not much more than yield stress, ranging from 355-365 MPa, except for at the cut-outs where the stresses are larger. IACS is based on plastic methods to dimension the scantlings, so some yielding is to be expected.

The maximum displacement is 34.3 mm and occurs at the middle of the plate field between two stiffeners. This is a rather high displacement. In the plate field this displacement is almost exclusively in the load direction. For the stiffeners there is some warping. This is due to the L-shape of the stiffeners, which causes rotation of the stiffeners. Because of this there is also significant displacement in longitudinal direction, normal to the load direction, in excess of 13 mm.

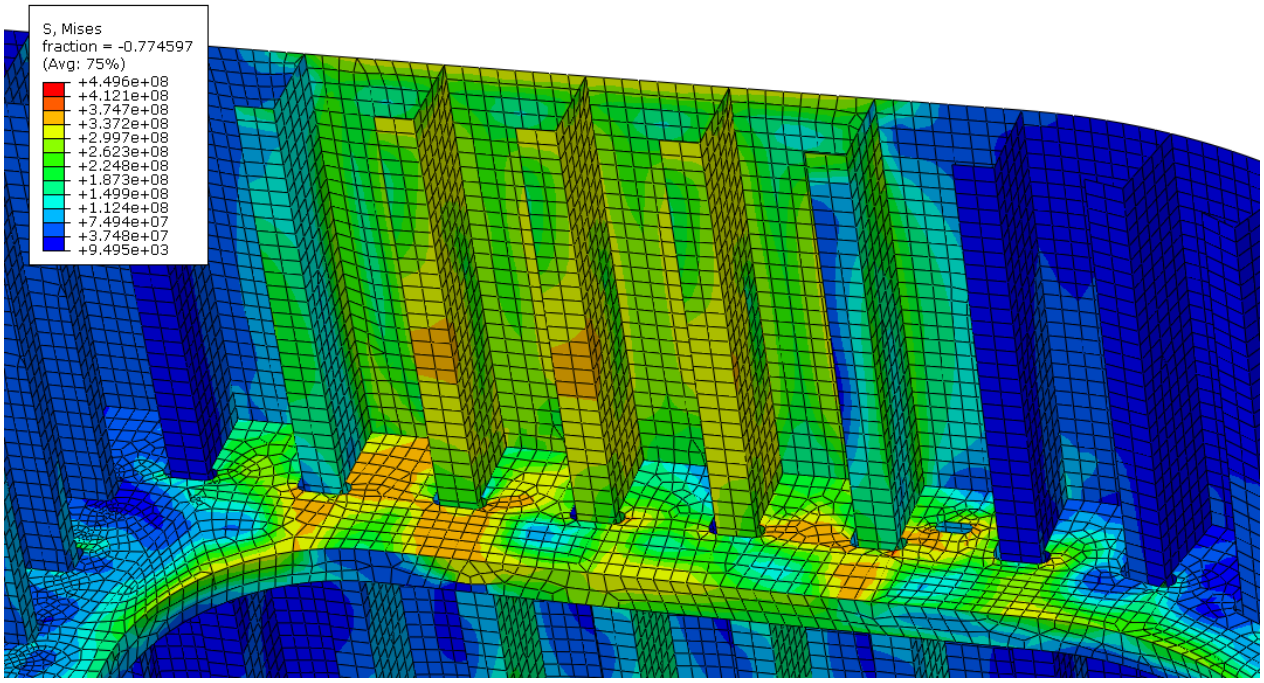

Figure 9.1: von Mises stress distribution due to IACS design load

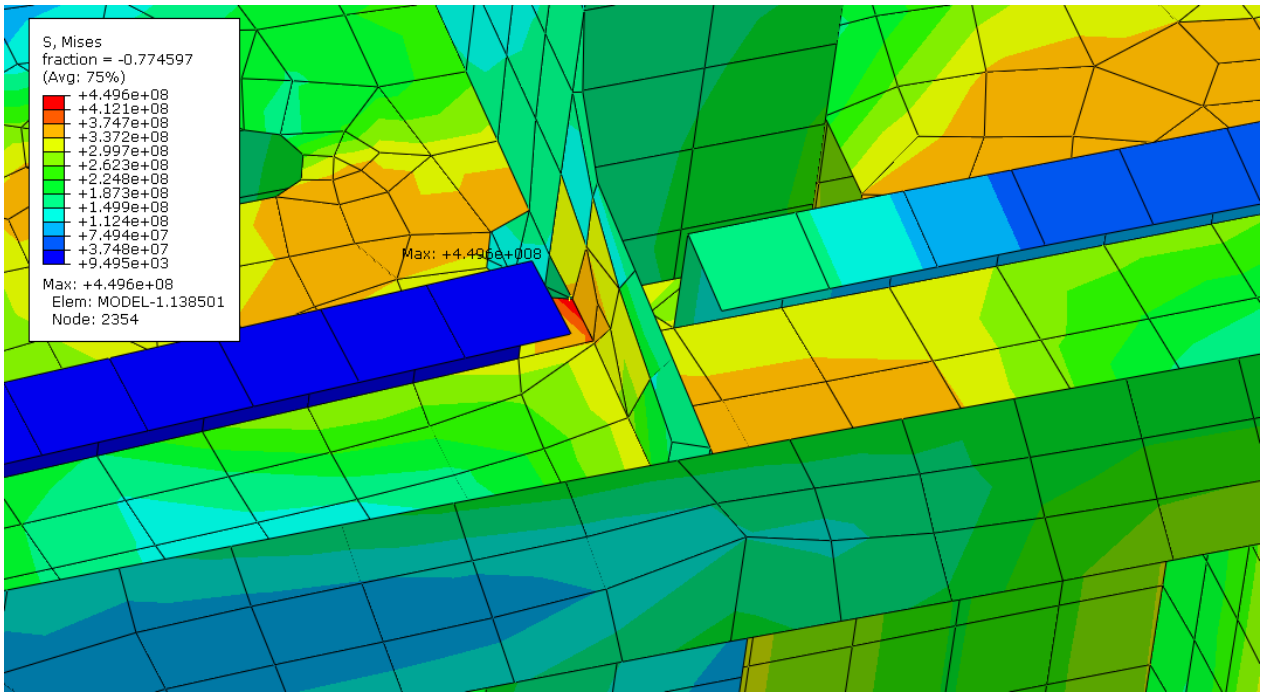

Figure 9.2: Maximum von Mises-stress due to IACS design load

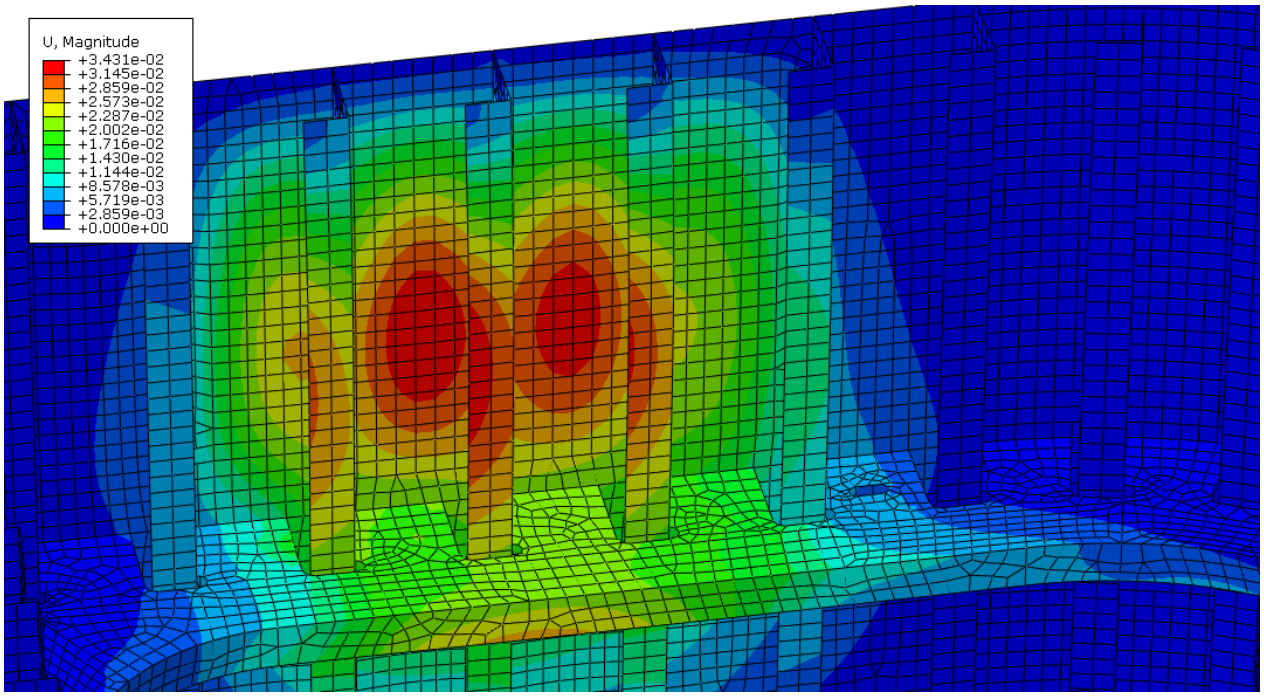

Figure 9.3: Displacements due to IACS design load

When the stiffener design load, with a magnitude of 5.69 MPa, is applied(see section 8.4.3) in combination with the average pressure of 4.74 MPa, a stress distribution as seen in figure 9.4 results. The maximum

von Mises-stress in the plate now becomes 339 MPa, while the maximum stress in the stiffeners is 349 MPa. This is right below yield stress, so there is a significant increase in the stress field. The same is seen in the stringer plate, where there is now extensive yielding. Due to the very quadratic shape of the load patch the increase in the force is big. Had the load patch been narrower and the loading acted over more stiffeners, the effect of the increased pressure load would not have been so extensive. Figure D.1 and D.2 in the appendix show the stress distribution in x-direction for the two load cases. The maximum stresses are 395 MPa and 419 MPa respectively, and the figures show the buckling mode of the plates if the pressure were to be increased. Figure D.3 and D.4 show the stress-strain plots in the middle of the plate area. The strains are excessive for the stiffener load condition.

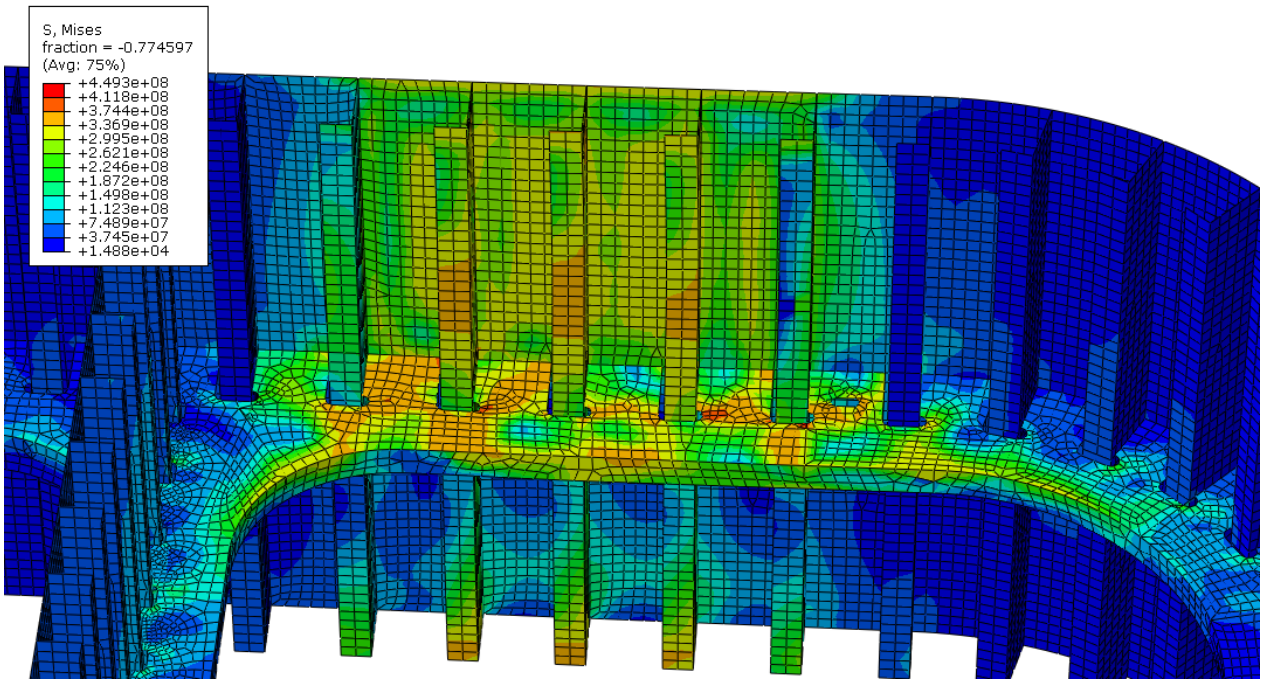

Figure 9.4: von Mises stress distribution due to stiffener design load

9.2 Response in Plating due to Local Ice Pressure

In this section the load cases presented in section 8.4.3, table 8.8, will be presented. Figure 9.5 shows the von Mises stress distribution in location 4, while figure 9.7 shows the distribution in location 1. The results show that the largest stresses in the plate field occur in location 1, which is quite surprising. The maximum von Mises-stress in location 1 is found to be 337 MPa which is the exact same as the yield strength of the material here. In location 4 the largest stress in the plate field is found to be 332 MPa.

Figure D.5 shows the plastic straining at location 1. The plastic straining is significant in the middle of the plate, this indicates that there has been significant redistribution of stress in this area. The same pattern is seen at location 4. The maximum stress occurs in the stringer plate for both locations, in the cut-off where the stringer intersects with the bracket, where a singularity point appears. The maximum deflection occurs in the middle of the plate field and has a magnitude of 17.3 mm at location 4 and 14.6 mm at location 1. One would expect the plastic straining would cause larger deformations at location 1 but this is not the case.

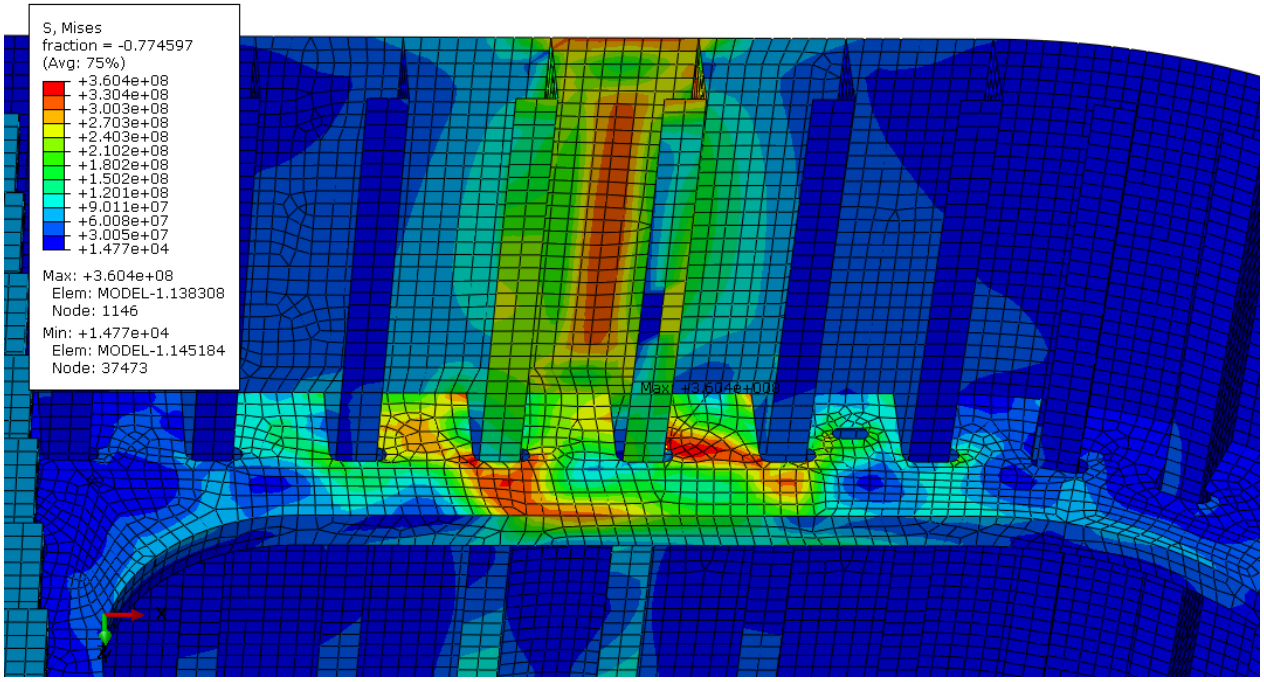

Figure 9.5: von Mises stress distribution for plating design load, location 4

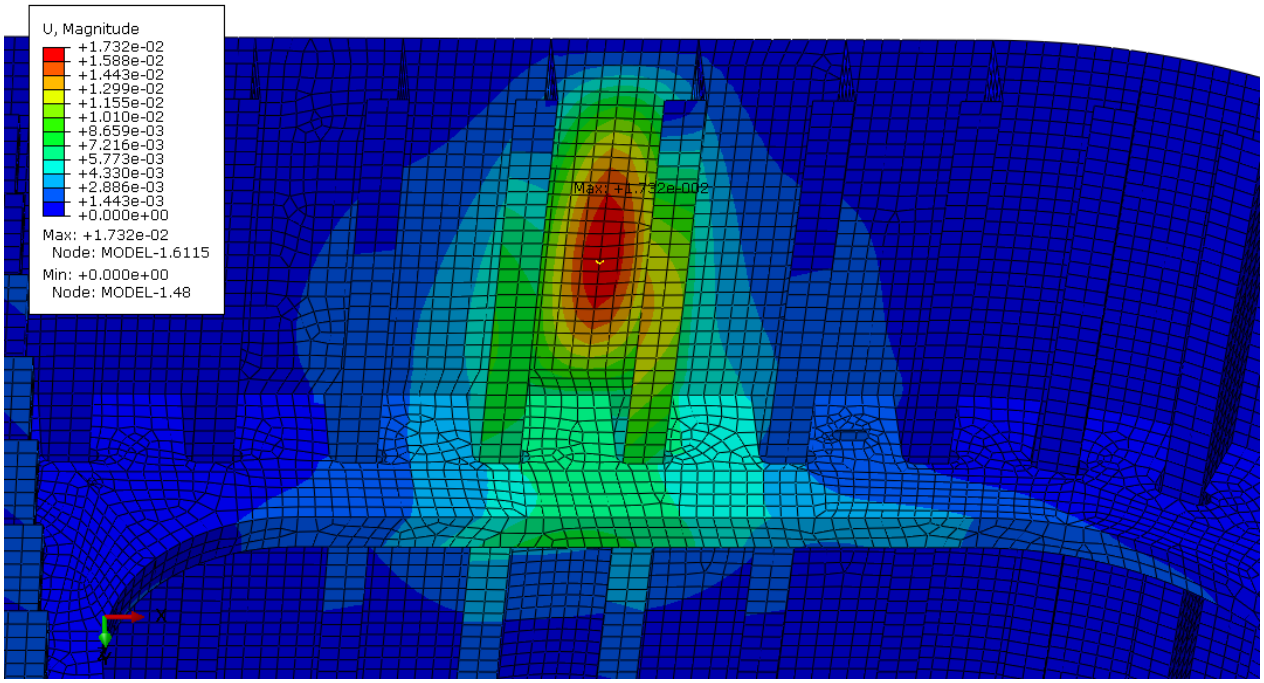

Figure 9.6: Displacement for plating design load, location 4

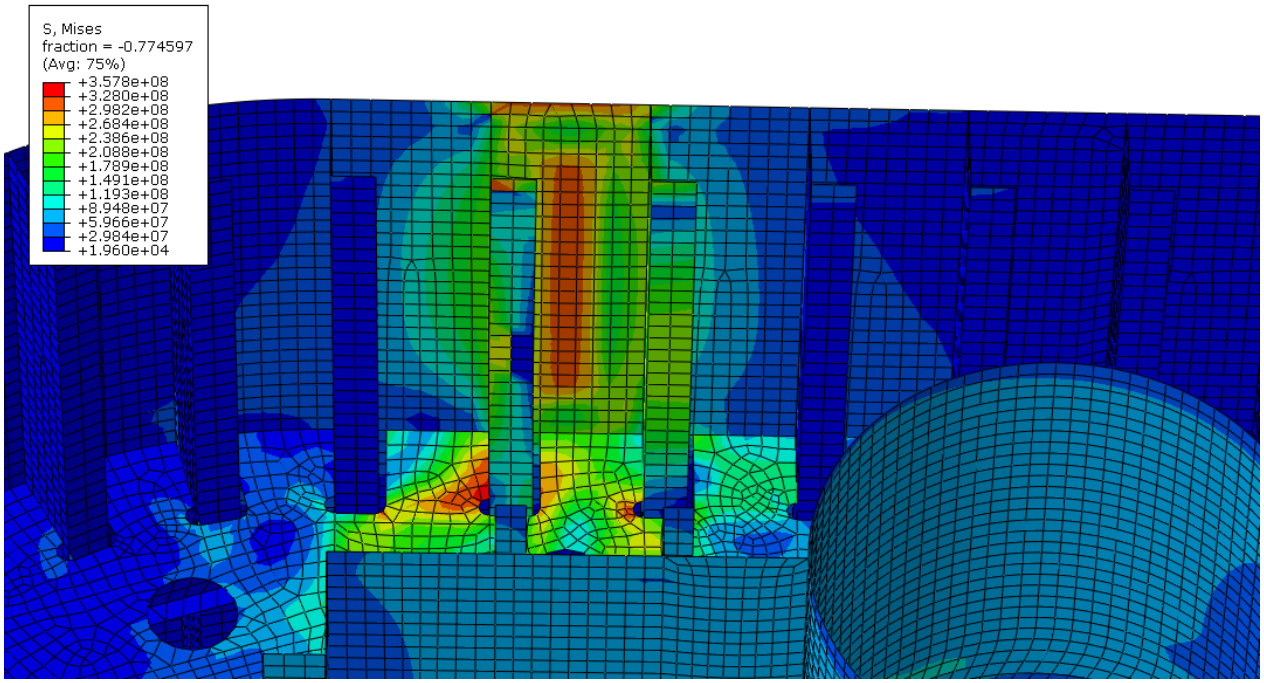

Figure 9.7: von Mises stress distribution for plating design load, location 1

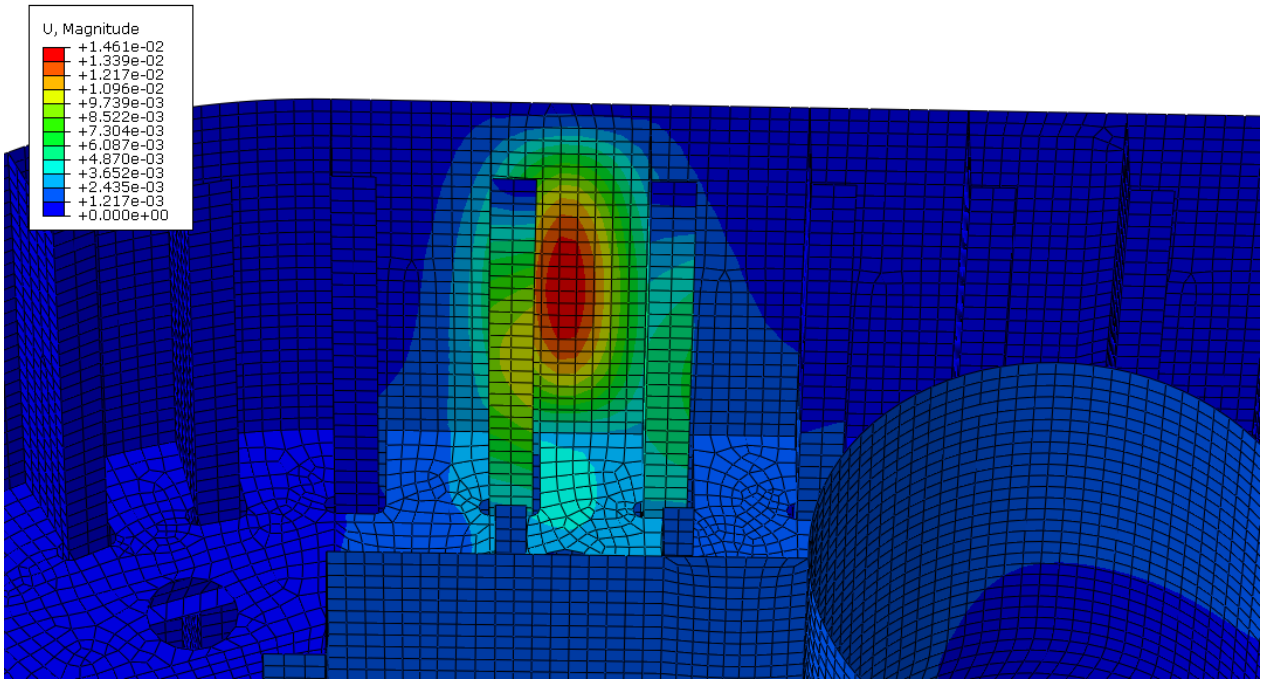

Figure 9.8: Displacement for plating design load, location 1

In the appendix the von Mises stress distribution and displacements are presented at location 2 and at the corner between location 3 and 4. In location 2 the maximum stress in the plate, which is seen in figure D.6, is found to be 303 MPa. This is well under the yield strength of the material. For this load case there is no yielding in the stringer plate either. The stresses in the stiffeners are moderate as well, so here it seems the stringer and the adjacent structure provides better strengthening than in location 1 for this load case. The maximum displacement is 7.5 mm which is moderate as well. The largest displacement occur in the stiffener. For the corner plate the maximum stress in the plate is 315 MPa. Some plastic straining is seen in the middle of the plate as the stresses are above the proportionality stress. There is significant yielding in the stringer plate due to the smaller area for the stresses to spread around. The maximum displacement is found to be 11.6 mm.

9.2.1 Parameter Study of Plating

A parameter study is performed in location 1 to see for what design load the plate will experience yielding. Figure 9.9 shows the maximum von Mises-stress in the plate, which occurs in the middle of the plate, as a function of the design ice pressure. It is observed that the stress crosses the yield strength for a design pressure in excess of 5 MPa. In this area a redistribution of stresses occur as the plate experiences plastic

straining of the material. It is seen in figure 9.10 that effects of buckling of the stiffener and plate are experienced(the effect is exaggerated here for illustrative purposes).

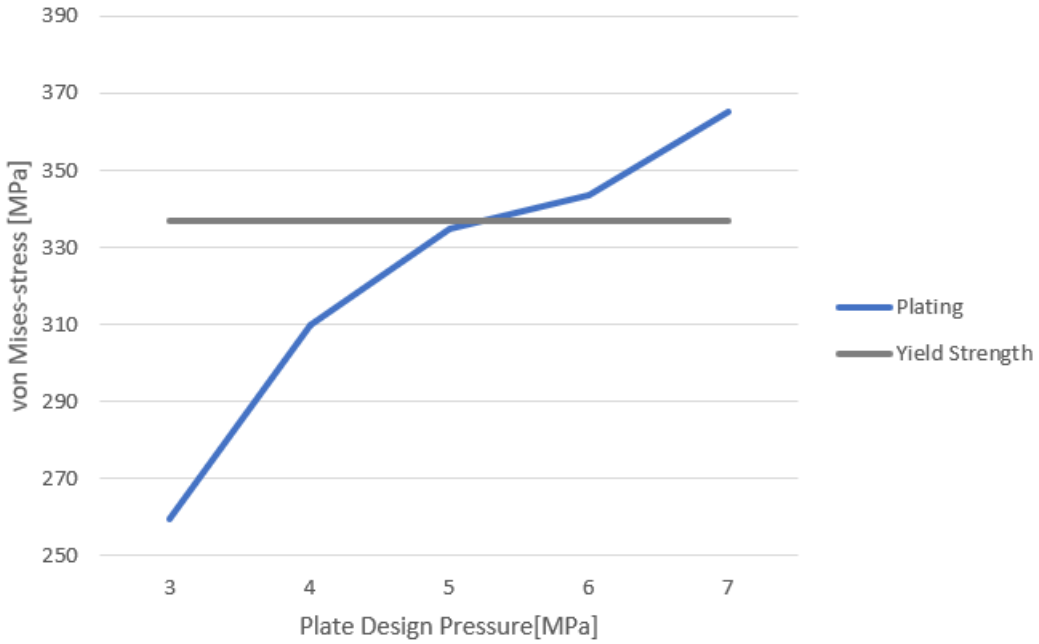

Figure 9.9: Maximum von Mises-stress vs design ice pressure in plate

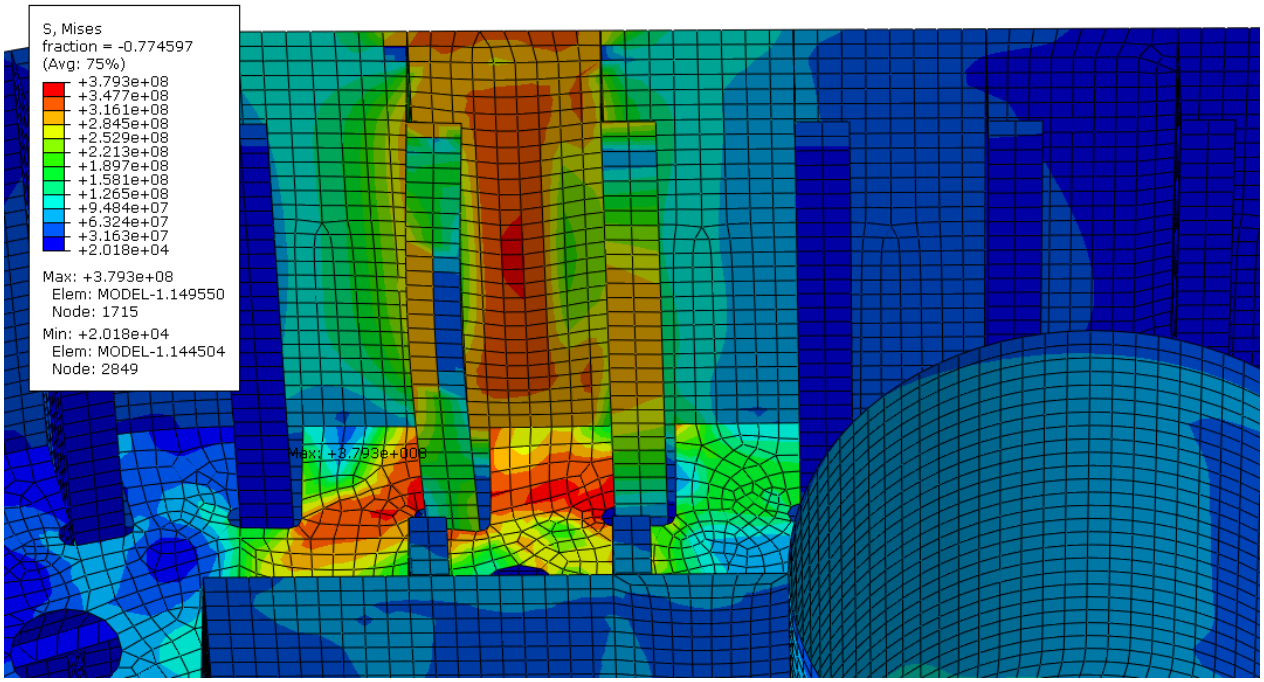

Figure 9.10: von Mises-stress distribution for a design pressure of 7 MPa

9.3 Response in Stiffener due to Local Ice Pressure

The stiffeners will be checked according to table 8.10, section 8.4.3. Figure 9.11 shows the von Mises-stress for the stiffener in location 4. The maximum stress occurs in the web with a magnitude of 307 MPa. This gives a safety factor of 1.10, so it is clear that the stiffener in this region is strong enough to carry the ice pressure it is exposed to. From figure D.10 that there is a small amount of plastic straining in the high stress area of the stiffener however. The flange experiences a maximum stress of 304 MPa. The stringer experiences some yielding in the region around the cut-out also for this load case. Figure 9.13 gives the stress distribution in location 5. In this case the stiffener chosen is further apart from the bulkhead, and this has an effect on the stresses it experiences. The maximum stress in the stiffener is here 308 MPa and 306 MPa in the web and flange respectively. The increase here is due to it being further away from the bulkhead, and thus having less stiffening in this area. The maximum displacement in location 4 is 11.7 mm, and occurs in the free end of the stiffener flange. The majority of the deflection is in y-direction, i.e. in load direction, with a magnitude of 10.4 mm. There is also significant sideways deflection, i.e. in longitudinal direction, with a magnitude of 5.2 mm. This is due to the L-shape of the stiffener, and this would probably not be observed if T-stiffeners were used. At location 5 the maximum deflection is 10.6 mm, and is also found at the free end of the stiffener flange.

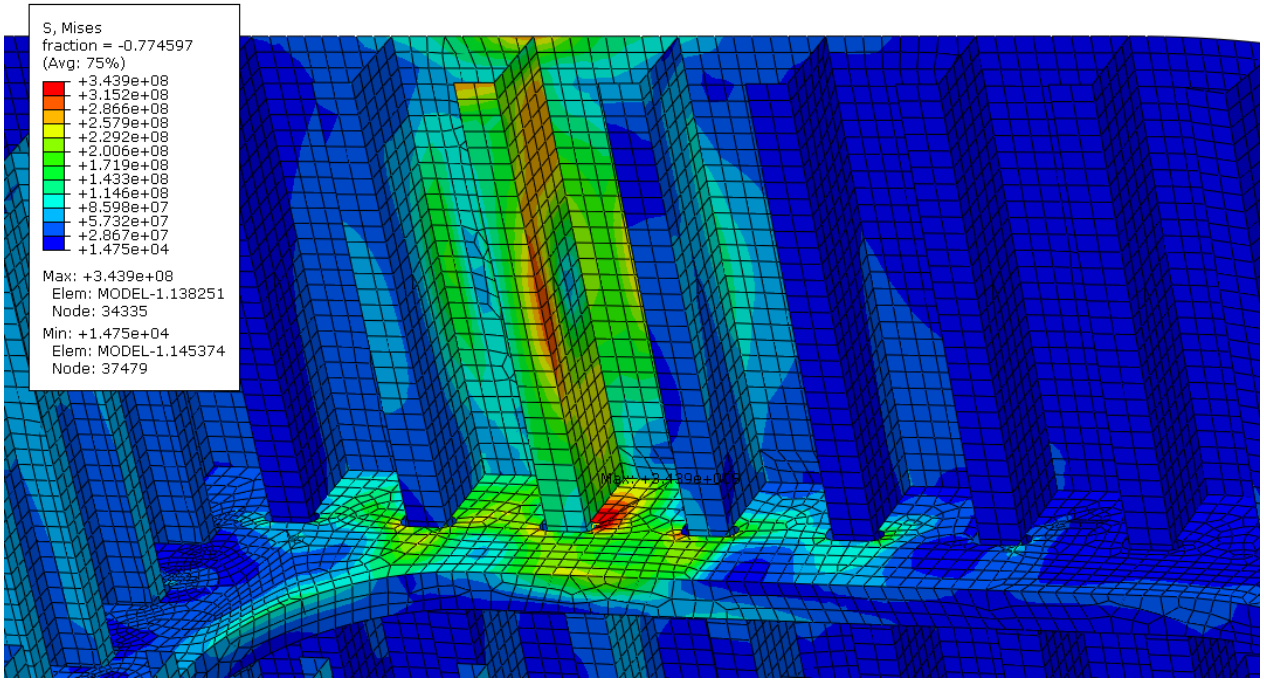

Figure 9.11: von Mises stress distribution for stiffener design load, location 4

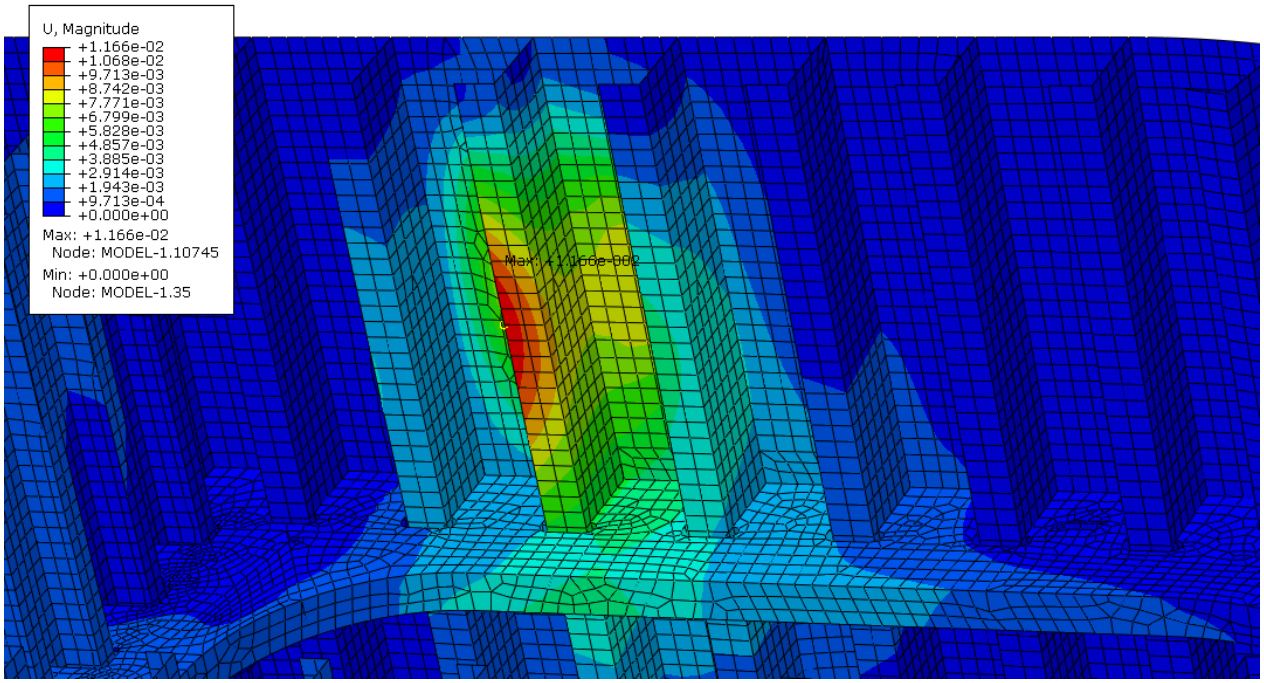

Figure 9.12: Displacement for stiffener design load, location 4

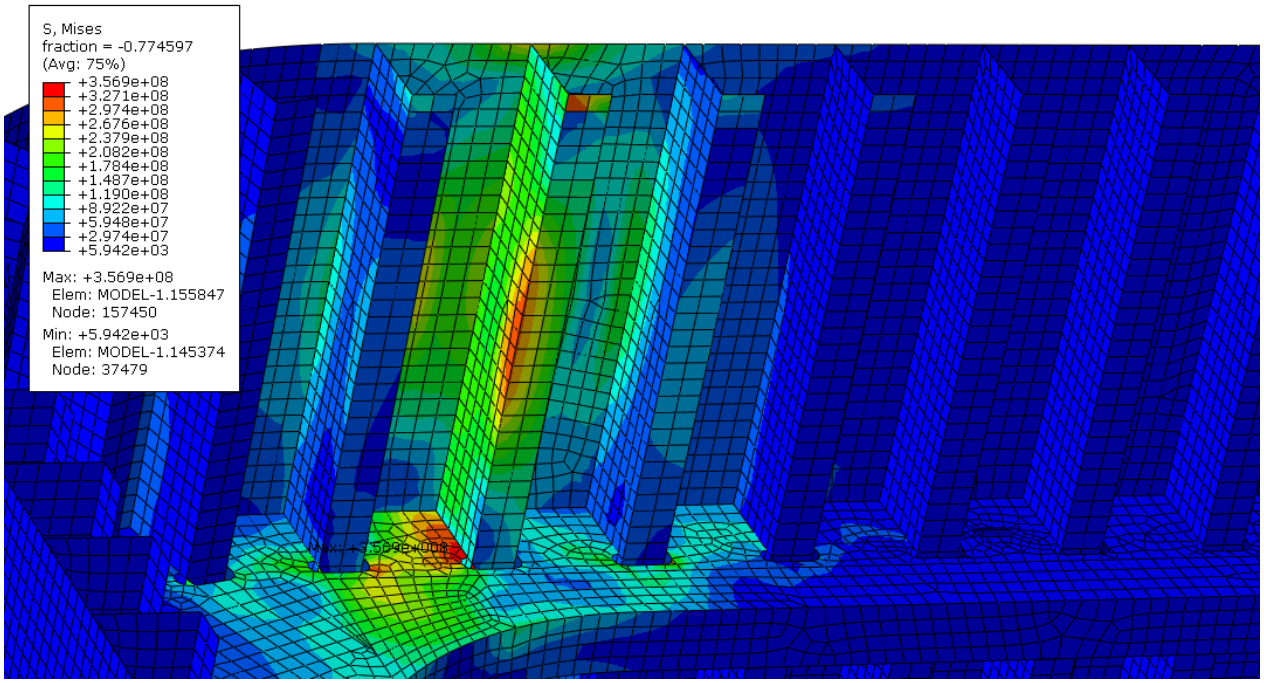

Figure 9.13: von Mises stress distribution for stiffener design load, location 5

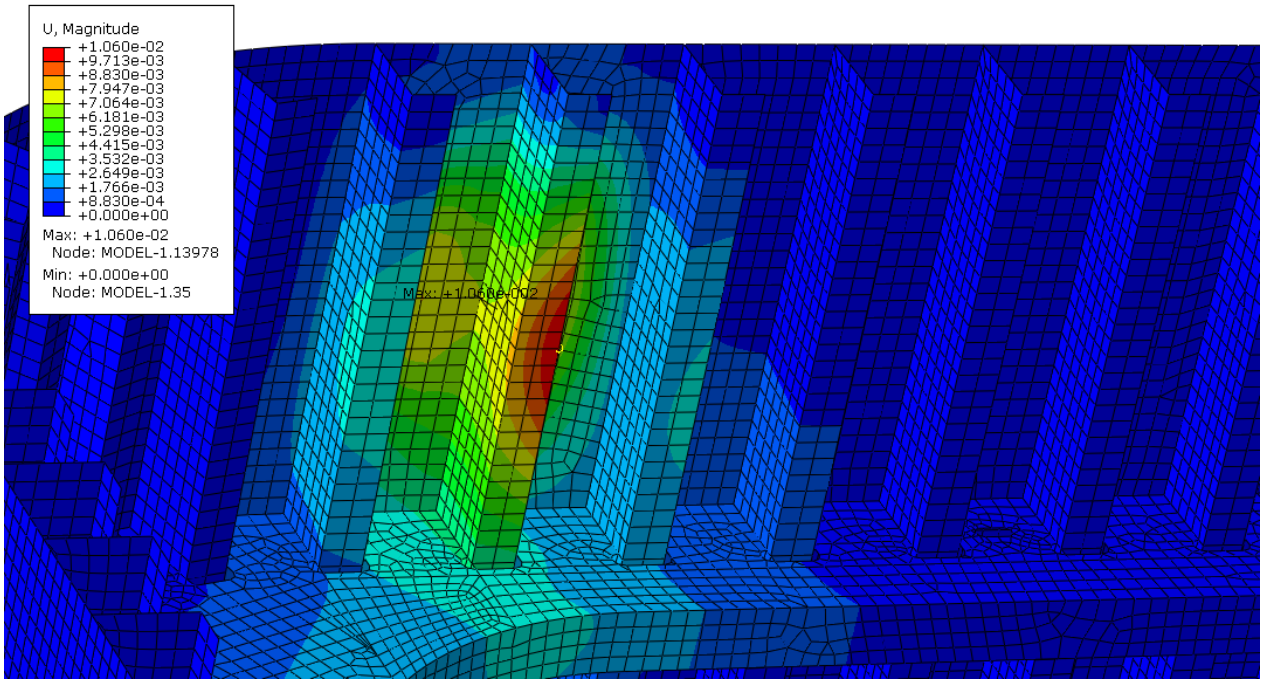

Figure 9.14: Displacement for stiffener design load, location 5

In appendix D the stress and displacement distribution is presented for location 3 and at the corner between location 1 and 2. Location 3 is a region with smaller stiffener spacing, and thus smaller area and larger pressure. The stiffener in location 3 is also here relatively close to the bulkhead, and the stresses are moderate with a maximum magnitude of 304 MPa in the connection between the web and flange. Also here some yielding is observed in the stringer plate, around holes and cut-offs. The maximum displacement is here 9.8, so this part of the structure is better strengthened, which is as expected. The stiffener at the corner between location 1 and 2 experiences the least amount of stress. Here the maximum stress in the stiffener is 247 MPa, with little to no yielding experienced in the stringer either. The deflection is small as well with a maximum value of 6.9 mm.

9.3.1 Parameter Study of Stiffener

Since the stiffeners all seem to be adequately designed to resist the ice actions they are exposed to, a parameter study will be performed on the stiffener in location 5. This location is chosen because it was the stiffener that experienced the largest von Mises-stresses and will thus be the governing response of the structure. Figure 9.15 shows the maximum von Mises-stress in the web and flange respectively, along with the yield strength of 336.9 MPa. It is observed that as the stresses approaches yield strength, the

maximum stress rises slower. This is due to redistribution of stresses in the stiffener as the material goes from behaving purely elastic to experiencing plastic deformations. The web reaches stresses in excess of the yield strength for a design ice pressure of 11 MPa, while for the flange it is for a pressure of 12 MPa. When the design ice pressure exceeds 13 MPa the maximum von Mises-stress shifts from the web to the flange. For a pressure of 14 MPa several components exhibit buckling behaviour. It is seen in figure 9.16(the deflections are exaggerated for illustrative purposes) how the stringer, bracket and stiffener all experience large deflections. It is also observed how the bracket helps in stabilizing and stiffening the vertical stiffener.

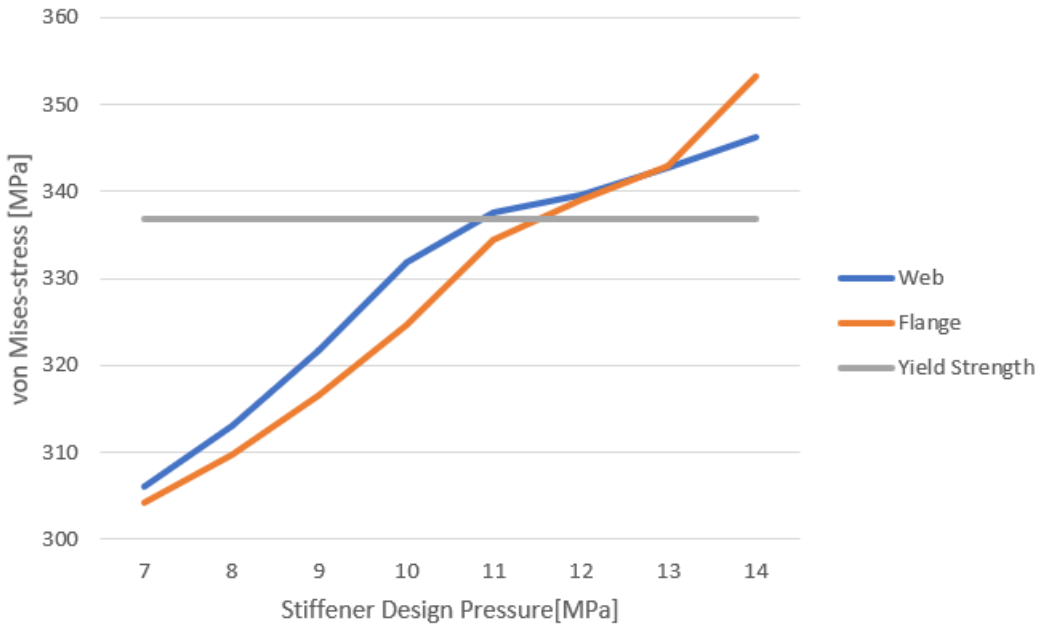

Figure 9.15: Maximum von Mises-stress vs design ice pressure in stiffener

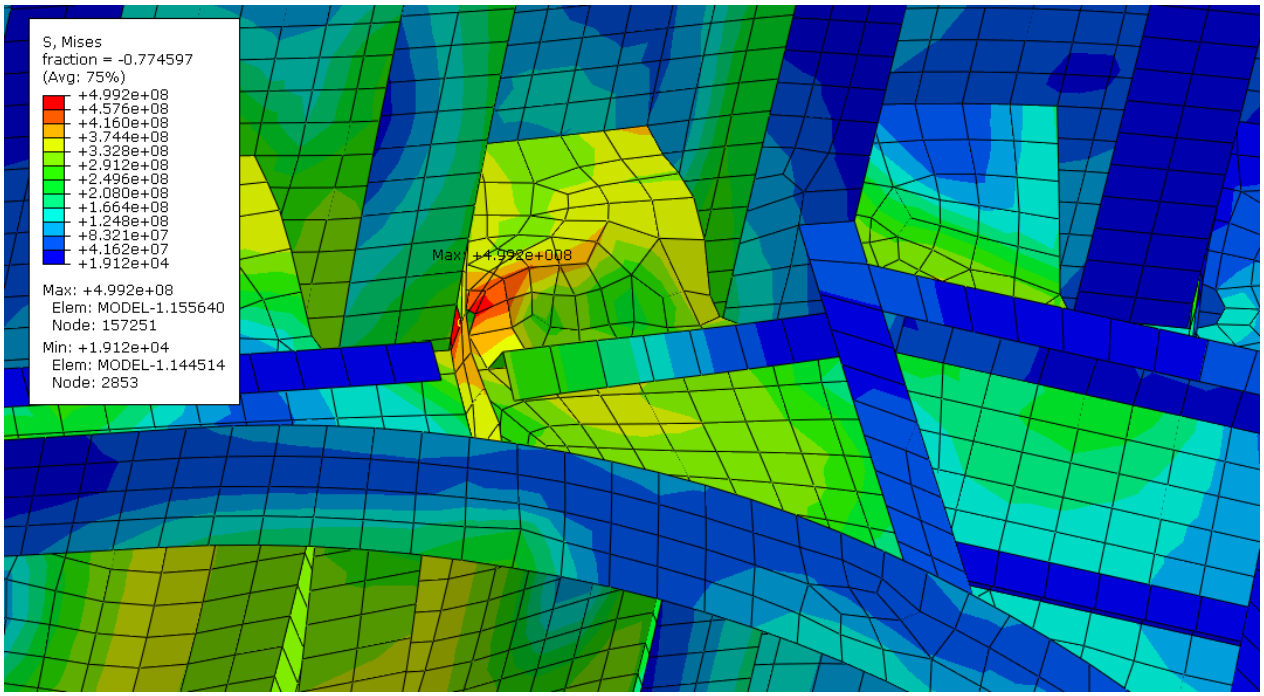

Figure 9.16: Buckling behaviour of stringer, bracket and stiffener

9.4 Response in Stringer due to Local Ice Pressure

The design loads applied for the stringer is found in table 8.12 in section 8.4.3. The stress distribution in the stringer plate can be seen in figure 9.17. There are large areas in the stringer that are yielding. The maximum stress is found between the second stiffener and the large hole in the stringer plate, with a magnitude of 393 MPa. The yield strength of the steel in the stringer is 357 MPa, so this is well above the yield strength of the material. This is also the only area with significant yielding, if the edges with cut-outs are ignored, as these are singularity points. Figure D.15 in the appendix shows this, the plastic strain is prominant in this area, but not elsewhere on the stringer. Figure 9.19 shows the stresses at location 8. It is clear that the structure has more area to carry the design pressure in this location. The maximum stress in the stringer, apart from the edges, is here 358 MPa, i.e. just above yield stress. The plastic straining seen for this design load is mainly contained to the red patch stretching from the stiffener to the hole on the left side as seen in figure 9.19, so there is some redistribution of the stresses. The maximum deflection at location 4 is 60 mm, which is significant. The location of the maximum deflection is seen in figure 9.18. The large deflection may suggest that buckling is occurring along this free edge. Away from the edges the maximum displacements are around 20 mm, which is still a significant amount. The majority of this deformation is downward. The best action to strengthen the stringer in this area would be to increase the

stringer plate thickness, and strengthening of the supporting stiffeners. This implies that the stringer is not sufficiently strengthened to be able to carry the design pressure. The maximum deflection at location 8 is 16.6 mm which is more reasonable. This can be seen in figure 9.20. Also here it happens along a free edge. Away from the edges the deformations are not that severe here either, with a maximum deflection of 10 mm.

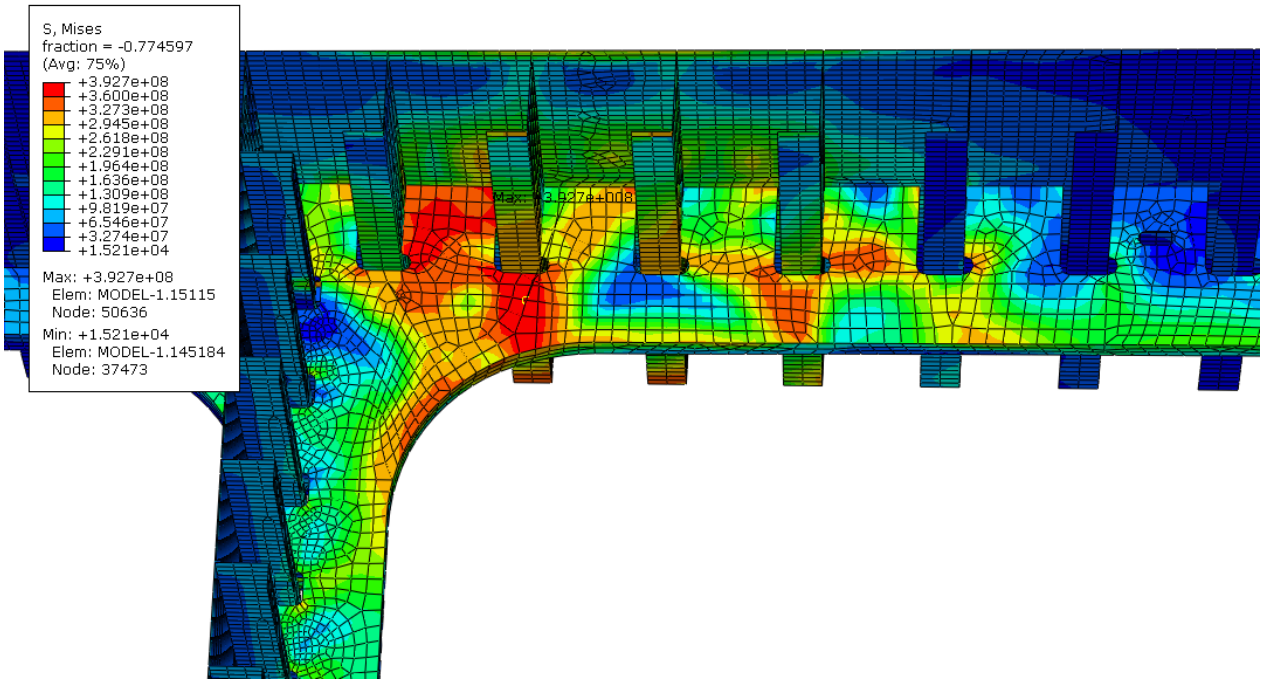

Figure 9.17: von Mises stress distribution for stringer design load, location 4

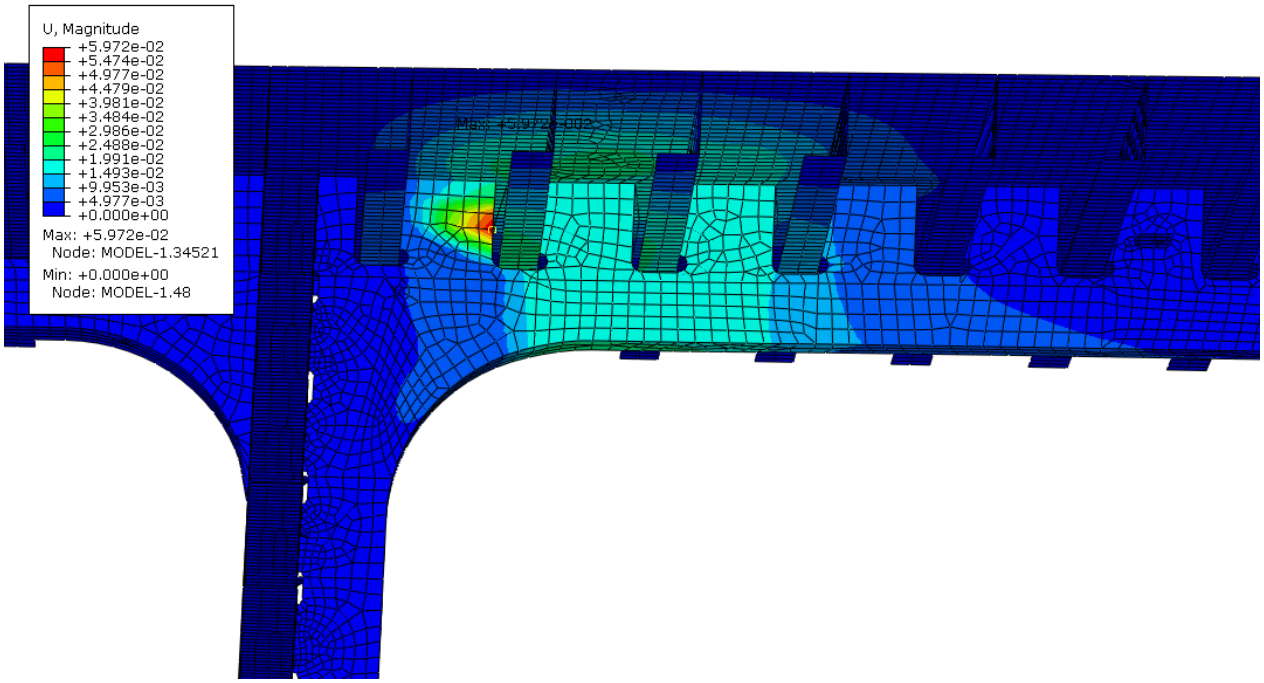

Figure 9.18: Displacement for stringer design load, location 4

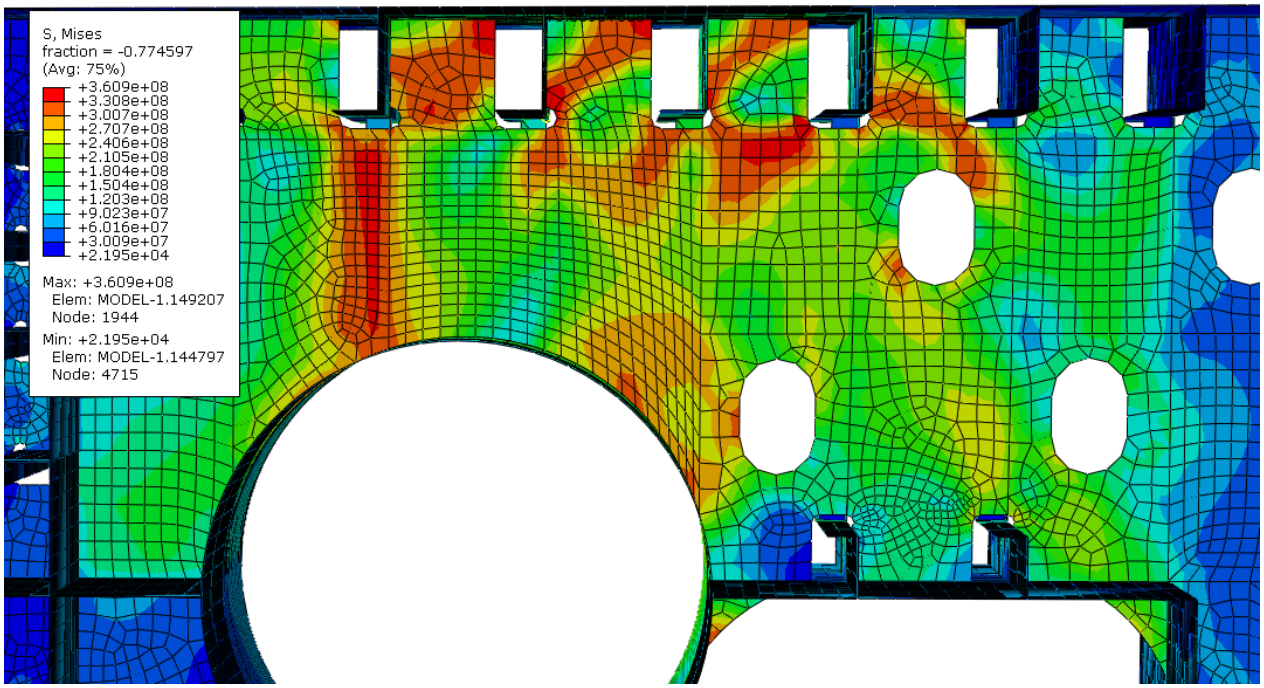

Figure 9.19: von Mises stress distribution for stringer design load, location 8

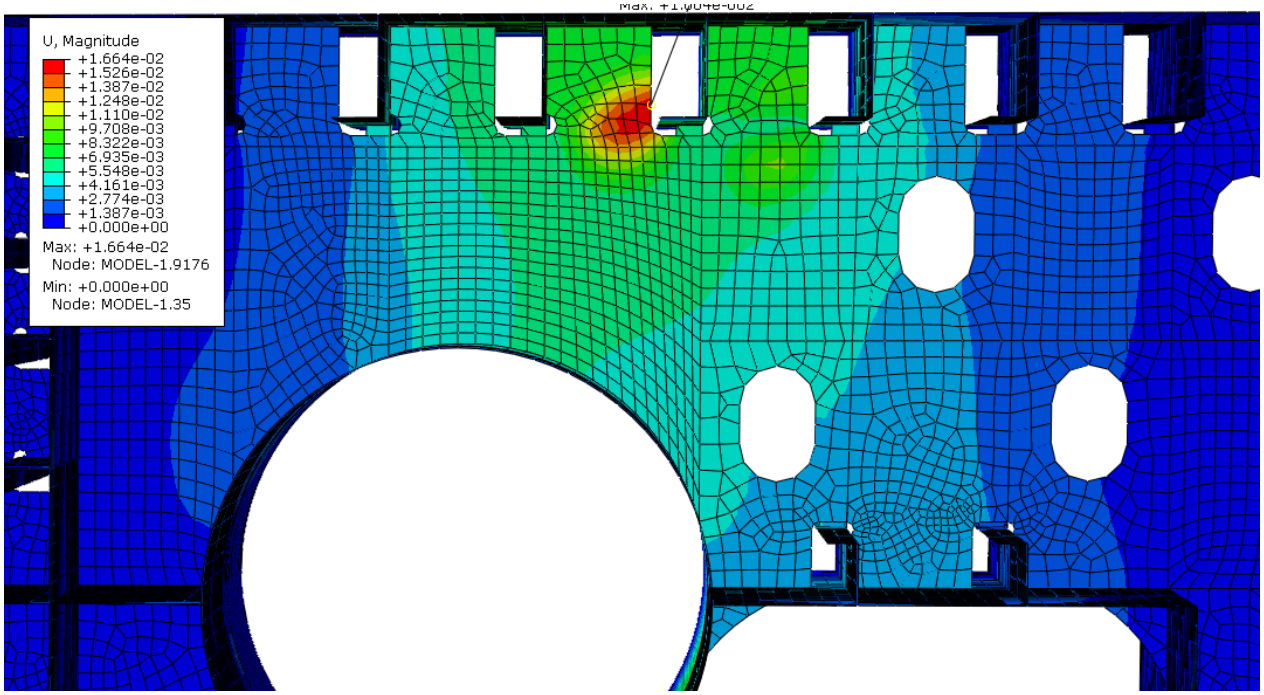

Figure 9.20: Displacement for stringer design load, location 8

The stress distribution at location 6 is found in Appendix D, figure D.16. In this area the stringer has more support from the bulkhead, decreasing the stresses throughout the stringer plate. Some yielding is still experienced, but this is mostly limited to the areas around the holes. Apart from this the stringer seems to be able to carry the design pressure. The maximum deflection is 18.4 mm, as seen in figure D.17. This is generally a stronger part of the structure, and will thus not be that affected by the pressure acting.

9.4.1 Parameter Study of Stringer

For the stringer the parameter study is performed at location 4, which is the critical location. In figure 9.21, the large stresses experienced by the stringer is observed. These large stresses occurring is mainly due to singularity spots and cut-outs leading to very high stresses in some parts of the stringer. The design ice pressure causes stresses in excess of the yield stress for a pressure of 2 MPa. It is difficult to quantify to what degree these results can be trusted, but a more refined model is probably needed to properly account for all the details in the stringer plate. But it is clear that lack of ice strengthening for the different parts on the stringer are not sufficient, and it is thus the weak spot of the structure, and would need considerable strengthening for use in ice infested waters.

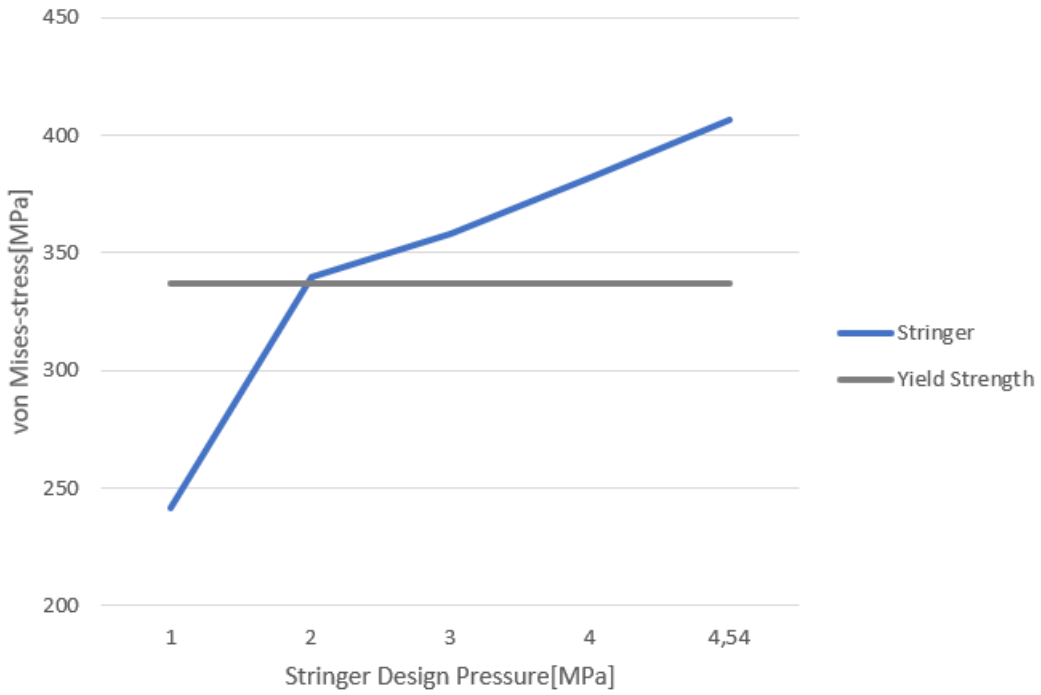

Figure 9.21: Maximum von Mises-stress vs design ice pressure in stringer

9.5 Response in Bulkhead due to Local Ice Pressure

The response of the bulkhead between location 4 and 5 due to the bulkhead design load can be seen in figure 9.22. The stresses are very moderate for this load case, with a maximum stress of 298 MPa. The yield strength in this area is 357 MPa, so in this case there is a safety factor of 1.20. From this it is obvious that the bulkhead is more than strong enough to carry the design load applied, and there is no plastic straining present. The maximum stress occurs in the top corner of the bulkhead. The maximum stresses for the bulkhead between location 2 and 3, see figure 9.24, also occurs at the top corner. The maximum stress is even lower here, with a magnitude of 253 MPa. I.e. this part of the structure does not need any local strengthening. The maximum deflection between location 4 and 5, as seen in figure 9.23, is 4.0 mm and occurs in the frame plate connected to the bulkhead. In the bulkhead itself the deflections are small, barely rising above 2 mm. For the bulkhead shown in figure 9.25 the maximum deflection is also observed in the outer frame, with a magnitude of 2.4 mm, and magnitudes of under 2 mm in the bulkhead itself.

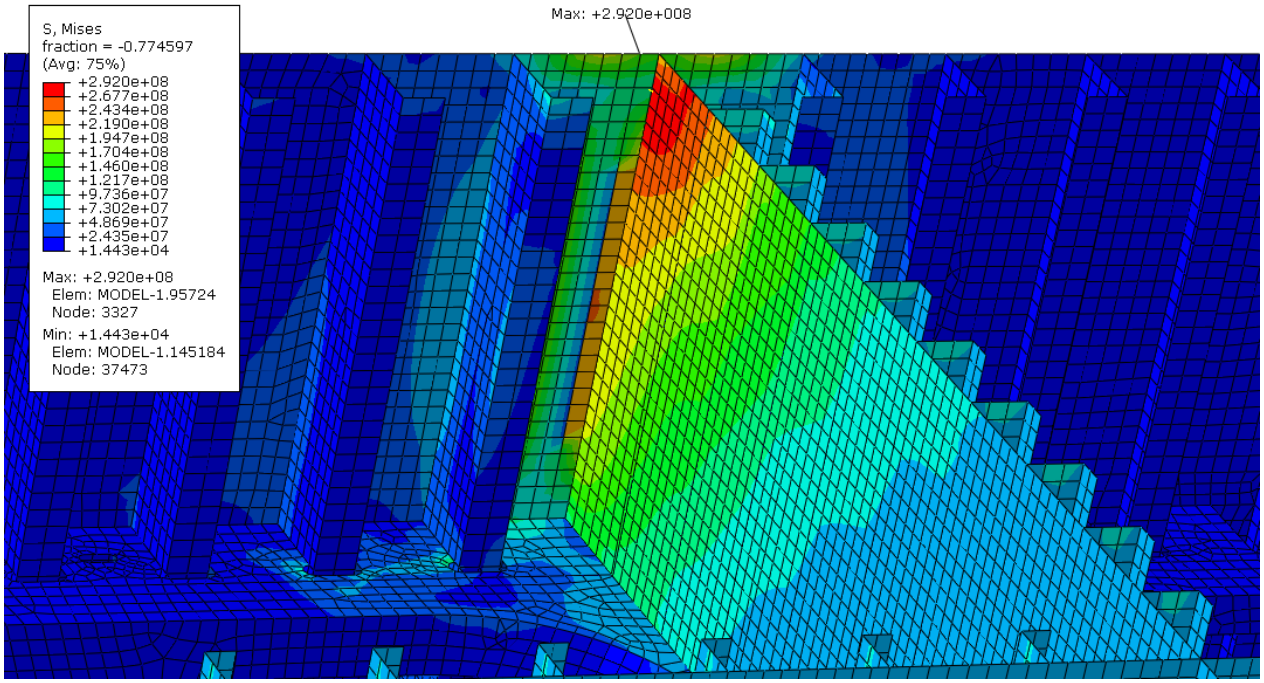

Figure 9.22: von Mises stress distribution for bulkhead design load, location 4/5

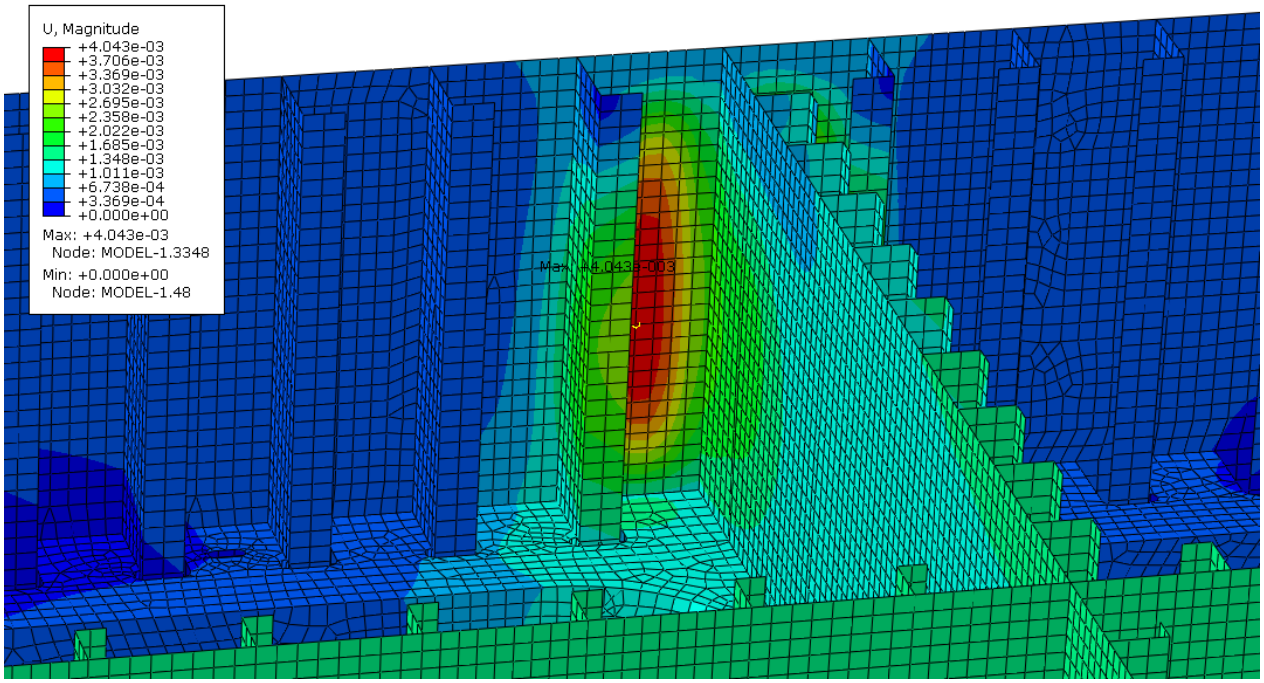

Figure 9.23: Displacement for bulkhead design load, location 4/5

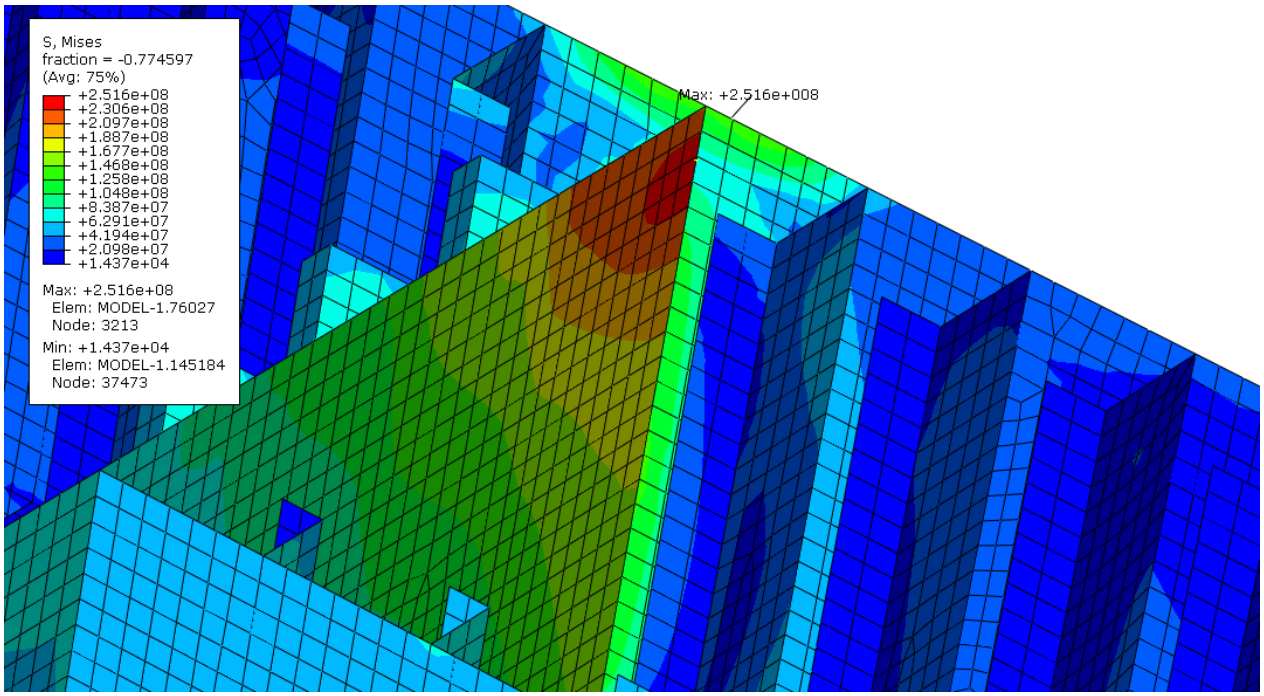

Figure 9.24: von Mises stress distribution for bulkhead design load, location 2/3

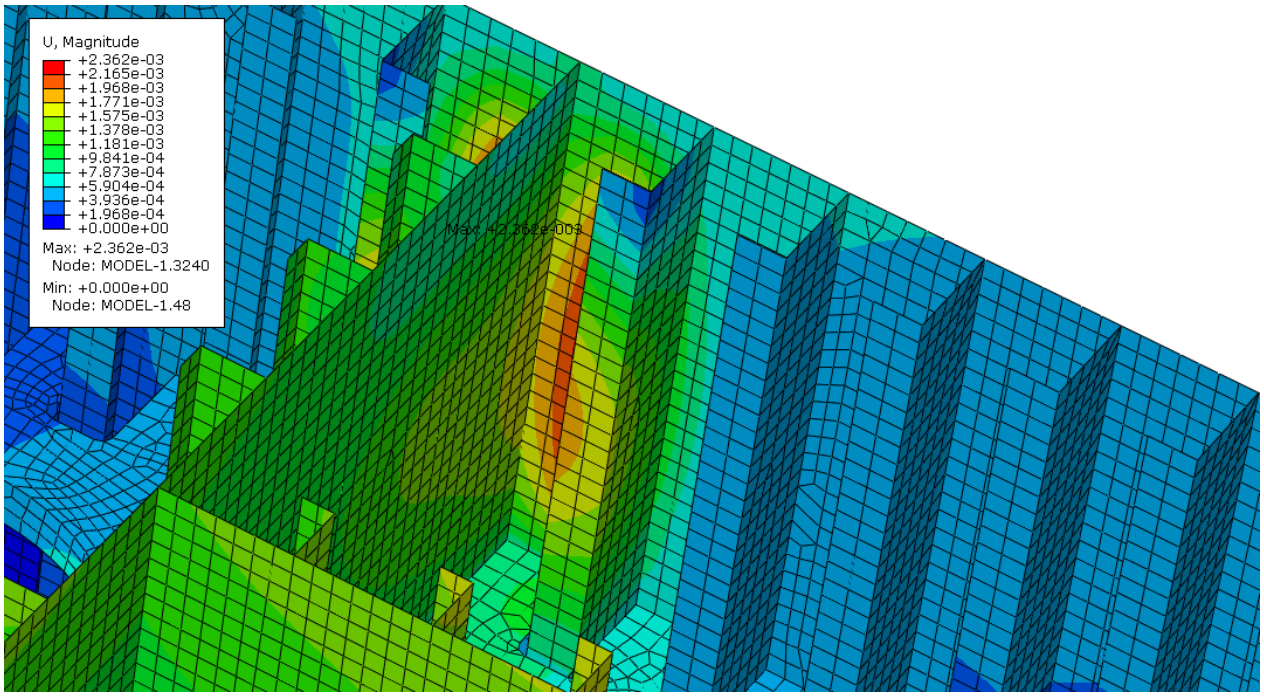

Figure 9.25: Displacement for bulkhead design load, location 2/3

9.5.1 Parameter Study of Bulkhead

The analyses of the bulkhead are not possible to perform for ice pressures above 8 MPa. This is because a large area is yielding at the boundary of the model. The output of the solver states that "The strain increment is so large that the program will not attempt the plasticity calculation at 159 points". This causes an error an the analysis is aborted. The maximum stress in the bulkhead at this instant is only about 330.5 MPa but there is still significant plastic straining in this area.

10 Conclusion

This master thesis has discussed some relevant load cases for a floating offshore structure intended for operation in the Arctic. The main part of the thesis involved an analysis of a local structural part of a semi-submersible subjected to ice actions. Three different load formulations were applied to check the structural capacity of the structure. The finite element analysis software Abaqus was utilized to conduct several non-linear analyses. In addition to this a literature study has been done on ice properties, ice mechanics and ice load formulations for floating hull structures.

The outer plate field with associated stiffeners are dimensioned according to *Requirements Concerning POLAR CLASS*. The minimum plate thickness and stiffener section modulus were calculated based on plastic methods, and the model was constructed accordingly. A sensitivity study was also performed on element size, and a comparison between different elements showed that the best suited element for this analysis was the S4R-element. The structural response of the model was analysed for three different load formulations. IACS design load for a glancing impact on the bow gave an average pressure of 4.74 MPa over an area of 7.14 m^2. Then the formulations of DNV GL for ships navigating and ice and ISO 19906 were compared. This resulted in ISO 19906 being used for load patch areas smaller than 1.6 m^2 and DNV GL being used for load patches equal to or larger than 1.6 m^2. These formulations were used to check the response for plating, stiffeners, stringer and bulkhead respectively.

The model is based on the assumption that the ice pressure is applied over a calculated contact area. In real conditions this is a simplification, as the ice interaction will vary constantly, both in time and space. It is therefore important to ensure that conservatism is applied in the calculations, and that the load patch is applied in an area that produces the largest response in the structure. The bottom boundary is assumed to only be free to rotate in vertical direction, while the top boundary is free to translate and rotate in vertical direction, while all other translations and rotations are fixed. This produced the most conservative stress and displacement response out of the cases checked.

The response due to IACS design load gave a maximum stress of 450 MPa, but this stress occurred in a singularity spot. In the plate the maximum stress was found to be 321 MPa, which is reasonably in magnitude. In the stiffener stresses of 340 MPa was found, which is just over yield stress for this area. IACS is based on plastic methods, so some yielding is expected for this load case.

For DNV's and ISO 19906's load cases, yielding was experienced for plating and stringer, while the stiffener's and bulkhead's stress response was beneath yield strength in magnitude. Parameter studies suggested that especially the stringer is a weak part of the structure, as it has not been much strengthened for interaction with ice, as large stresses occurred for large parts of the stringer plate. The many details and cut-outs in this part of the structure does make it even more important for a detailed and refined model.

11 Recommendations for Further Work

Several uncertainties have been addressed throughout the master thesis, regarding dimensioning, boundary conditions, loads and elements. More work need to be done to make any definite conclusions about the response of the model.

The drawing provided in order to construct the model was limited in regards to details. In order to get obtain more accurate results this is critical, especially for the stringer plate. Having information about the other parts of the structure is also critical in modelling realistic boundary conditions. A global analysis should first be conducted, and from this the correct boundary condition can be gathered. Another possibility is introducing spring stiffness at the boundary.

Finding the optimum load locations in order to obtain conservative results is challenging, and more time and thought should be put into this. Some basic calculations were done to find the best locations for the loads, but far from every possibility was considered, so it is hard to say if the loads used are conservative enough, or maybe even too conservative. The same can be said about the load patches constructed, more analyses has to be performed to be sure this provides acceptable results.

The stringer should be investigated further, and rules for ice strengthening should be implemented. It is clear that this part of the model is not strengthened enough, which causes difficulties for the rest of the structure. Large stresses and deformations occur for relatively small design pressures, and singularities appear as the details of the stringer are not sufficiently modelled. This should be further pursued.

References

Abaqus (2014). ABAQUS 6.14 documentation, http://abaqus.software.polimi.it/v6.14/index.html. Accessed: 2019-05-25.

AMSA (2009). *Arctic Marine Shipping Assessment 2009 Report*. Arctic Council.

CARA (2008). *Ice mechanics, a brief introduction*. Circum Arctic Resource Appraisal. Estimates of Undiscovered Oil and Gas North of the Arctic Circle, USGA Fact Sheet 2008-3049, US Department of the Interior, U.S. Geological Survey.

Daley, C. (2000). *IACS Unified Requirement for Polar Ships. Background Notes to Design Ice Loads*. Memorial University.

Diamond, H. J. (2019). *Arctic Sea Ice Extent*. PhD; Climate Science Program Manager at NOAA's Air Resources Laboratory, http://akclimate.org/node/1592.

DNV (2013). *Ships for navigation in ice. Rules for Classification of Ships Part 5, Chapter 1*. Det Norske Veritas.

DNV (2016). *Determination of structural capacity by non-linear fe analysis methods. Recommended practice DNV-RP-C208*. Det Norske Veritas.

Fequet, D. (2005). *MANICE: manual of standard procedures for observing and reportingice conditions*. In:Environment Canada.

Frederking, R. M. and Timco, G. W. (1984). *Measurement of shear strength of granular/discontinuous-columnar sea ice*. Cold Regions Science Tech., Vol. 9, pp. 215-220.

Høyland, K. (2015). *Ice mechanics, a brief introduction*.

IACS (2011). *Requirements concerning polar class*. Technical report, International Associationof Classification Societies, Geneva, Switzerland.

ICEX1979 (1979). *Ice and Climate Experiment. Report of Science and Application Working Group*. Goddard Space FlightCenter, Greenbelt, Maryland, USA, 90 p.

ISO (2010). *Petroleum and natural gas industries - arctic offshore structures*. SO 19906, Inter-national Organization for Standardization, Geneva, Switzerland.

J.P., D. (1999). *Scale effects on the in-situ tensile strength and fracture of ice. Part II:first-year sea ice*. Intentional Journal of Fracture 95, 347–366.

Kovacs, A. (1996). *Sea Ice Part 1. Bulk salinity versus ice floe thickness*. CRREL Report 96-7,Hanover, NH, USA.

Løset, S. and et al (2006). *Actions from ice on arcctic offshore and coastal structures*. LAN.

Moan, T. (2003). *Finite element modelling and analysis of marine structures*. Department of Marine Technology, NTNU.

Muhonen, A. (1991). *Medium scale ice indentation tests*. Test results from a program of ice indentation tests made at Hobson's Choice Ice Island in the Canadian Arctic on May 1st-24th, 1990, 65 p.+ app. 175 p.

Ottosen, N. and Petersson, H. (1992). *Introduction to the Finite Element Method*. Prentice Hall.

Palmer, A. and Croasdale, K. (2013). *Arctic offshore engineering*. Singapore, World Scientific.

Petroleumstilsynet (2017). *Odfjell Drilling*. https://www.ptil.no/tilsyn/samsvarsuttalelser/sutgitt/deepsea-stavanger-odfjell-drilling/.

Riska, K. (2011). *Design of ice breaking ships*. Course material NTNU.

Riska, K. (2018a). *ICE ACTION ON SHIP HULL*. Course material NTNU.

Riska, K. (2018b). *Ship-ice interaction in ship design: Theory and practice*. Course material NTNU.

Sanderson, T. (1988). *Ice mechanics: risks to offshore structures*. Graham Trotman, London.

Skjetne, E. H. (2015). *Local Structural Analysis of a Semi-Submersible Exposed to Ice Loads*. Master's thesis, Norwegian University of Science and Technology, Department of Marine Technology.

T., T. (1993). *Total Ice Forces on Multi-Legged Offshore Structures*. Pro-ceedings of the 3rd ISOPE Conference, 6–11 June. Vol. II, pp. 36–39.

Timco, G. and O'Brien, S. (1994). *Flexural strength equation for sea ice*. Cold Regions Science Tech., Vol. 22, pp. 285-298.

Timco, G. and Weeks, W. (2010). *A review of the engineering properties of sea ice*. Cold Regions Science and Technology, 60(2):107-129.

Timco, G. W. and Frederking, R. M. (1990). *Compressive Strength of Sea Ice Sheets*. Cold Regions Science and Technology (17), pp. 227–240.

Timco, G. W. and Frederking, R. M. (1996). *R.M.W.A Review of Sea Ice Density*. Cold Regions Science Tech., Vol. 24, pp. 1-6.

Timco, G. W. and Pratte, B. D. (1985). *The Force of a Moving Ice Cover on a Pair of Vertical Piles*. Proceedings Canadian Coastal Conference, St. John's, Newfoundlend, Canada, pp. 349–362.

Vershinin, S., Truskov, P., and Kouzmichev, K. (2006). *The impact and influence of ice*. OAO Institute Giprostroymost, Moscow, p. 205.

WMO (1989). *Sea Ice Nomenclature*. World Meterological Organization, http://www.aari.ru/gdsidb/docs/wmo/nomenclature/WMO_Nomenclature_draft_version1-0.pdf. Accessed: 2019-02-21.

Appendices

A Drawing of Stringer

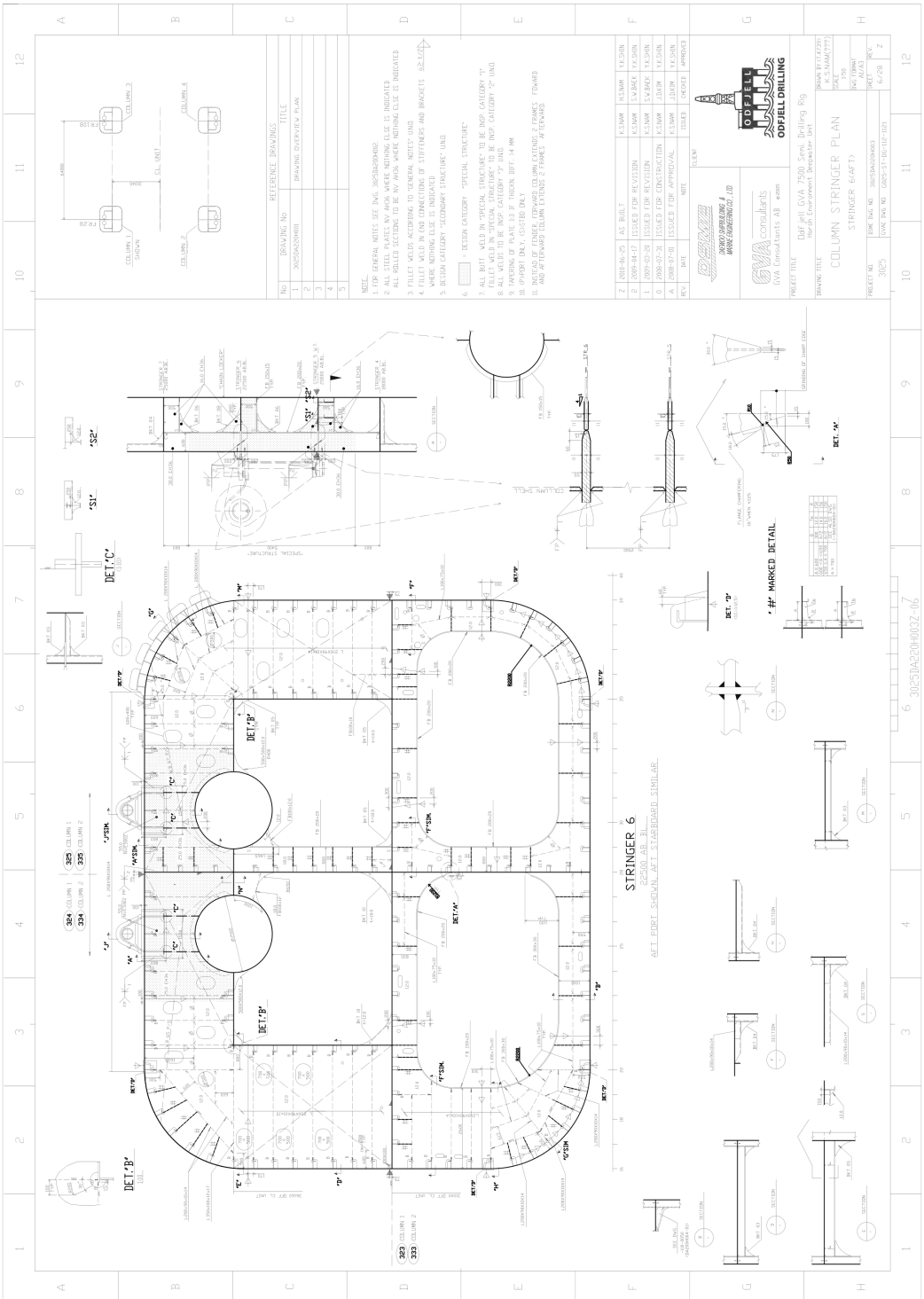

Figure A.1: Drawing of stringer used in model

B Dimensioning according to IACS

```
wh = 530;
wt = 50;
fw = 240;
ft = 50;
tpn = 45.4; %net shell plate thickness
s = 848; %transverse frame spacing
LL = 2.35; %length of loaded portion of span
a = 2.75; %frame span

aw = (wh+ft)*(wt-2.5)/100; %net effective shear area

apn = wh*(wt-2.5)+fw*(ft-2.5); %net cross-sectional area
apn = apn/100;
afn = fw*(ft-2.5); %net cross-sectional area of flange
afn = afn/100;

%net effective plastic section modulus
Zp = apn*tpn/20 + wh^2*(wt-2.5)/2000 + afn*(wh+(ft/2))/10;

at = 275.5; %net effective shear area
y= 1 - 0.5*(LL/a);
j=2;
a1=at/aw;
kw=1/(1 + 2*(afn/aw));
zp=((1/4)*fw*(ft-2.5)^2 + (1/4)*(s*0.5)*tpn^2)/1000;
kz = zp/Zp;
a1a=1/(1+(j/2)+kw*(j/2)*((1-a1^2)^(0.5) - 1));
a1b=(1-(1/(2*a1*y)))/(0.275 + 1.44*kz^0.7);

if a1a > a1b
    A1 = a1a;
else
    A1 = a1b;
end

%net effective plastic section modulus of frame
zpt = (100^3*LL*y*(s*10^-3)*1.2*4.72*a*A1)/(4*355);
```

C Convergence Analysis

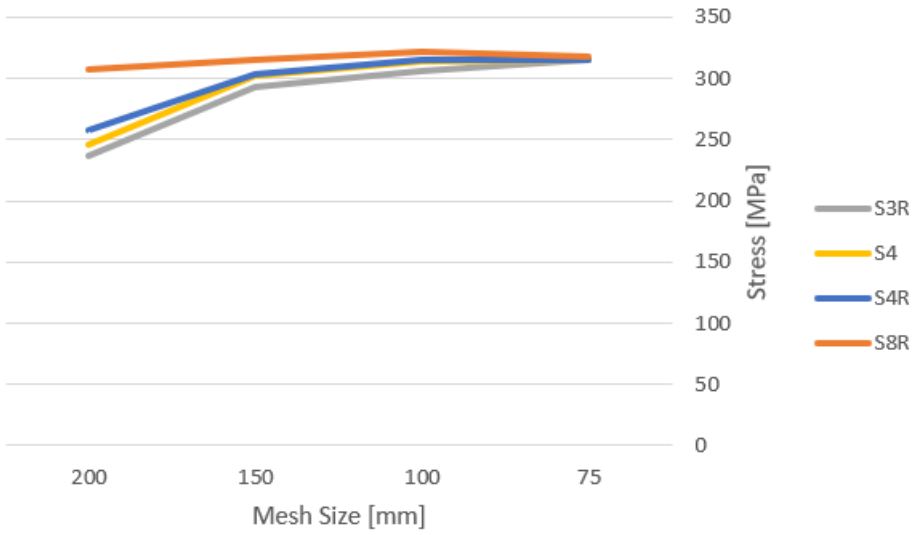

Figure C.1: Convergence of stresses at point of maximum displacement

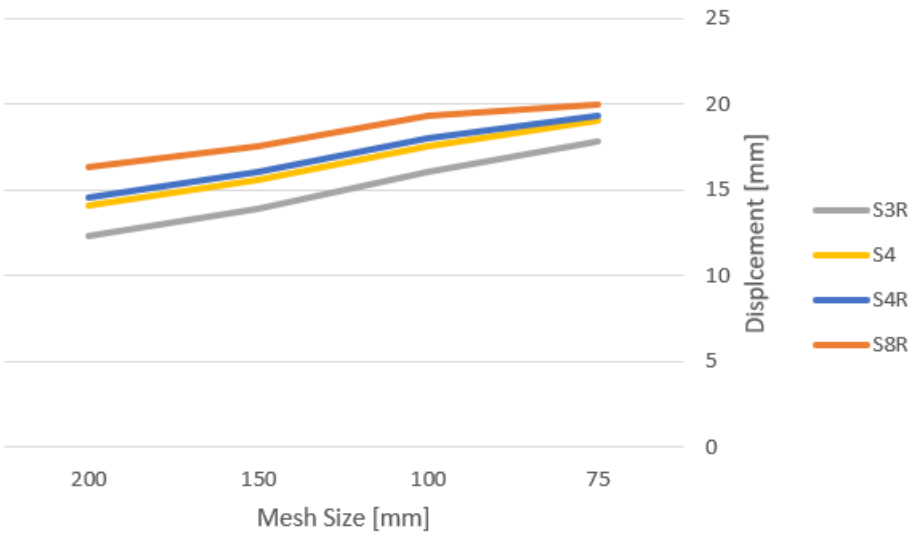

Figure C.2: Convergence of stresses at point of maximum displacement

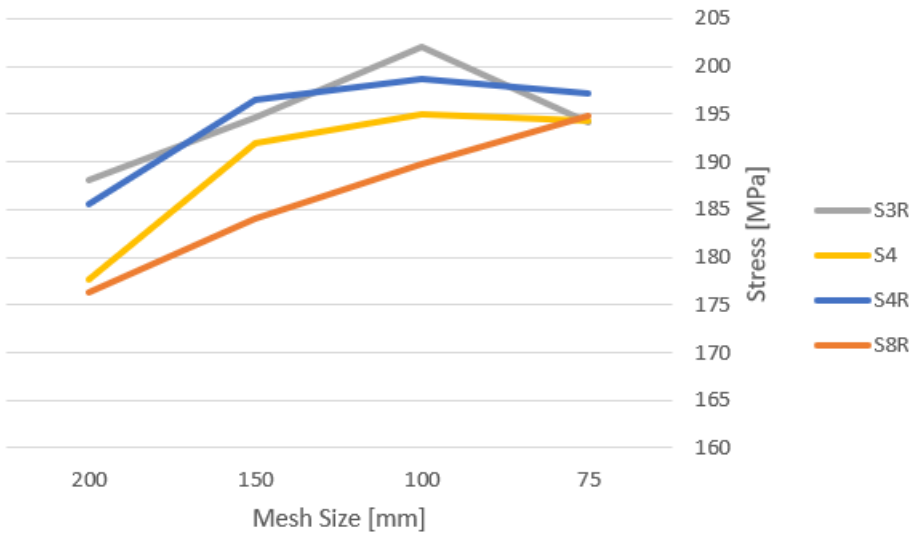

Figure C.3: Convergence of stresses at low stress area

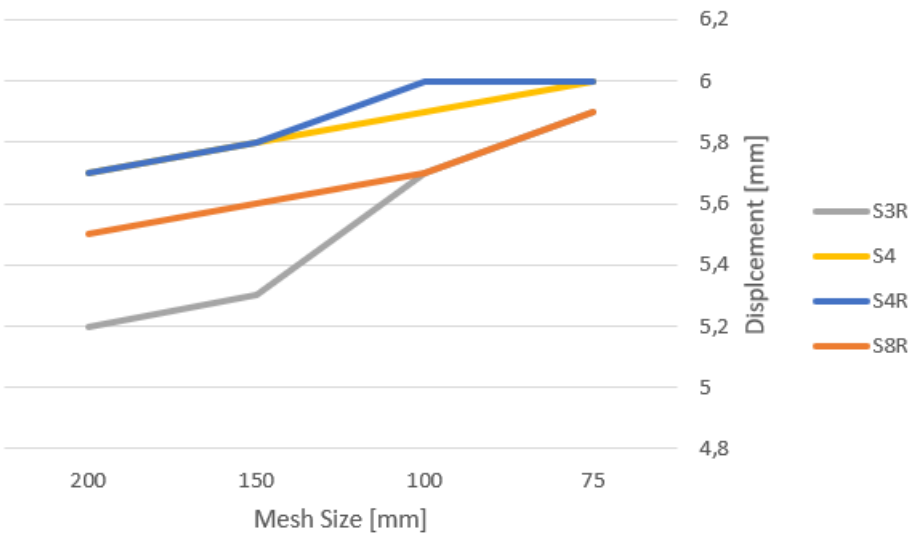

Figure C.4: Convergence of displacements at low stress area

D Results

D.1 Response due to IACS Design Load

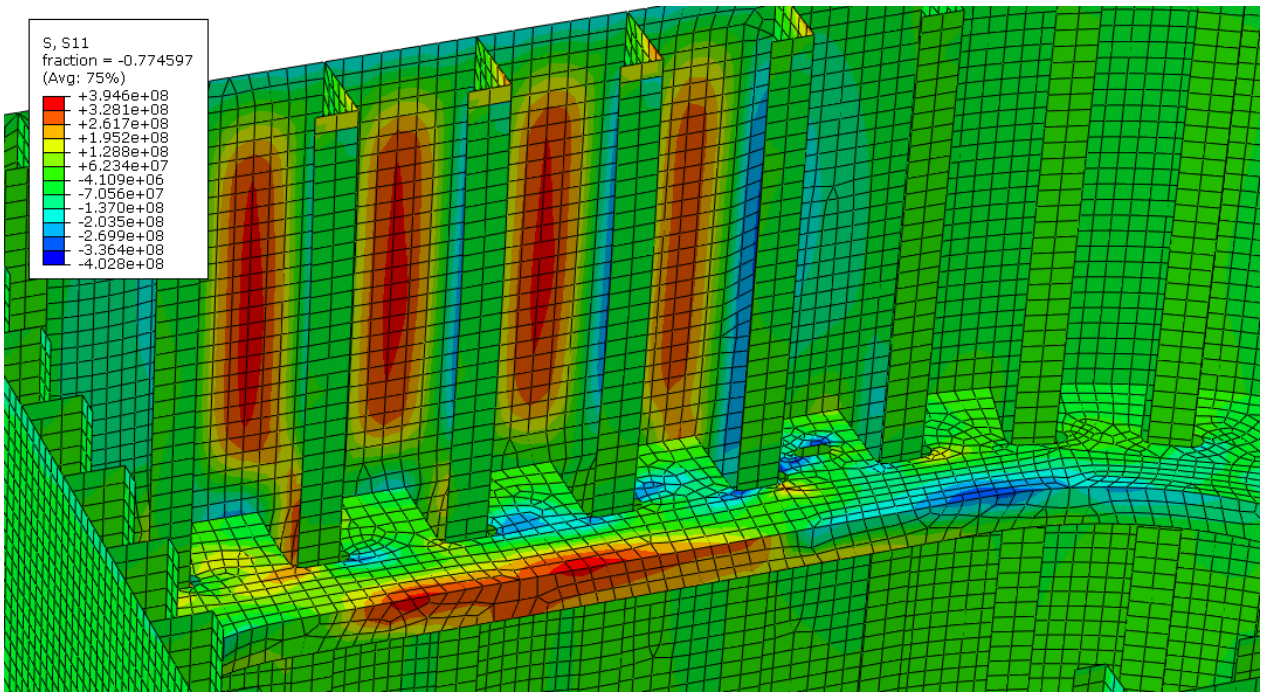

Figure D.1: Stress distribution in x-direction due to IACS design load

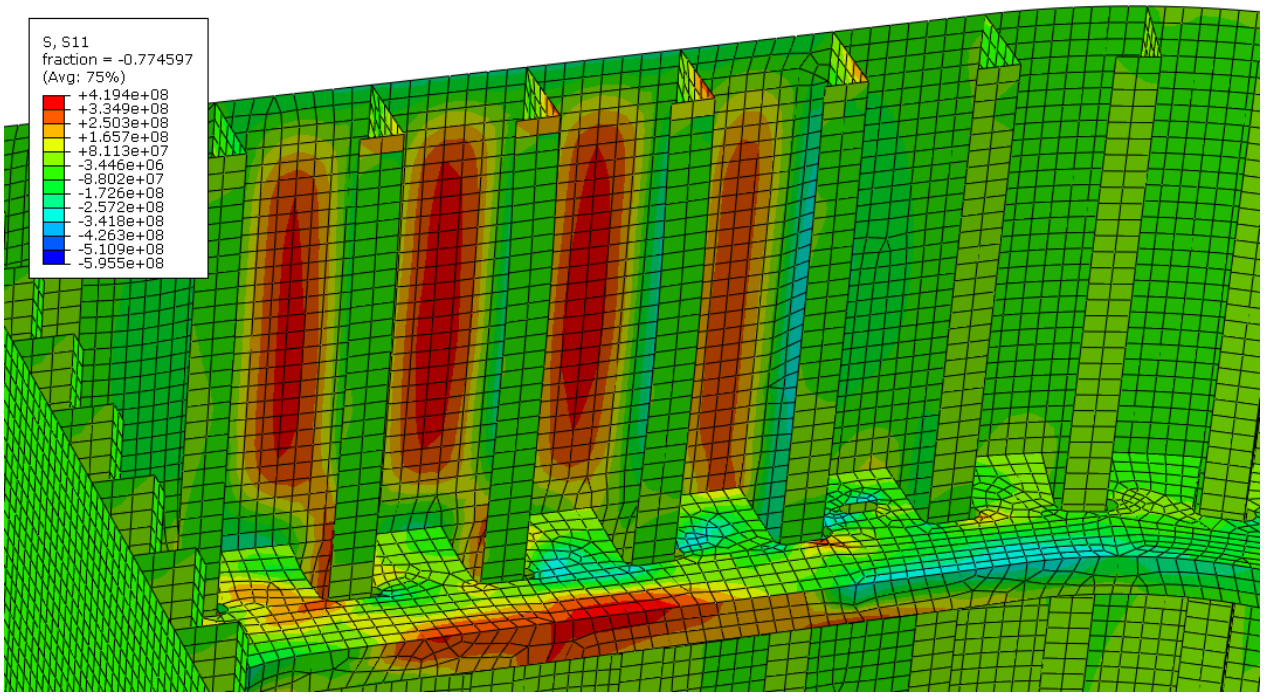

Figure D.2: Stress distribution in x-direction due to IACS stiffener design load

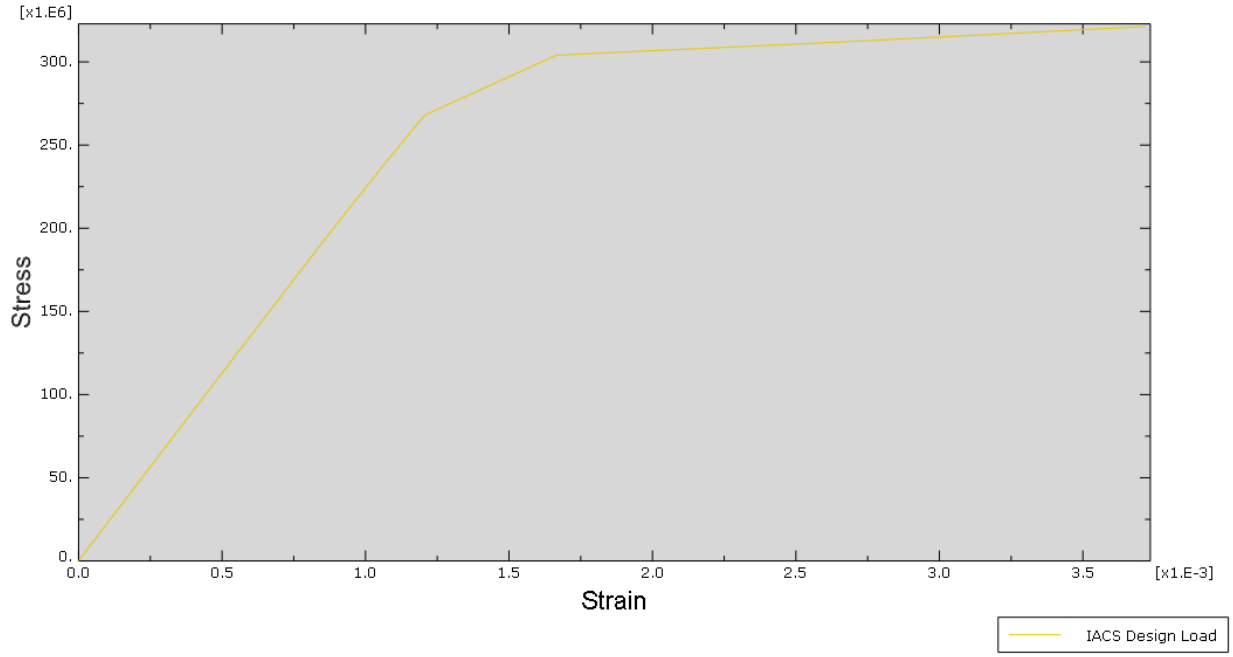

Figure D.3: Stress-strain curve in the middle of plate due to IACS design load

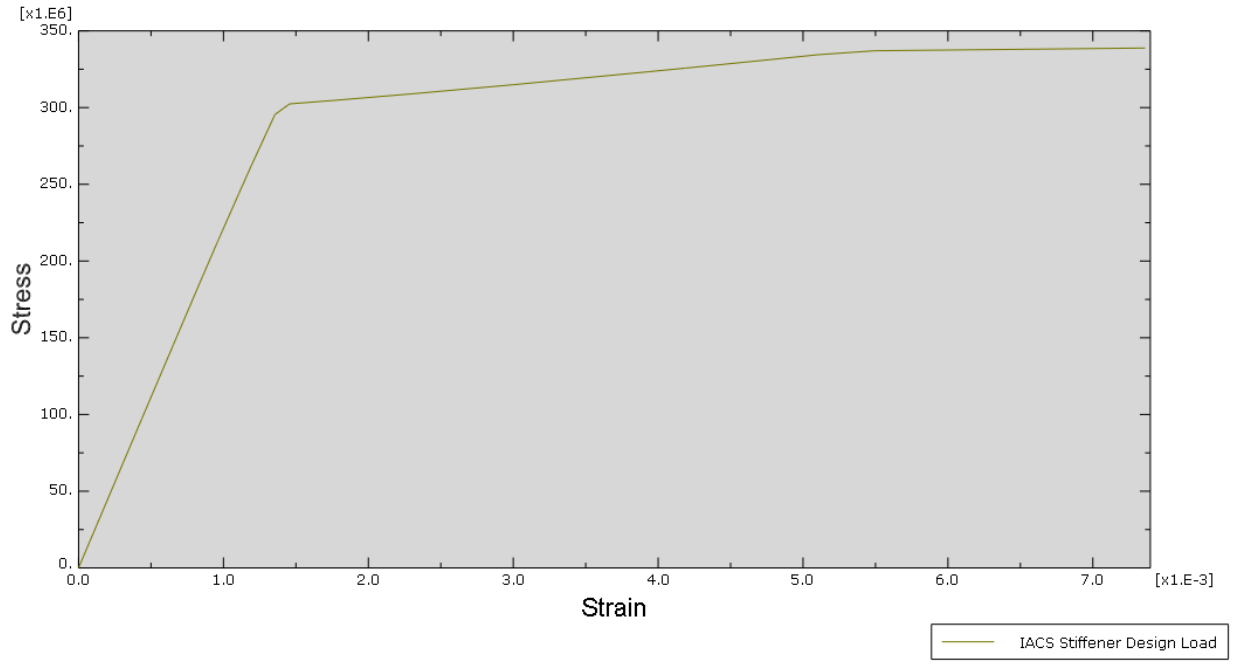

Figure D.4: Stress-strain curve in the middle of plate due to IACS stiffener design load

D.2 Response in Plating due to Local Ice Pressure

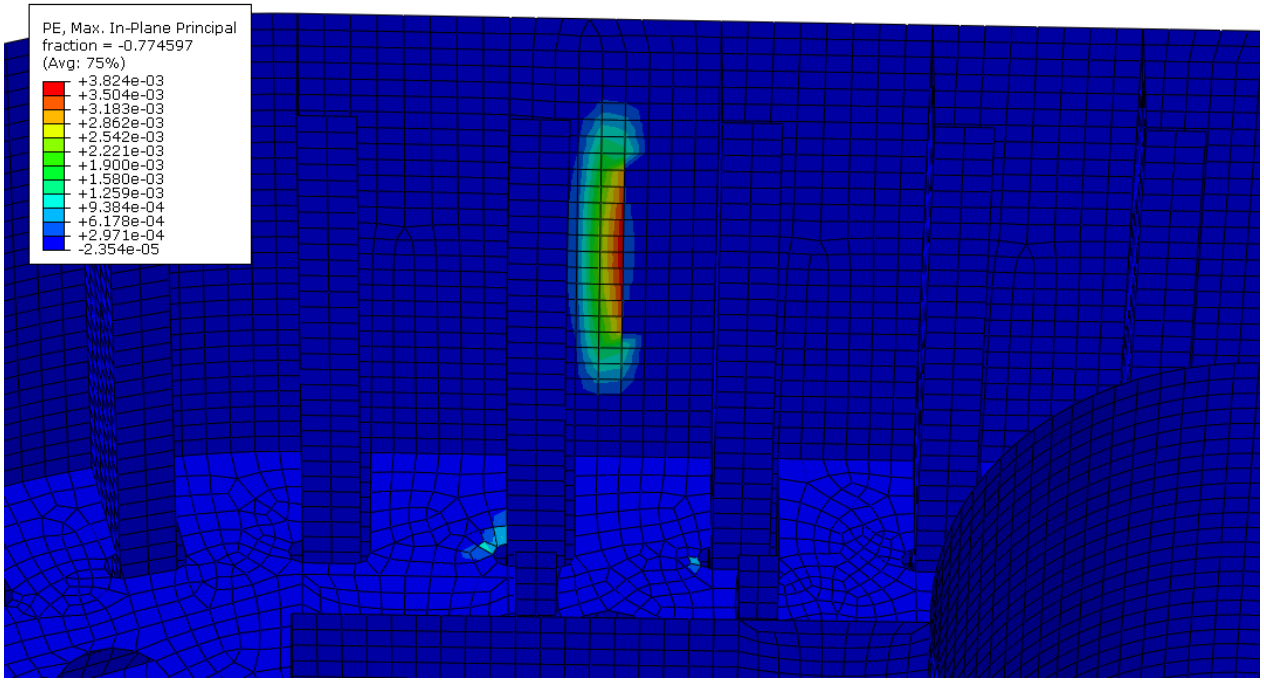

Figure D.5: Plastic straining for plating design load, location 1

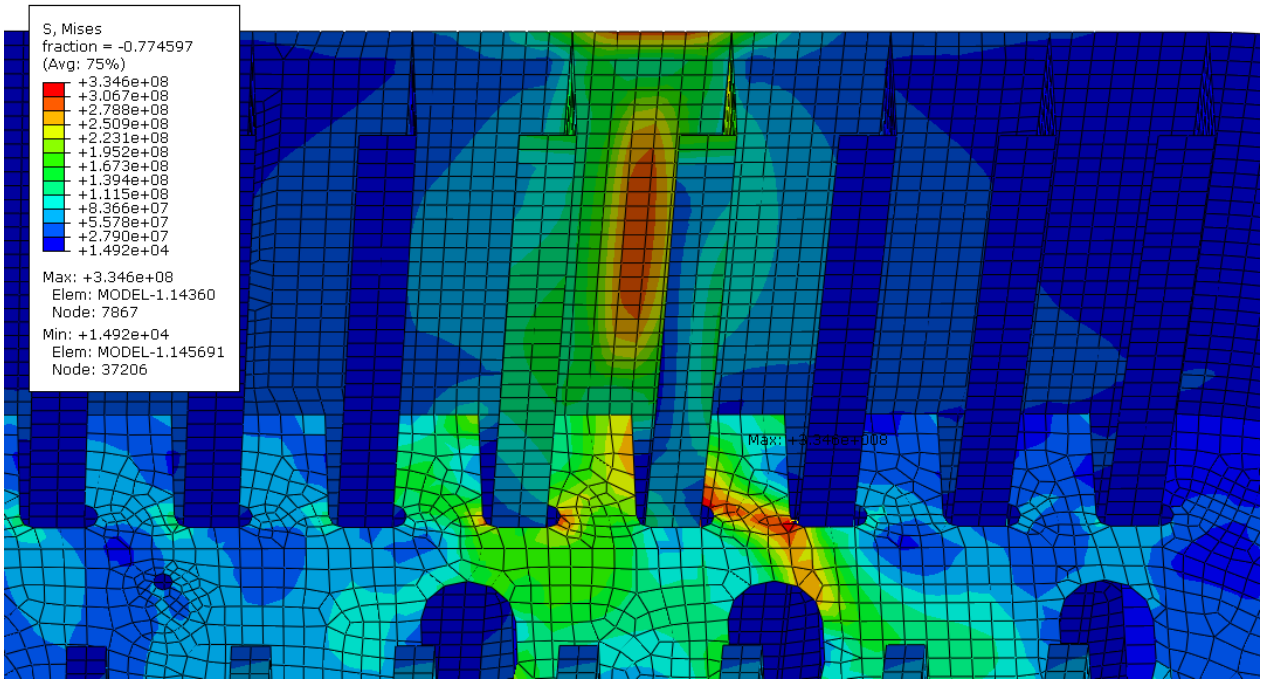

Figure D.6: von Mises stress distribution for plating design load, location 2

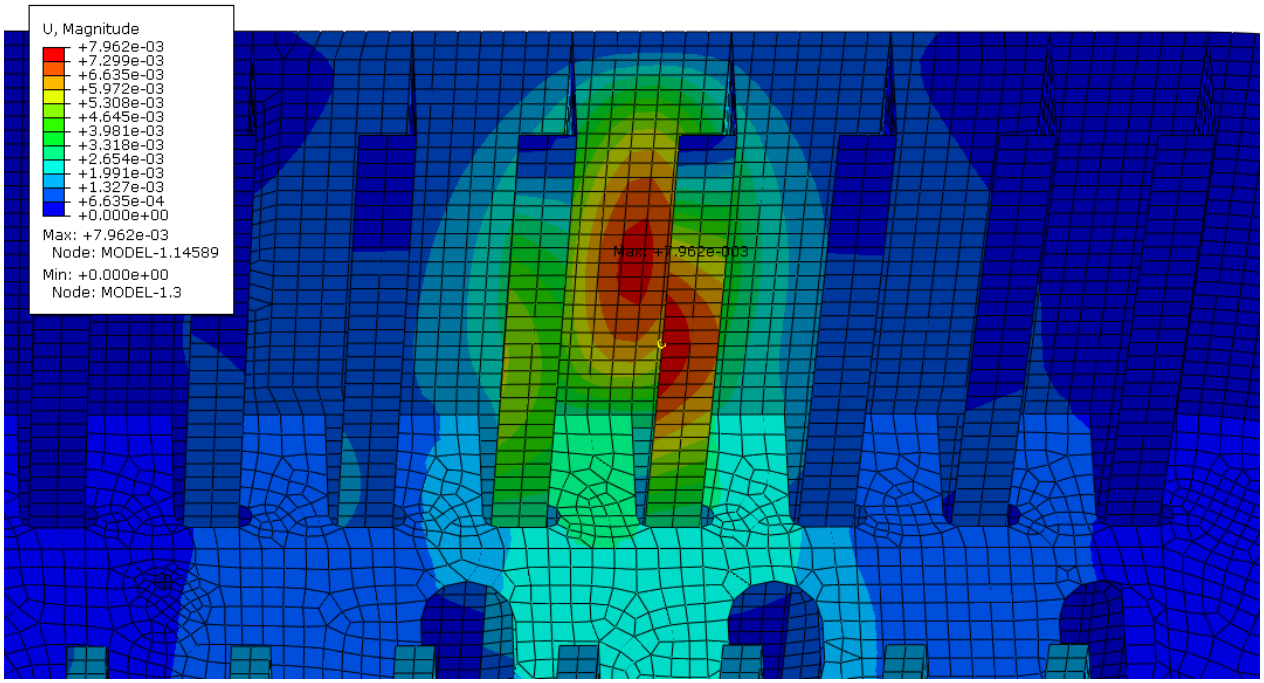

Figure D.7: Displacement for plating design load, location 2

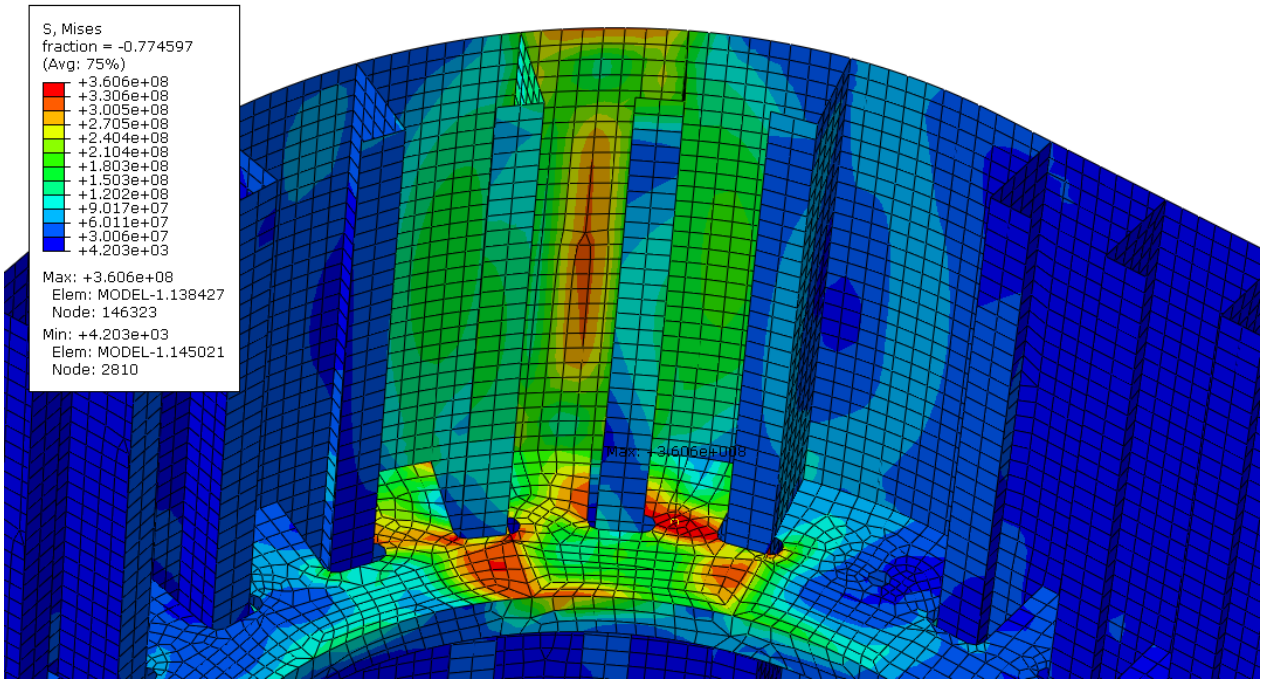

Figure D.8: von Mises stress distribution for plating design load, corner 3/4

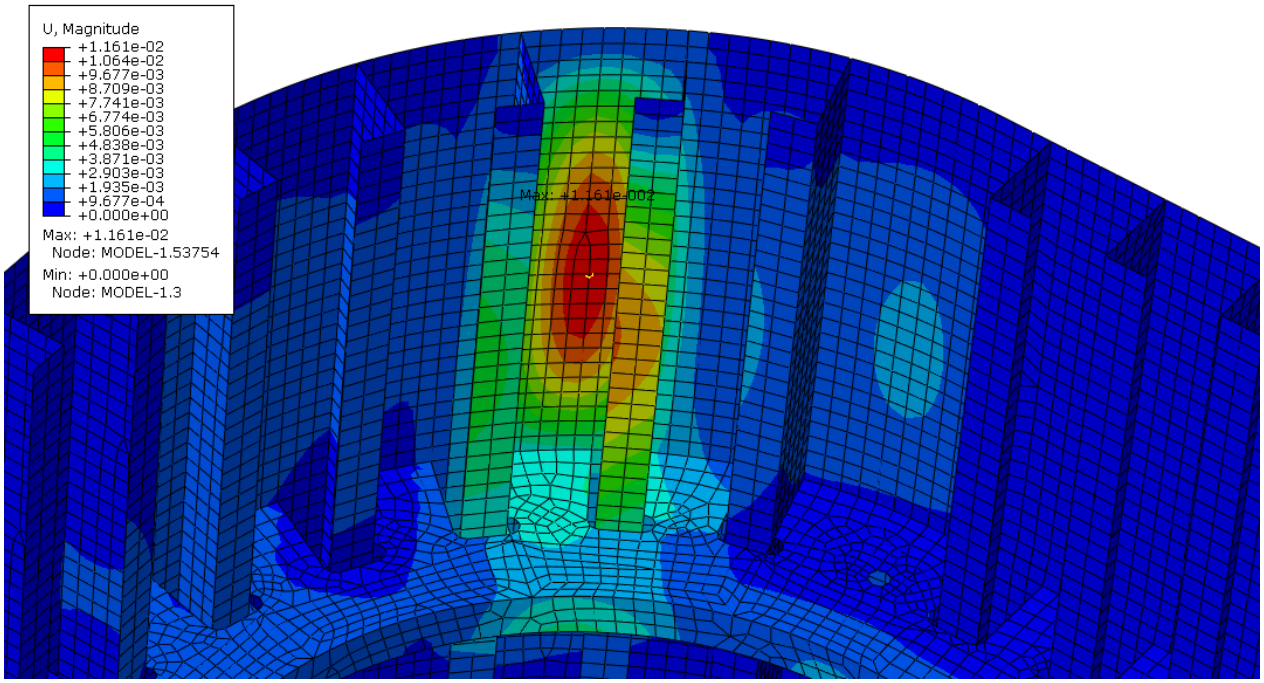

Figure D.9: Displacement for plating design load, corner 3/4

D.3 Response in Stiffener due to Local Ice Pressure

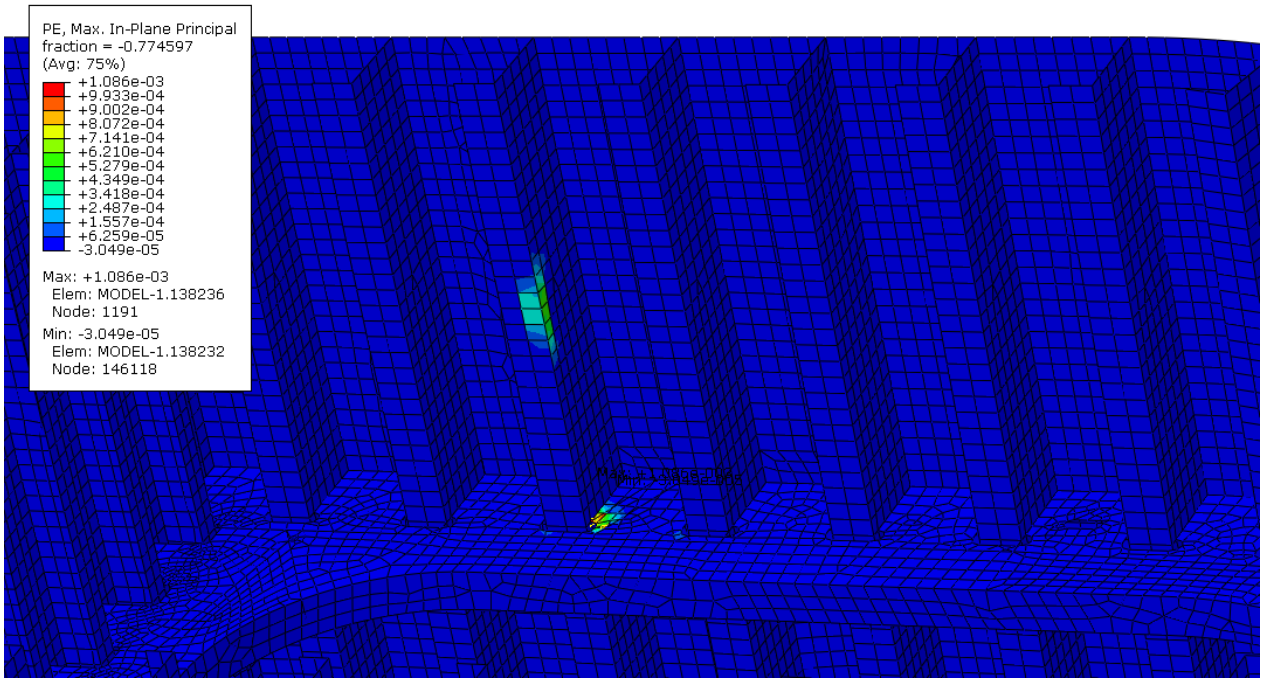

Figure D.10: Plastic straining for stiffener design load, location 4

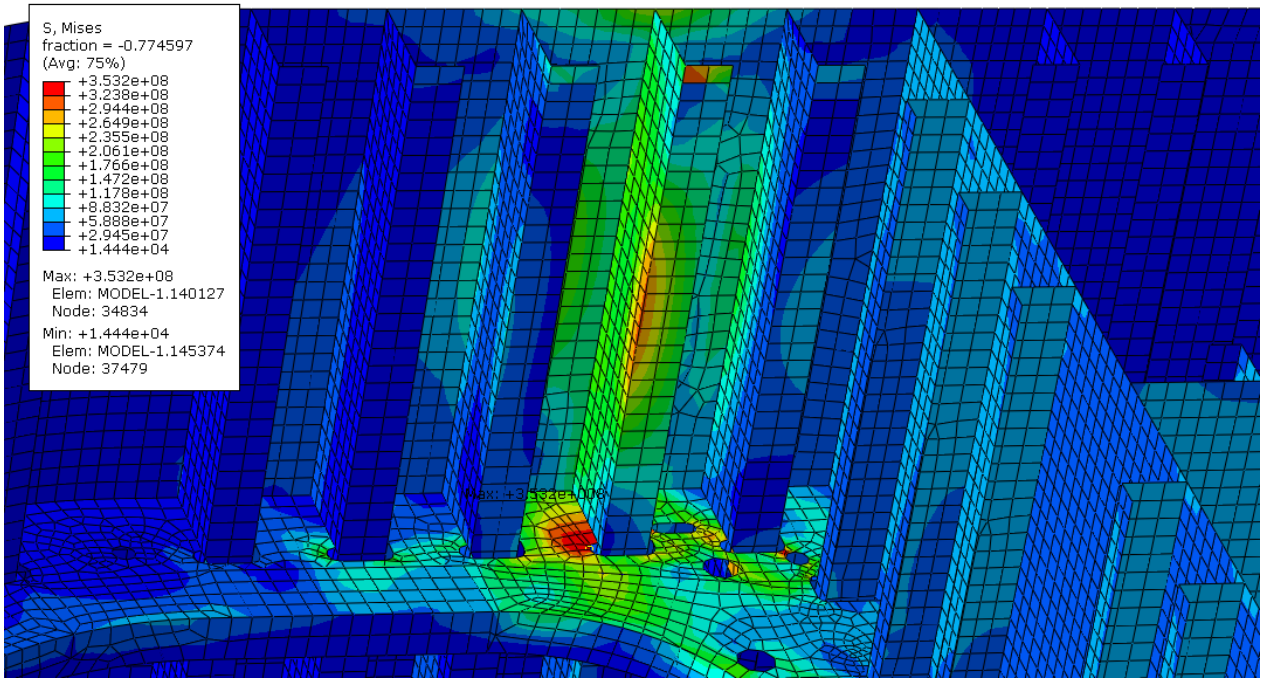

Figure D.11: von Mises stress distribution for stiffener design load, location 3

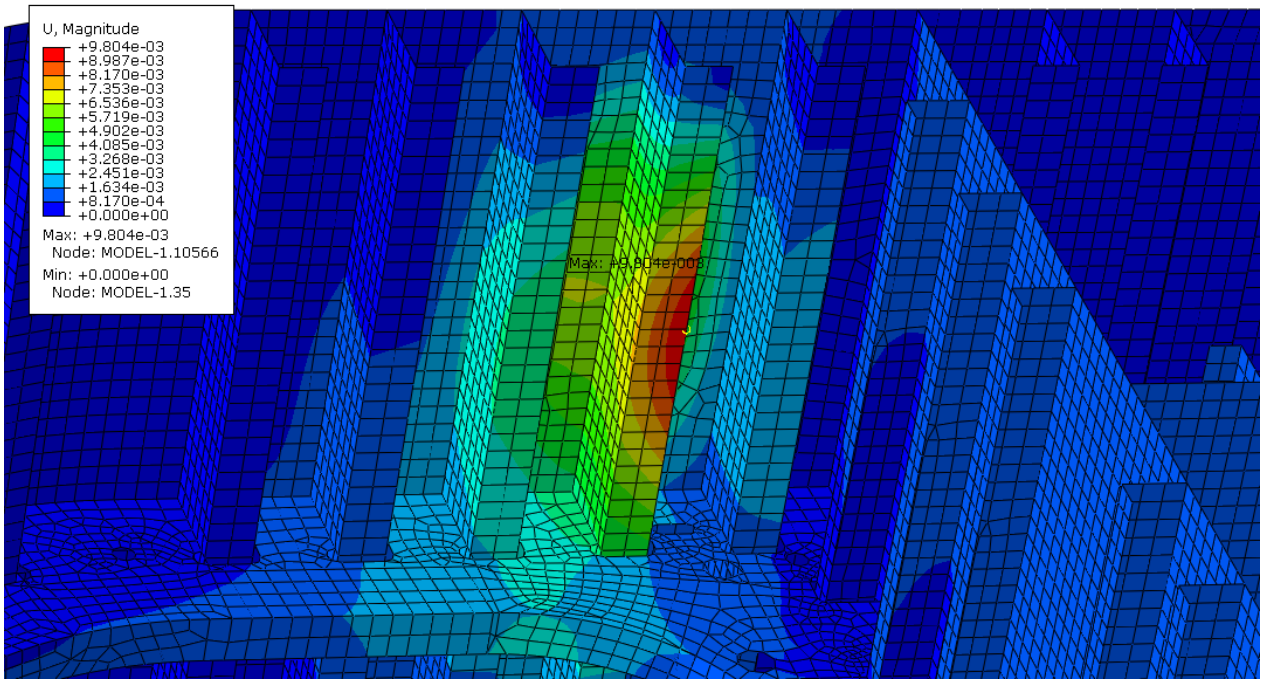

Figure D.12: Displacement for stiffener design load, location 3

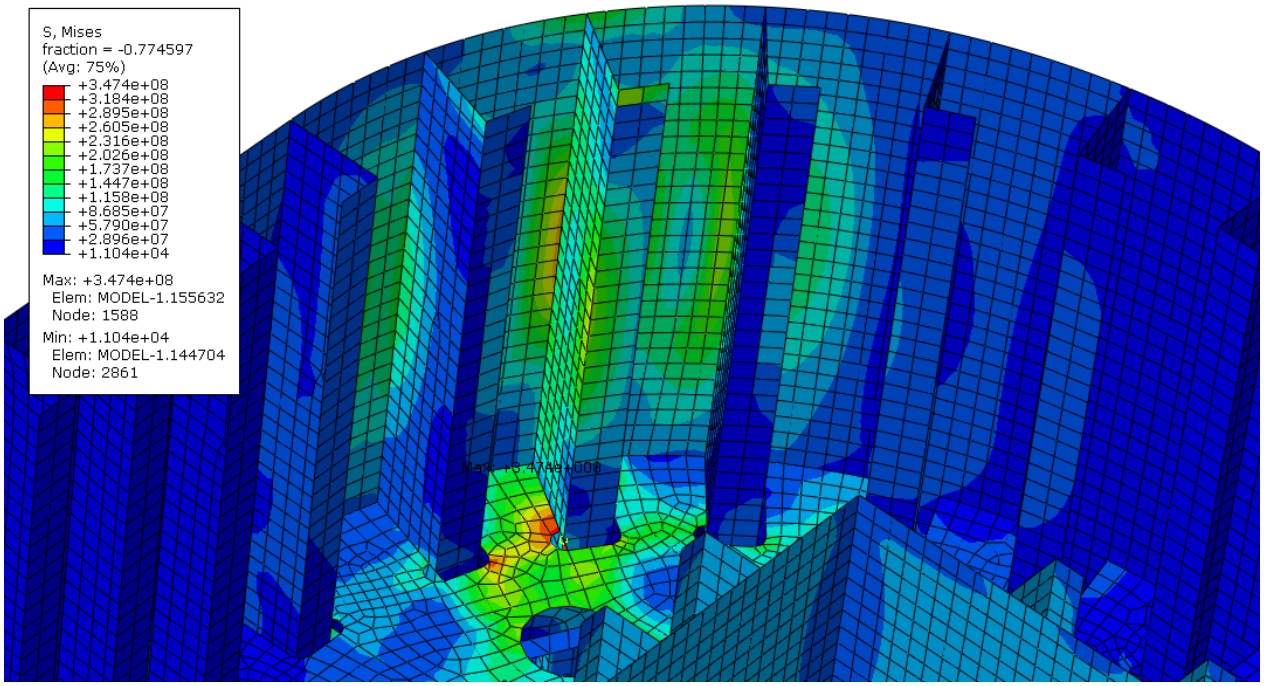

Figure D.13: von Mises stress distribution for stiffener design load, corner 1/2

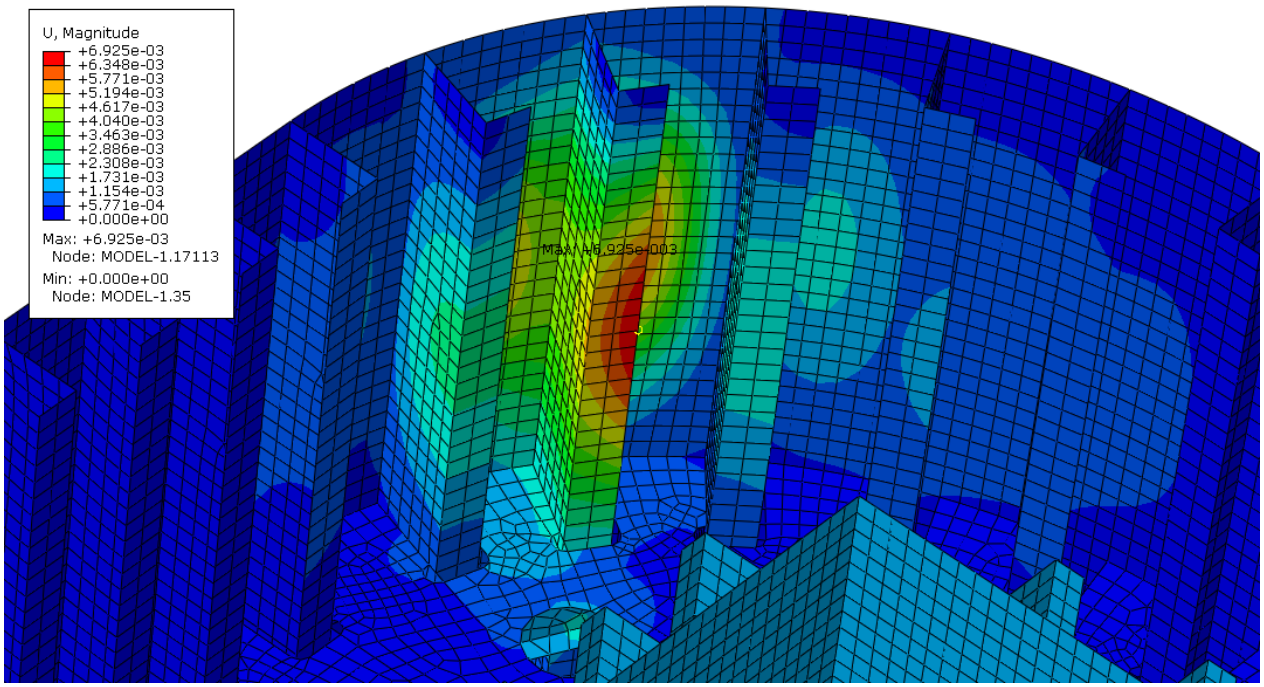

Figure D.14: Displacement for stiffener design load, corner 1/2

D.4 Response in Stringer due to Local Ice Pressure

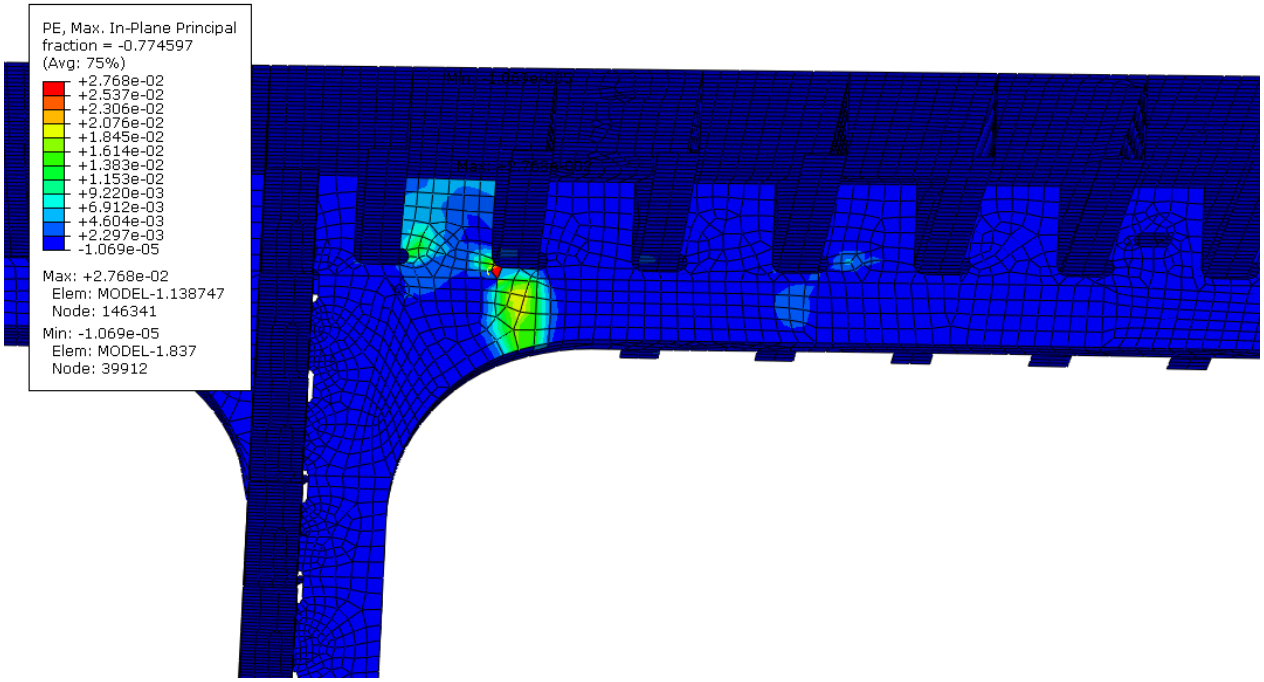

Figure D.15: Plastic straining for stringer design load, location 4

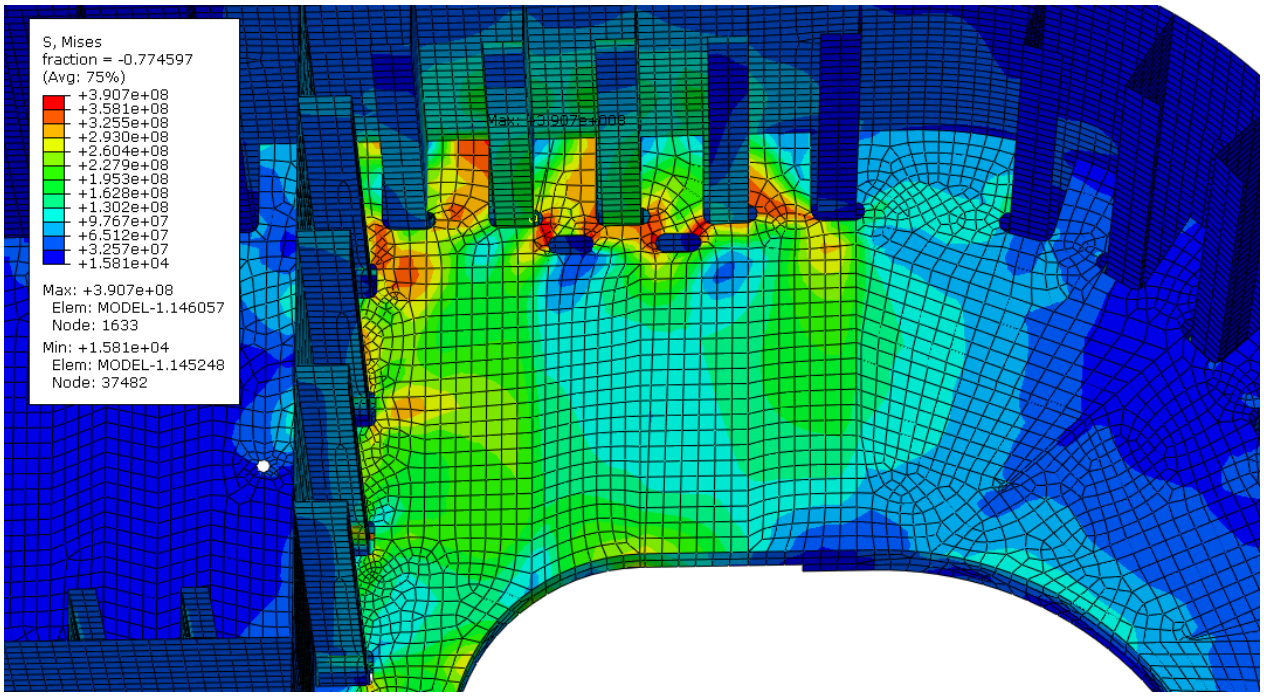

Figure D.16: von Mises stress distribution for stringer design load, location 6

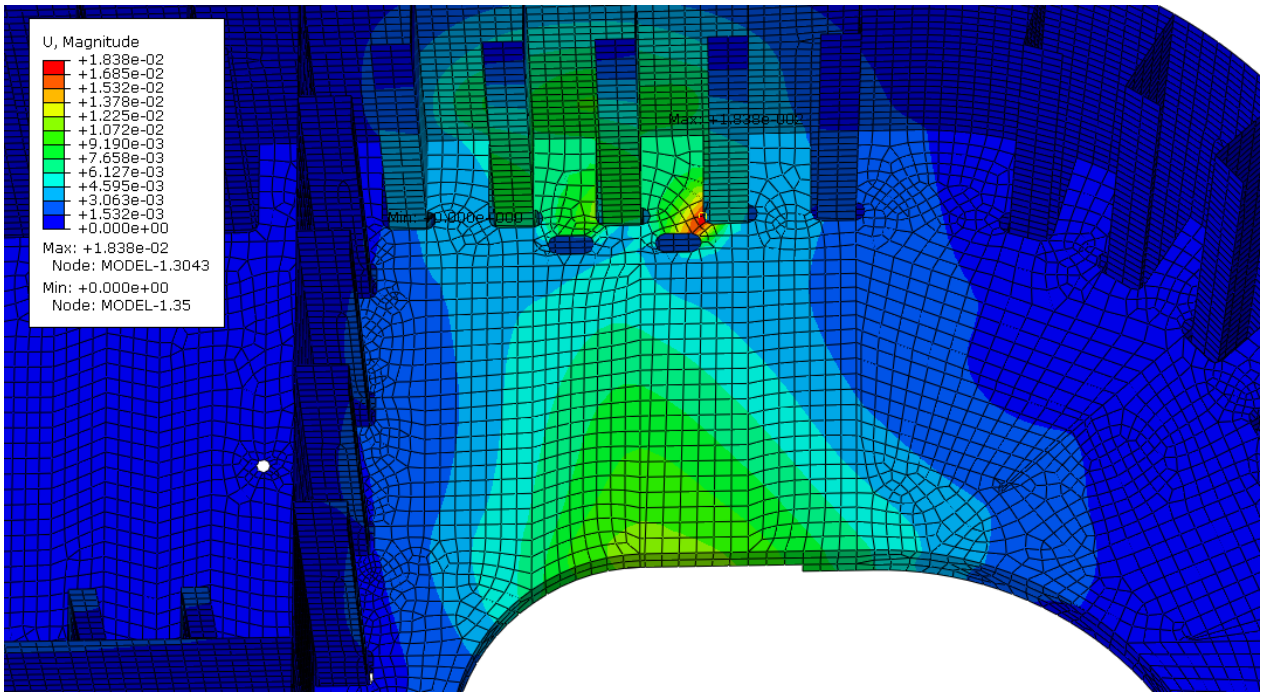

Figure D.17: Displacement for stringer design load, location 6

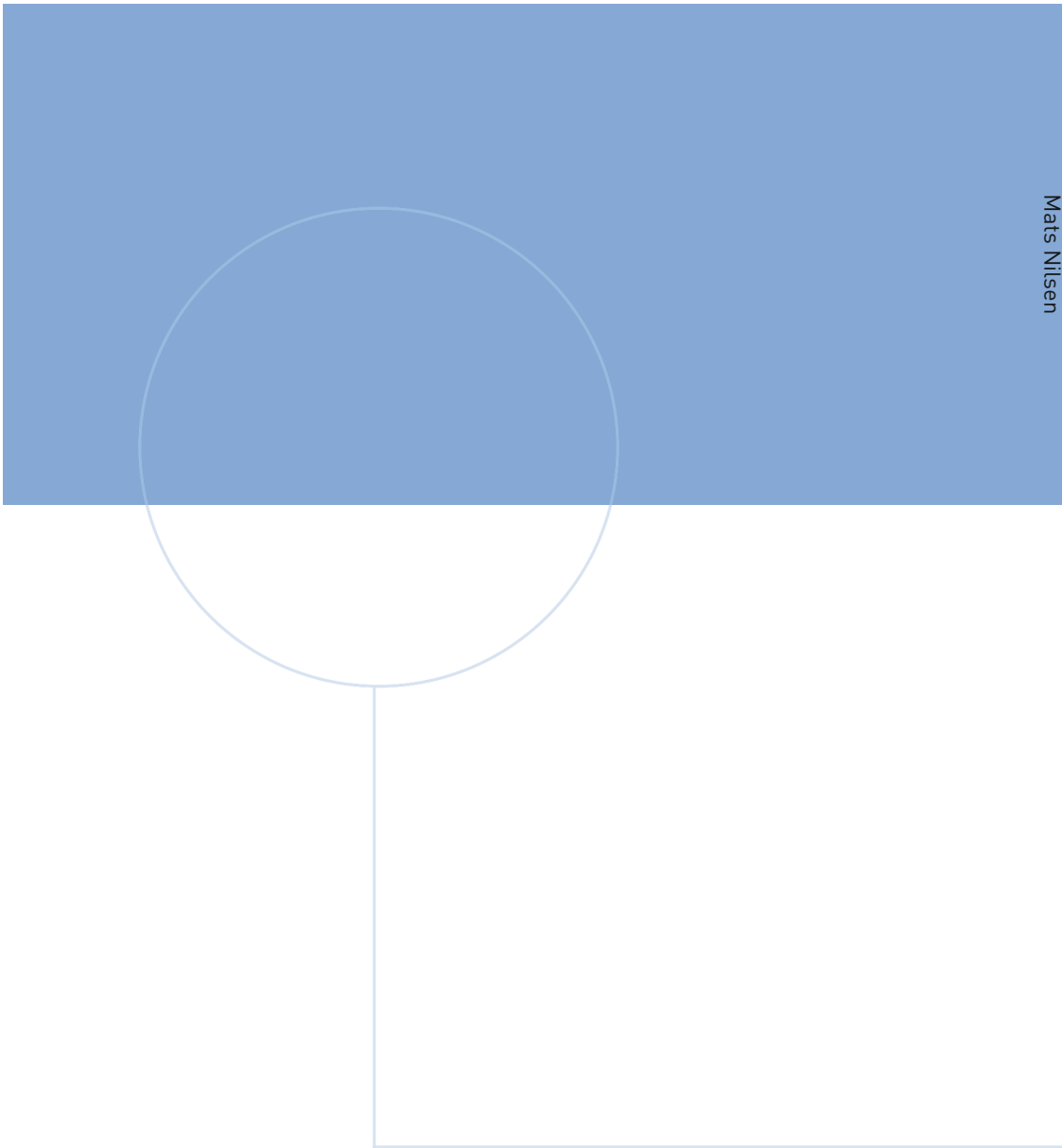

Mats Nilsen

NTNU
Norwegian University of
Science and Technology